AN ABSTRACT OF THE THESIS OF

CURTIS ALLAN COLLINS (Name) for the DOCTOR OF PHILOSOPHY (Degree)

in OCEANOGRAPHY (Major) presented on July 20, 1967 (Date)

Title: DESCRIPTION OF MEASUREMENTS OF CURRENT VELOCITY AND TEMPERATURE OVER THE OREGON CONTINENTAL SHELF, JULY 1965-FEBRUARY 1966

Redacted for Privacy

Abstract approved: Dr. June G. Pattullo

Currents and temperature were measured continuously above the continental shelf off Oregon during four periods lasting 25 days each. The data were obtained in July, September, and October of 1965 and in February 1966. Data are described using, where appropriate, elementary statistics, progressive vector diagrams, covariance functions, and power spectra.

In July and September the waters above the Oregon continental shelf were well stratified and shear existed between currents at 20 and 60m; this was true not only for the mean flow, but for low frequency and tidal currents. In February, when conditions were nearly isopycnal between 50 and 75m, currents at 50m were similar to currents at 75m for all frequencies studied.

Northerly currents were common and dominated September and

October flow. In July, flow at 10, 20 and 60m was usually to the south. Mean speeds varied from 13 cm sec^{-1} to 27 cm sec^{-1}. Flow was usually parallel to local topography.

Variations with a period of about one week dominated most low frequency (0 to 0.5 cpd) data. Low frequency variations of sea level and longshore velocity were in phase. A geostrophic current width of 75 km was obtained from the relationship between sea level and longshore velocity in July and September. For frequencies less than 0.2 cpd, sea level and longshore wind were in phase; an increase of one m sec^{-1} of southerly wind was associated with a one cm rise of sea level.

Spectra of sea level had bands of energy at one and two cpd. Current velocity spectra had, in addition to significant one and two cpd energy, a peak at the inertial frequency, 1.4 cpd. Inertial currents were associated with storm passage. Temperature spectra for July, September, and October lacked well defined peaks at one and 1.4 cpd and were dominated by energy at two cpd. The amplitude of the two cpd temperature oscillation required considerable baroclinic response.

High frequency (7-144 cpd) temperature spectra had significant peaks near two and four cph. Further, at a given depth, values of energy density were inversely proportional to the temperature gradient; this indicates that weak vertical stability enhanced high frequency oscillations.

Description of Measurements of Current Velocity and Temperature over the Oregon Continental Shelf, July 1965-February 1966

by

Curtis Allan Collins

A THESIS

submitted to

Oregon State University

in partial fulfillment of
the requirements for the
degree of

Doctor of Philosophy

June 1968

APPROVED:

Redacted for Privacy

Professor of Oceanography
in charge of major

Redacted for Privacy

Chairman of the Department of Oceanography

Redacted for Privacy

Dean of Graduate School

Date thesis is presented July 20, 1967

Typed by Gwendolyn Hansen for Curtis Allan Collins

ACKNOWLEDGEMENT

I would like to thank my major professor, Dr. June Pattullo, for her professional guidance and instruction, and especially for her humor.

I would like to acknowledge the assistance provided by Mr. Chris Mooers. Chris has made substantial contributions to this work.

This study has been part of a project and the help of many has been necessary. The National Science Foundation has provided financial support. The logistic support which made field operations feasible was provided by Chevron Research Company, Standard Oil Company of California, and Western Offshore Drilling and Exploration Company. The computer facilities of Western Data Processing Center were used extensively.

The encouragement and understanding of my wife, Judy, have been most necessary.

TABLE OF CONTENTS

LIST OF FIGURES

LIST OF TABLES

DESCRIPTION OF MEASUREMENTS OF CURRENT VELOCITY AND TEMPERATURE OVER THE OREGON CONTINENTAL SHELF, JULY 1965-FEBRUARY 1966

CHAPTER 1. INTRODUCTION

This is a descriptive study contributing to our understanding of the physical oceanography of the sea over the Oregon continental shelf.

The continental shelf and its overlying sea constitute a border between the continent and the ocean. The waters of the shelf must certainly be derived principally from the adjacent ocean, and on the shelf rivers add fresh water, sediment load, and man's wastes. The momentum of the ocean waters is transferred to the shelf where shallow water and variegated topography serve to rechannel flow and to dissipate energy. Above the continental shelf waters, winds are modified by adjacent land masses so that wind stress on the shelf sea may differ considerably from wind stress on the adjacent ocean. Tides are important on the continental shelf, often affecting water flow and water properties in complex ways. Understanding these processes and their interactions is not an easy task.

The complexity of shelf processes is somewhat offset by the availability of the shelf to man. Incentive is provided by the major fisheries and mineral deposits which are found on the shelf, as well as in recreational and military requirements. However, along the

Pacific coast the lack of good ports, fog and other bad weather, and low population density have discouraged use and study of the continental shelf and its sea.

The basis for this study are four 25-day time series of temperature and current velocity obtained in July, September, and October of 1965 and in February 1966. Time series of current velocity are described, in part by use of progressive vector diagrams. The data are split into three sets, each set pertaining to one frequency domain, by numerical filtering. The low frequency domain, from zero to one-half cycle per day (cpd), is described using autocovariance and cross-covariance functions; transfer functions are used to investigate relationships between variables. The intermediate frequency domain, from one-half to seven cycles per day, is described using power spectra, cross-spectra, and traditional harmonic analyses. In the high frequency domain, from seven to 144 cycles per day, only temperature variations are studied and power spectra are used.

CHAPTER 2. LITERATURE REVIEW

George Davidson was the first to describe ocean currents along the Pacific Coast. His work, which he did from 1865 to 1906, is summarized by Jones (1918):

> . . . Professor Davidson concluded that there existed, from 50 to 100 miles offshore, a southerly setting current of unknown width and velocity and that inside of this, following closely along the general trend of the coast was a northerly setting current which he named the 'Davidson Inshore Eddy Current.'
>
> . . . The data on which Professor Davidson's conclusions were based were necessarily meager. He had observed such northerly setting currents at various anchorages while engaged on survey work along the coast, and had also ascertained that logs of the redwood (which does not grow north of California) were frequently found on the shores of Washington, British Columbia, and even Alaska, the wood being well known to the natives of these regions.
>
> Professor Davidson was too good a scientist to attempt to promulgate a theory more definite than was justified by the available data and there is, so far as known, nothing to indicate that in naming this current he had in mind anything more than a general tendency to a current flowing in a northerly direction, which tendency might at any time disappear or be reversed by the prevailing weather conditions.

Jones concludes, from Davidson's work and further measurements of ships' drift, that ". . . in the summer months when the winds are northwesterly, the tendency of the current is toward a southerly set, and in the winter when the winds are southeasterly to southwesterly, the currents will in general be northerly."

The prevailing equatorward flow which dominates the surface waters off the west coast of the United States is termed the California Current. Measurements of ships' drift have indicated that the width of the California Current is about 300 miles and that its average speed is about 0.2 knots (USC&GS , 1951). Measurements of ships' drift have also indicated that the current extends from 50° N to 30° N although north of 45° N the set is usually northward from November through February (USC&GS, 1951). The depth of the California Current, inferred from the distribution of temperature and salinity, is less than 500m (Wooster and Reid, 1963). When compared with other surface currents of the world, the California Current may be characterized as broad, slow and shallow (Wooster and Reid, 1963).

Recent studies of Oregon State University have directly measured the current off this coast. Stevenson (1966) reported on current measurements made with parachute drogues 45 miles west of Newport, Oregon (44.7° N). Direction of flow was variable with speeds usually 5 to 10 cm sec^{-1}. The net drift was slow and to the south at all depths from the surface to 500m (Stevenson, 1967). Lee (1967) computed meridional geostrophic flow from 65 to 165 miles west of Newport using the well known dynamic (geostrophic) method. He found weak and irregular currents, generally 5 cm sec^{-1} or less, and an average close to zero. However his computations indicated a seasonal pattern: within 105 nautical miles of the coast, flow was

southward in summer, northward in winter; beyond 105 nautical miles, flow directions were reversed.

From September to April, a northerly flow may occur nearshore and is called the Davidson Current (as noted above). Schwarzlose (1964) has used drift bottles to infer that

> . . .the Davidson Current develops along the Washington and Oregon coasts in September, first close to shore and later widening. By October, it appears as far south as Point Conception. The countercurrent appears to be at least 50 miles wide and with speeds of at least 0.5 to 0.9 knots for distances of several hundred miles. . . .In the spring, the process is reversed. The countercurrent disappears in April off central California and in May off Oregon and Washington.

Similar results were obtained by Reid and Schwartzlose (1962) who measured the Davidson Current off central California with parachute drogues: in October northward flow was irregular but in January northward flow was well established. Burt and Wyatt (1964) interpret drift bottle returns from 165 miles west of Newport as evidence that the Davidson Current may extend offshore to this station; they also indicate that the Davidson Current may flow as far north as 50°N.

The cause of the Davidson Current is obscure. Although Munk (1950) attributed the current to the curl of the local wind stress, Reid and Schwartzlose (1962) have shown that off central California the Davidson Current begins before the winds shift from the northeast and remains after they shift back to the northeast. Data presented by Burt and Wyatt (1964) indicate that the Davidson Current off

Oregon was a direct result of local wind stress. Marmer (1926) found that the direction of nontidal flow at the Columbia River Light Vessel was well correlated with wind direction, i.e. northwesterly currents were associated with southerly winds and southwesterly currents with the northerly winds (the westerly component of current was due to river discharge). Sverdrup, Johnson, and Fleming (1942) suggested that the Davidson Current might be a surface manifestation of the subsurface California Countercurrent.

A subsurface countercurrent, the California Countercurrent has been observed off the California coast (Reid, 1962). It appears to extend northward along the Oregon coast as a tongue of warm salty water; this is shown by geopotential charts constructed by the Norpac Committee (ΔD400/1000) (1960) and Dodimead, et al. (ΔD200/1000 and ΔD500/1000) (1962), among others. Reid's measurements (1962) with drogues indicated that the countercurrent lay adjacent to the coast, extended seaward for 60 miles, and had a maximum velocity of 0.44 knots at its center. Direct current measurements reported by Stevenson (1966) did not reveal the presence of any strong permanent subsurface current off Oregon. The cause of this subsurface countercurrent is not understood (Reid, et al., 1958).

Concepts of a zonal flow pattern for the Oregon coast involve the phenomena of upwelling. Upwelling has been defined by Smith (1964):

> Upwelling. . .(is). . .an ascending motion of some minimum duration and extent by which water from subsurface layers is brought into the surface layer and is removed from the area of upwelling by horizontal flow.

Along the Oregon coast upwelling is the result of northerly winds which transport surface water offshore.

The zone between upwelled and non-upwelled water forms a surface front across which density, temperature, and salinity change abruptly (Collins, 1964). The circulation pattern associated with an equatorial front is illustrated in Figure 1; surface convergence, sinking within the front, and divergence at depth have been observed (Cromwell and Reid, 1956). Although the Oregon coastal front is less intense than equatorial fronts, the circulation pattern should be similar.

In many cases meridional gradients can be neglected when examining a time series of zonal hydrographic sections, such as Figure 2 or Figure 3. Then changes in area between isograms of conservative properties, such as temperature, salinity, specific volume, etc., can be interpreted as onshore or offshore flow. Smith, Pattullo, and Lane (1966) have deduced the zonal current pattern for an early stage of upwelling off the Oregon coast from changes of isograms of temperature and salinity (Figure 2). They found offshore flow at the surface and at 50 meters and onshore flow at 20 meters and 100 meters; the 20m onshore flow might not have occurred

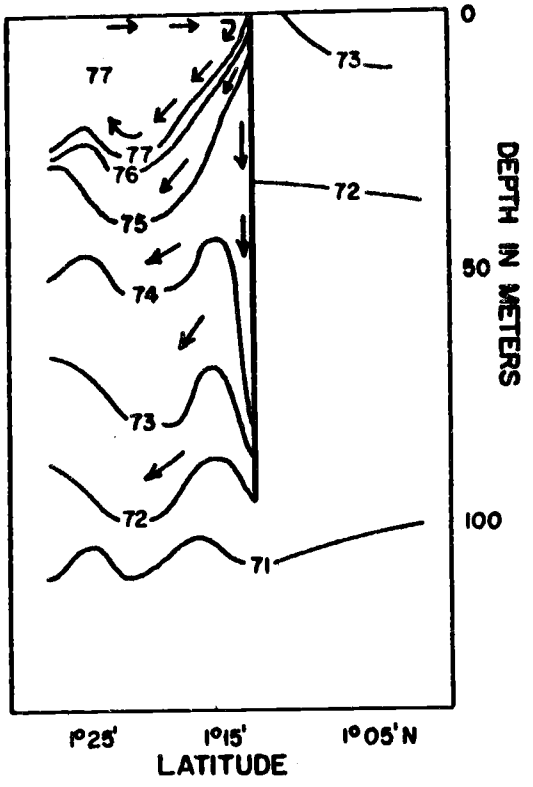

Figure 1. Vertical temperature distribution across an equatorial front at 120°11'W on October 27, 1952. Basic circulation is indicated by arrows. (from Cromwell and Reid, 1956)

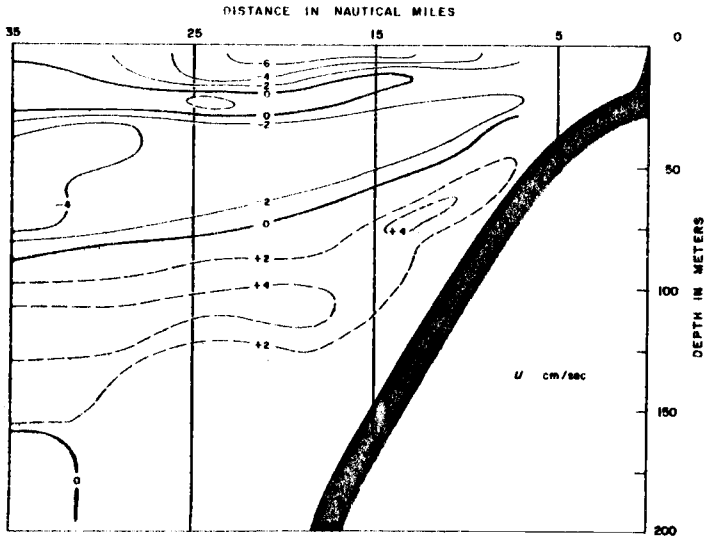

Figure 2. Mean onshore velocity for an early stage of upwelling along the Oregon Coast (from Smith, Pattullo, and Lane, 1966).

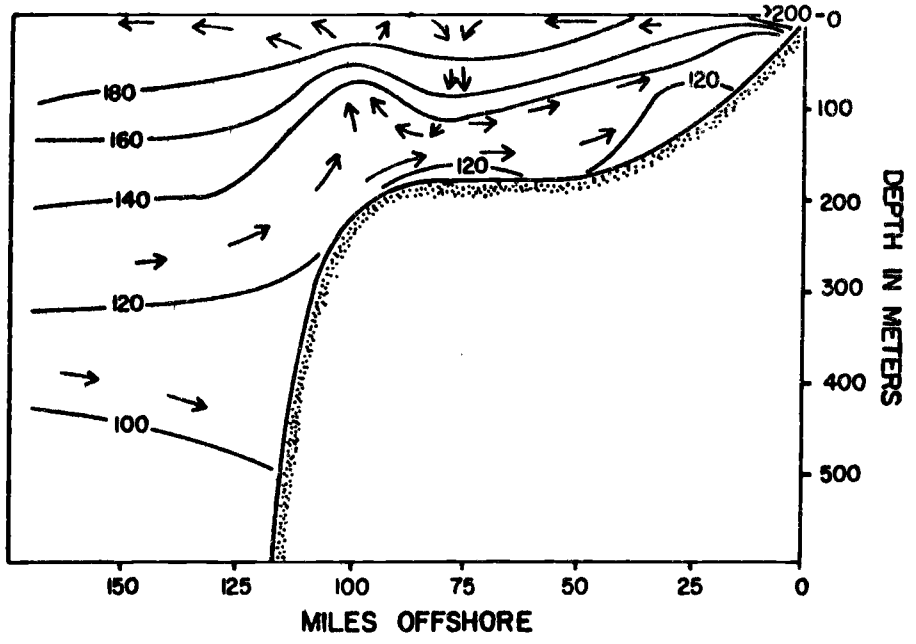

Figure 3. Upwelling in the Benguela Current. Vertical section normal to the coast in latitude 28°40'S showing isosteres and probable direction of water movement in the vertical plane (from Curie, 1953).

and may be an effect of mixing (Smith, Pattullo, and Lane, 1966).

Collins (1964) has computed zonal flow in surface and pycnocline layers off Newport due to displacements of sigma-t surfaces 25.5 and 26.0. He found offshore flow in the surface layer from May to mid-October, onshore flow from mid-October to January, and a period from February to April in which no significant onshore-offshore flow occurred. Flow within the pycnocline layer was usually in the same direction as that in the surface layer. Rates of flow were small, about one cm sec^{-1} (Collins, 1964).

The zonal circulation pattern deduced for an upwelling front in the Benguela Current is illustrated in Figure 3 (Curie, 1953). Note that Figure 3 extends offshore to a distance of 175 miles and that Figure 2 extends offshore only 35 miles. Curie (1953) noted a surface convergence with vertical circulation similar to an equatorial front at a distance of 75 miles from the coast; a region of surface divergence was observed further offshore. Near the coast, circulation was similar to that obtained by Smith, Pattullo, and Lane (1966).

Stevenson (1966) found that mean zonal transport 45 miles west of Newport reversed direction in the pycnocline (the pycnocline was between 100 and 200m). In the surface layer the transport was toward the east; below the pycnocline the transport was toward the west. Within the pycnocline there was little east-west transport. This indicates that a convergence zone existed within 45 miles of the

coast.

In coastal water, tidal currents may dominate. Marmer (1926) summarized surface current measurements made at the Columbia River light vessel during 1915-1920; tidal currents were found to be rotary, clockwise, semidiurnal, with a maximum velocity of $\frac{1}{4}$ knot and with little diurnal inequality. Barnes and Paquette (1954) have measured currents in deep water off the coasts of Oregon and Washington with parachute drogues and a GEK; inertial currents were observed to have an amplitude as great as 22.5 cm sec^{-1} and tidal currents (semidurnal) had an amplitude of between seven and eleven cm sec^{-1}. Stevenson (1966) observed both tidal and inertial currents in deep water off the Oregon coast; the former dominated his data and speeds were 5-12 cm sec^{-1}.

CHAPTER 3. HYDROGRAPHY

Introduction

Pattullo and Denner (1965) have summarized the hydrography of Oregon shelf waters:

> Temperature decreases rapidly with depth only in the upper layer; salinity increases rapidly with depth to about 150m. (Below 200m, all gradients are small. Temperatures decrease to 5 or 6C at 400m; salinity increases to 34.0 or 34.1 ‰). Lowest temperatures and highest salinities at 200m occur during summer. The annual ranges at this depth are approximately 2C and 0.2 ‰. Surface variations are much larger. During 1961 and 1962, temperatures 5 to 25 miles offshore ranged from 6 to 17C with a mode between 10 and 11C and a mean of 11.6C. Salinities varied from 18.0 to 33.5 ‰ with a mode between 32.5 and 33.0 but a mean of only 30.96 ‰.
>
> These cool, low salinity waters reflect both the water masses from which they are derived and local modifications by climatic processes and mixing. Oregon coastal waters are largely derived from Subarctic waters.

Local processes which modify the salinity appreciably are rainfall, runoff (mainly from the Columbia River), and upwelling (Pattullo and Denner, 1965).

Hydrographic Data

Density stratification varied from month to month. Representative data are illustrated in Figure 4. July profiles were averaged from 25 hourly profiles obtained with BT casts and Frautchy bottles

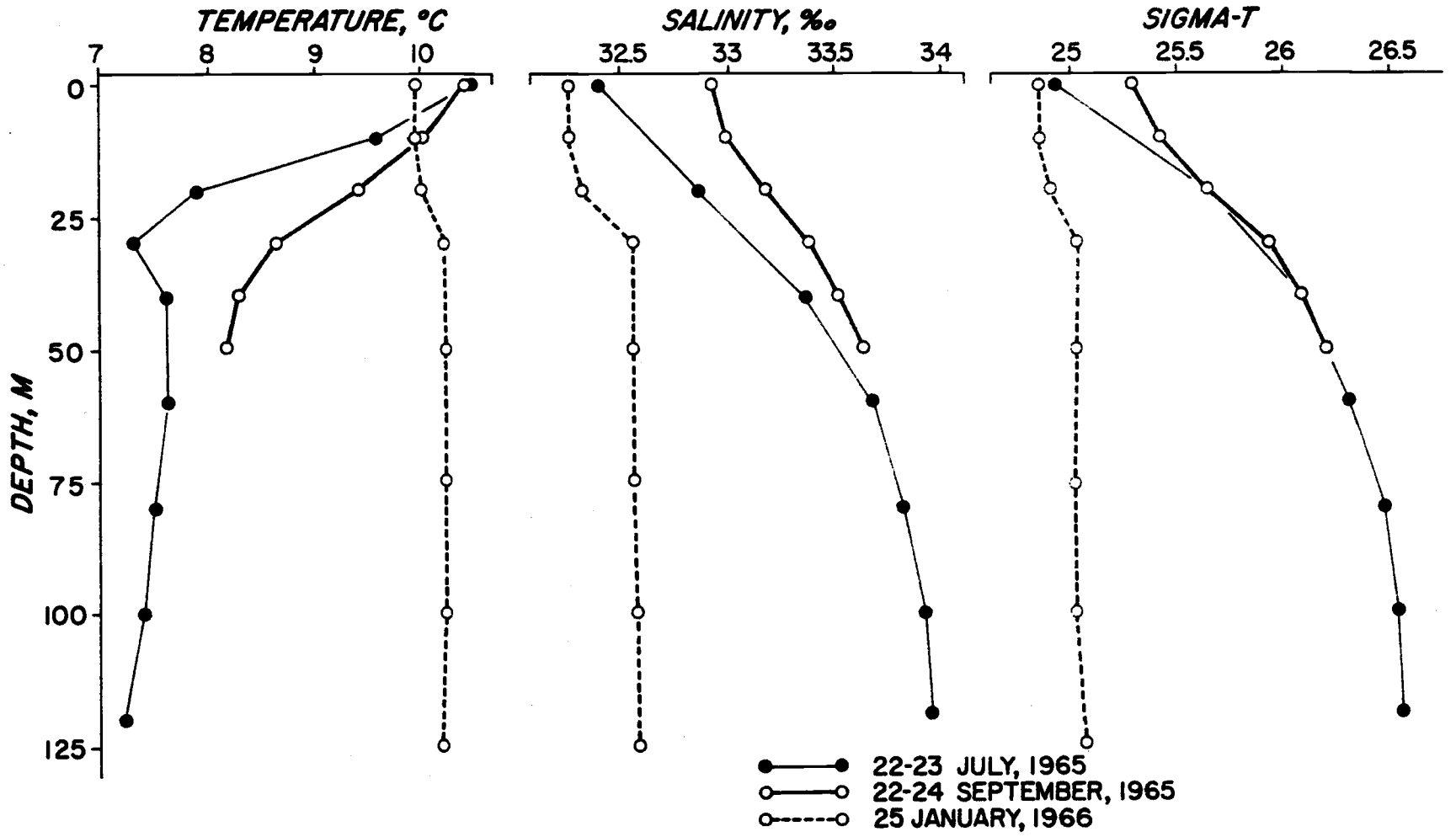

Figure 4. Temperature, salinity, and sigma-t versus depth.

$8\frac{1}{2}$ miles west-northwest of Depoe Bay, Oregon.[1] The seasonal thermocline was well developed and resulted in a decrease in temperature from 10.4C at the surface to 7.3C at 30m. A weak temperature inversion resulted in a temperature maximum of 7.6 or 7.7C between 40 and 60m. Below this depth the temperature decreased slowly to 7.4C. The maximum salinity gradient occurred between 20 and 40m (0.025 ‰ /m). The average surface salinity was 32.4‰; the salinity at 60m was 33.7‰; below 60m salinity increased slowly.

Although the pycnocline was strongest between the surface and 10m in July, it extended to a depth of 60 or 80m. The density increased from 24.8 sigma-t units at the surface to 26.3 sigma-t units at 60m (a gradient of 0.025 sigma-t units m^{-1}).

September profiles were constructed from 49 hourly profiles obtained from BT and in-situ salinometer casts on Stonewall Bank (See Footnote 1). Gradients of temperature, salinity, and density were less than in July. Water was warmer and saltier at each depth than in July. Water above 20m was denser than in July; water below 20m was more dense in July than in September. In September, maximum gradients occurred at depth: temperature decreased most rapidly from 20 to 30m (-0.078C m^{-1}); salinity (0.021 ‰ m^{-1}) and

---

[1] Exact positions are given in Table 2.

density (0.0286 sigma-t units m^{-1}) increased most rapidly from 20 to 30m.

February profiles were obtained from a hydrographic cast at a station 25 miles west of Newport. The water was nearly homogeneous between 30 and 125 m: 10.2C, 32.6‰, 25.0 sigma-t units. This water is fresher and warmer than water at these depths in July and September. However a temperature inversion was maintained at the surface by a freshening of surface water so that February surface temperatures were colder than in July or September.

Summary

Density stratification varied from month to month. The largest density gradient between 20 and 60m existed in July; this gradient was slightly less in September. In February conditions were isopycnal between these depths.

A temperature inversion was present at 40m in July. This will complicate the interpretation of the time series obtained in July at this depth.

CHAPTER 4. OBSERVATIONAL PROGRAM

A sensor array consisting of current meters and thermographs was moored off Depoe Bay in July 1965 and February 1966 and on Stonewall Bank in September and October 1965.

Instrumentation

Current Meters

Current velocity was measured by Braincon type 316 Histogram current meters (Braincon Corporation, 1965, and Sunblad, 1965). Performance characteristics for the current meter are given in Table 1. Current speed was sensed by a Savonius rotor; the output of the rotor is integrated over the recording period (9 or 19 minutes[2]) on photographic film as arc length. The Savonius rotor has two advantages as a speed sensor: (i) it is insensitive to small vertical motions (Gaul, 1963) and (ii) output is nearly a linear function of speed (Sexton, 1964). However a disadvantage is that response is omnidirectional and all horizontal motion contributes to speed.

Current direction is sensed by a vane which is about one meter square. During the recording period, direction is continuously

---

[2] The current meter takes an additional minute to reset itself.

Table 1. Performance specifications for the Braincon Type 316 Histogram Current Meter (Braincon Corporation, 1965)

Current Speed Sensor	
Speed Range	0.05 to 5 Knots
Calibration Threshold	0.05 Knots (Minimum)
Minimum Starting Velocity	0.01 Knots
Sensitivity	83 R. P. M. /Knot
Current Speed Output	
Sensitivity	78.85°/Knot
Accuracy	± 3% of Full Scale (5.0 Knots) When used with calibration curve and corrected for Tilt when required, including total error band
Current Direction Sensor	
Sensitivity	$\pm 5^{\circ}$ at 0.05 Knots
Current Direction Output	
Sensitivity	$\pm 0.5^{\circ}$
Accuracy	$\pm 1^{\circ}$ (± 0.3% Full Scale)
Instrument Tilt Sensor	
Tilt Range	0° to 40°
Instrument Tilt Output	
Sensitivity	$\pm 0.5^{\circ}$ Tilt, $\pm 0.5^{\circ}$ Tilt Direction
Accuracy	$\pm 1.0^{\circ}$ Tilt Angle, $\pm 1.0^{\circ}$ Tilt Direction
Timing Mechanism	
Accuracy	± 10 seconds/day, Rate adjusted

recorded on photographic film in a circular format.

The dimensions of the vane and the rotor are such that response is complete for currents with a period greater than 30 seconds (Sunblad, 1965). Hence, for a 19 minute recording period, the current meter determines (approximately) the mean speed and the most frequent direction of at least 38 velocity vectors. For the purposes of this study, this defines current velocity.

Note that this definition of current velocity (the mean speed and most frequent direction) could differ considerably from the vector average flow during the recording period, especially if direction varied a great deal. Since direction is recorded continuously, a range for current direction can be obtained for each recording period. If current direction is assumed to have a normal distribution during the recording period, then the range is about four standard deviations of direction (Sunblad, 1965). For 20m currents in July 1965, the mean value of the range of direction during the sampling period was 42^{o}. Hence the standard deviation of direction, during a sampling period, averaged 11^{o}. Similar values were obtained in other months and at other depths. Since direction had a low standard deviation during the recording period, it was acceptable to consider the output of the current meter as current velocity.

The current meter also measures and records instrument tilt.

Thermographs

Water temperature was measured by Braincon type 146 recording thermographs. These were fitted with -2C to +25C mercury-in-glass thermometers. In this instrument the thermometer is between a phosphorescent source and photographic film, so that temperature is recorded as a thick dark line where the mercury prevents film exposure. The film was advanced every five minutes. The thermograph achieves 95% of final value in ten minutes (Brainard, 1964). Thermometer readout accuracy is ± 0.1C (Brainard, 1964).

For any given thermometer, the lag coefficient, λ , is defined as the time required for a difference in temperature to be reduced to 1/e of its initial value (Middleton, 1942). For the Braincon thermograph, the lag coefficient is three minutes (Brainard, 1964). The frequency response of the thermograph, R(f), is given by

$$|R(f)| = (1+4\pi^2 f^2 \lambda^2)^{-\frac{1}{2}} \qquad (3\text{-}1)$$

$$\phi = \tan^{-1}(-2\pi f \lambda)$$

(Holloway, 1958). For a frequency of seven cycles per day,

$$|R(f)| = 1.0$$

$$\phi = 5.0^{\circ}$$

and it is possible to neglect the effect of the lag coefficient for frequencies less than seven cycles per day.

Instrument Array

A diagram illustrating the system used to moor these instruments is given in Figure 5. Details concerning the hardware are as follows:

Subsurface Floats - Two 42-gallon hot water tanks bridled by means of chain or flat bar cages; pressurized with 50 lbs of air. When submerged, the depth of the top of the subsurface float was 15 meters.

Diesel-Filled Floats - Five Geodyne #B-322 mooring floats filled with diesel oil and used to provide additional buoyancy at depth.

Main Anchor - A 55-gallon drum filled with scrap steel and concrete; total weight about 1350 lbs.

Ground Line - $\frac{1}{4}$-inch non-rotating galvanized performed wire rope; 400-700 meters of wire were laid between the main anchor and the secondary anchor. The secondary anchor was attached to the ground line with $\frac{1}{4}$-inch pendants and wire rope clips; the wire from the surface float to the main anchor was continuous.

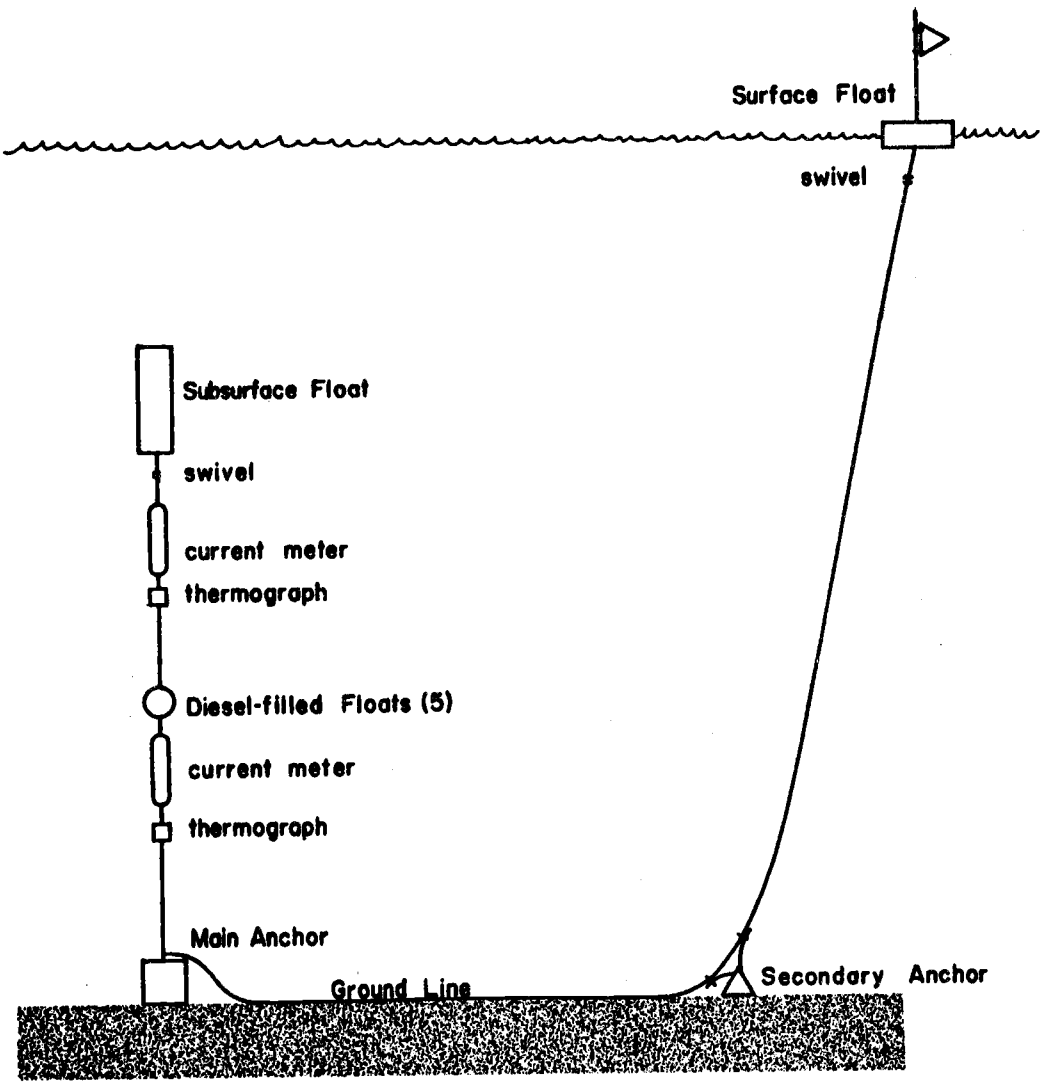

Figure 5. Diagram of the instrument array.

Secondary Anchor - Seven 35-lb shackles and one 25-lb Danforth anchor.

Surface Float - Five air-filled PVC floats (Geodyne #B-322).

The surface float was provided with a 2:1 scope.[3] Components of the instrument array were fastened together with 7/16-inch galvanized chain safety shackles and 3/16-inch 6 x 19 preformed stainless steel wire rope was used in the instrument array. Half-inch swivels were used below the subsurface float and the surface float.

Measurements

The sensor array was moored on the Oregon shelf on four occasions.

July

The mooring was set at 44°51.3'N, 124°15.3'W in 60 fathoms of water at 1700 PDT 11 July 1965 by the M/V Big Tide and retrieved by the M/V Big Tide at 0900 PDT 2 August 1965. Useful data were obtained from current meters at 20 and 60 meters and thermographs at 20 and 40 meters for the period 2140 PDT 12 July to 0840 PDT 2 August. Current observations were made every 20

---

[3] $\text{scope} = \frac{\text{length of wire between anchor and float}}{\text{depth of water}}$

minutes.

September

The R/V Yaquina set the mooring at 44°28.9'N, 124°26.7'W at 2100 PDT 28 August 1965 in 40 fathoms of water. Retrieval was accomplished by the Yaquina at 1515 PDT 24 September. Data were obtained for the interval 0010 29 August to 1205 PDT 23 September by current meters at 20 and 60 meters depth and by thermographs at depths of 20 and 40 meters. Current observations were made every 10 minutes.

October

The array was immediately remoored by the R/V Yaquina at the September position. Only the current meter at 20 meters and the thermograph at 20 meters operated, giving a data record which extended from 2010 PDT 24 September to 2005 PDT 19 October. The current meter cycled at 10 minute intervals and the thermograph cycled at 5 minute intervals.

February

The array was set by the R/V Yaquina at 44°51.2'N, 124°14.3' W in 60 meters of water at 1200 PST 24 January 1966. The Yaquina retrieved the array at 1245 19 February 1966. Current meters were

placed at depths of 25, 50, and 75 meters and thermographs at 25 and 50 meters. All instruments yielded data from 1210 PST 24 January to 1150 PST 19 February 1966 although the rotor on the 25m current meter jammed. The current meters recorded at 20 minute intervals.

In July, September, and October, the sensor array was moored within two miles of the oil drilling barge WODECO III. The drilling barge served as a navigational aid, a shield against offshore shipping, and also as a platform from which additional oceanographic observations were made. In July and September, meteorological, sea level, and ten meter current observations were made by Chevron Research Corporation at the WODECO III (Burke, 1966). Meteorological observations at the drilling platform Bluewater no. 2 were provided by Shell Oil Company during September, October, and February periods. Geographic coordinates for barge positions are given in Table 2.

Table 2. Drilling barge positions

Barge	Month	Position		Description
		Latitude, N	Longitude, W	
Wodeco III	June-July, 1965	44°-13'-29"	124°-16'-41"	off Depoe Bay
	September, 1965	44°-29'-47"	124°-28'-54"	on Stonewall Bank
Bluewater no. 2	August-Oct., 1965	44°-13'-16.4"	124°-28'-11.4"	on Heceta Bank
	February, 1966	46°-02'-50"	124°-29'-55"	near Tillamook Head

Data Processing

Processing of the data has been described by Collins, Creech, and Pattullo (1966). The process of obtaining useful numbers from analog records was arduous and time consuming. It was necessary to optically project the analog film record and measure the quantities recorded. These measurements, unprocessed data, were placed on punched cards and processed by computer. The result was referred to as "processed" data.

Processed data were plotted by computer; this was done at Western Data Processing Center with program BMDO5D. Computer plots were used to look for errors in the data. If an observation differed appreciably from those which immediately preceded and followed, it was checked by rereading the original film record.

No attempt was made to correct current meter records for mooring motions. Neither were current meter records compensated for the effect of surface swell.

Mooring Motion

The motion of an instrument array has been studied by Fofonoff (1965, 1966) and by Paquette and Hendersen (1965). Paquette and Hendersen (1965) studied a slack-line moor buoyed by a surface float; the vertical displacement of the surface float (caused by surface

waves) imparted considerable horizontal motion to instruments attached to the line, even at depth. A taut-line moor buoyed by a subsurface float overcomes much of this difficulty so we used a taut-line moor.

Fofonoff (1965) considers a taut-line moor. Neglecting inertia, and requiring horizontal drag force to be equal to horizontal restoring force at the surface float, he obtains

$$1/2\rho C_D A V^2 = F_B r L^{-1} \qquad (3\text{-}2)$$

where ρ is water density, C_D drag coefficient, A effective mooring cross section, V water speed, F_B float buoyancy, r horizontal displacement of the float, and L mooring length. Equation (3-2) can be written

$$r = KV^2 \qquad (3\text{-}3)$$

where

$$K = 1/2\rho C_D A L F_B^{-1}$$

The parameter K is a measure of the "softness" of a mooring. From Table 3, the instrument array used in this study had a K of 23 $sec^2 cm^{-1}$; Fofonoff (1965) states that deep water moorings with good performance characteristics have a K of 5 to 20 $sec^2 cm^{-1}$.

Table 3. Characteristics of the mooring

Components (with fittings)	Weight in air (lbs.)	Weight in water (lbs.)	Cross-sectional Area (A) (ft^2)	C_d
Subsurface Float 2	138	-219	6.5	1.2
Subsurface Float 3	162	-195	6.5	1.2
Current Meter	95	67	2.7	1.2
Thermograph	23	6	.6	1.2
Diesel Filled Float	96	-15	2.1	0.6
One Foot of Wire	.065	.053	.015	1.2

Since the current meter measures tilt, as well as speed, it is possible (with Fofonoff's assumptions) to obtain an "observed" K by regression (Equation 3-3). The "observed" value of K is 0.5 $sec^2 cm^{-1}$. Differences between observed and computed K are indicative of the degree to which Fofonoff's model approaches nature. It seems that the model is a useful approximation and that the array used in this study had good performance characteristics. Table 4 indicates that instrument tilt was minimized and supports the latter view.

For low or intermediate frequency rotary currents, the ratio of mooring speed r_ω to current speed V_0 is

$$\frac{r_\omega}{V_0} = \frac{2\pi [Kr_0]^{\frac{1}{2}}}{T}$$

where

T = rotation period of the current

r_0 = an initial displacement

for Fofonoff's model (Fofonoff, 1965). For a semidiurnal tidal current and an initial displacement of 875 cm,[4]

$$\frac{r_\omega}{V_0} = \frac{1}{60}$$

i.e. a 60 cm sec^{-1} rotary semidiurnal tidal current will be underestimated by 1 cm sec^{-1}. This effect is negligible.

Table 4. Instrument tilt

Month	Depth (m)	Mean (°)	Variance (°2)	Maximum (°)
July	20	0.3	1.0	5.0
	60	0.3	0.6	5.0
September	20	0.0	0.4	4.0
	60	0.0	0.2	7.0
October	20	0.3	1.0	6.0
February*	25	0.1	0.0	2.0
	50	0.3	0.5	4.0
	75	0.9	0.0	6.0

*Read by Braincon Corporation.

[4] 875 cm = sin 5° x 100m

Response to Swell

Extreme wave conditions occurred on 4 October when 18-24 foot, 10 sec waves were observed and on 5 February when 27 foot, 9 sec waves were observed. The former result in 56 cm sec^{-1}, 5 sec horizontal speed oscillations at 20m (using Airy wave theory); the latter result in 21 cm sec^{-1}, $4\frac{1}{2}$ sec horizontal speed oscillations at 50m. It is important to know how the current meter might respond to these motions.

The dimensions of the direction vane, lm by lm, preclude its participation in this motion. Variability of the direction vane and tilt indicator were normal during periods of heavy sea conditions.

Gaul, Snodgrass, and Cretzler (1963) summarize their attempts to determine the dynamical response of a Savonius rotor:

> The Savonius rotor is a highly inertial device. Response to acceleration can be several times faster than to deceleration (when the flow past the meter is stopped) and response factors are strongly dependent on the magnitude of speed changes.

However they note that "when the (true) speed varied almost sinusoidally with a period of roughly 4 seconds. . .the speed (indicated by the Savonius rotor) followed the mean trend but failed to indicate the variations."

Speed data have been examined thoroughly for swell effects. Since it is expected for current speed as well as wave height to

increase with wind speed, a current speed-wave height relationship is ambiguous. So a qualitative approach was used. Peak sea height occurred at the same time as maximum wind and each led the maximum of smoothed current speed[5] by 8-16 hours (Table 5). In the absence of wind, or with only light breezes, current speed seemed independent of swell height, but in this case the amplitude of the swell was seldom more than a meter. Hence, the effect of swell on the current meter did not seem to mask most variations in mean flow.

---

[5]Current speed was smoothed to remove tidal and inertial variations which would mask response to the slower buildup of swell (equation (5-1)).

Table 5. Response of the current meter to swell, September-October, 1965

Wind Maxima			Swell Maxima		20m Smoothed Current Maxima	
Date, time	speed mph	direction	Date, time	height ft	Date, time	speed $cm\ sec^{-1}$
8/29, 1800	30	355	8/29, 2300	11	8/30, 0000	20.1
9/16, 2130	30	335	9/16, 2200	9	9/18, 1200	7.7
9/23, 1200	30	020	9/23, 0800	12	9/25, 1200	10.4
10/2 , 1800	20	175	10/2 , 2100	8	none	---
10/4 , 1300	60	200	10/4 , 1300	21	10/5 , 0130	24.1
10/14, 0600	50	175	10/14, 0600	16	10/15, 1200	13.6

CHAPTER 5. ANALYSIS METHODS

Progressive Vector Diagrams

Current velocity time series are graphically presented as progressive vector diagrams. Progressive vector diagrams, or vector displacement diagrams, are constructed by plotting the locus of

$$\sum_{t=0}^{N} \vec{V}(t)\Delta t$$

It is convienent to think of a progressive vector diagram as a particle trajectory, but this can be misleading. A progressive vector diagram would coincide with a particle trajectory only in the special case where the field of motion is independent of position over the spatial scale of the vector diagram (Webster, 1964).

A vector average is defined

$$\overline{|\vec{V}|} = (\bar{u}^2 + \bar{v}^2)$$

$$\bar{\theta} = \arctan(\bar{u}/\bar{v})$$

This is the vector which connects the origin and the final position of a progressive vector diagram.

Filtering Scheme

Two smoothed time series, $\overset{\approx}{x}(t)$ and $\tilde{x}(t)$, were obtained from the original data, $x(t)$, using a numerical cosine filter as follows:

$$\overset{\approx}{x}(t) = \frac{1}{2m+1}\sum_{k=-m}^{m}[1+\cos\frac{2\pi(t-k)}{2m+1}]x(t-k),\ t = m, m+1, \ldots, N-m+1 \qquad (5\text{-}1)$$

$$\tilde{x}(t) = \frac{1}{2p+1}\sum_{k=-p}^{p}[1+\cos\frac{2\pi(t-k)}{2p+1}]x(t-k),\ t = p, p+1, \ldots, N-p+1$$

where

$$\frac{m}{\text{no. samples/hr.}} = 24 \text{ for } \overset{\approx}{x}$$

and

$$\frac{p}{\text{no. samples/hr.}} = 5/6 \text{ for } \tilde{x}.$$

Using $\overset{\approx}{x}(t)$, $\tilde{x}(t)$, and $x(t)$ three 'new' variables were defined:

$$\overset{\approx}{y}(t) = \overset{\approx}{x}(t)$$

$$\tilde{y}(t) = \tilde{x}(t) - \overset{\approx}{x}(t)$$

$$y(t) = x(t) - \tilde{x}(t).$$

Note that

$$\overset{\approx}{y}(t) + \tilde{y}(t) + y(t) = x(t)$$

The frequency response of the filter used to obtain $\overset{\approx}{x}(t)$ is defined

$$R_{\approx\atop x}(f) = \frac{1}{2m+1}\sum_{k=m}^{m}(1+\cos\frac{2\pi k}{2m+1})\cos 2\pi fk$$

where frequency, f, is cycles per data interval (Holloway, 1958). Similarily,

$$R_{\sim\atop x}(f) = \frac{1}{2p+1}\sum_{k=-p}^{p}(1+\cos\frac{2\pi k}{2p+1})\cos 2\pi fk\ .$$

Then

$$R_{\approx\atop y}(f) = R_{\approx\atop x}(f)$$

$$R_{\sim\atop y}(f) = R_{\sim\atop x}(f) - R_{\approx\atop x}(f)$$

$$R_{y}(f) = 1 - R_{\sim\atop x}(f)$$

$R^2_{\approx\atop y}$, $R^2_{\sim\atop y}$, and R^2_{y} are plotted in Figure 6. The frequency cutoff of a filter is defined as the frequency at which $R = e^{-1}$. $R^2 = e^{-2}$ is indicated in Figure 6.

This filtering technique effectively divides the variance into three frequency domains: (i) the low frequency domain from zero to one-half cycle per day $(\tilde{\tilde{y}}(t))$; (ii) the intermediate frequency domain from one-half to seven cycles per day $(\tilde{y}(t))$; (iii) the high frequency domain from seven to 144 cycles per day. This classification makes sense physically. The low frequency domain includes response to meteorological storms and long period shelf waves. The intermediate frequency domain contains tidal and inertial variations. The high frequency domain contains stability oscillations. Each domain is

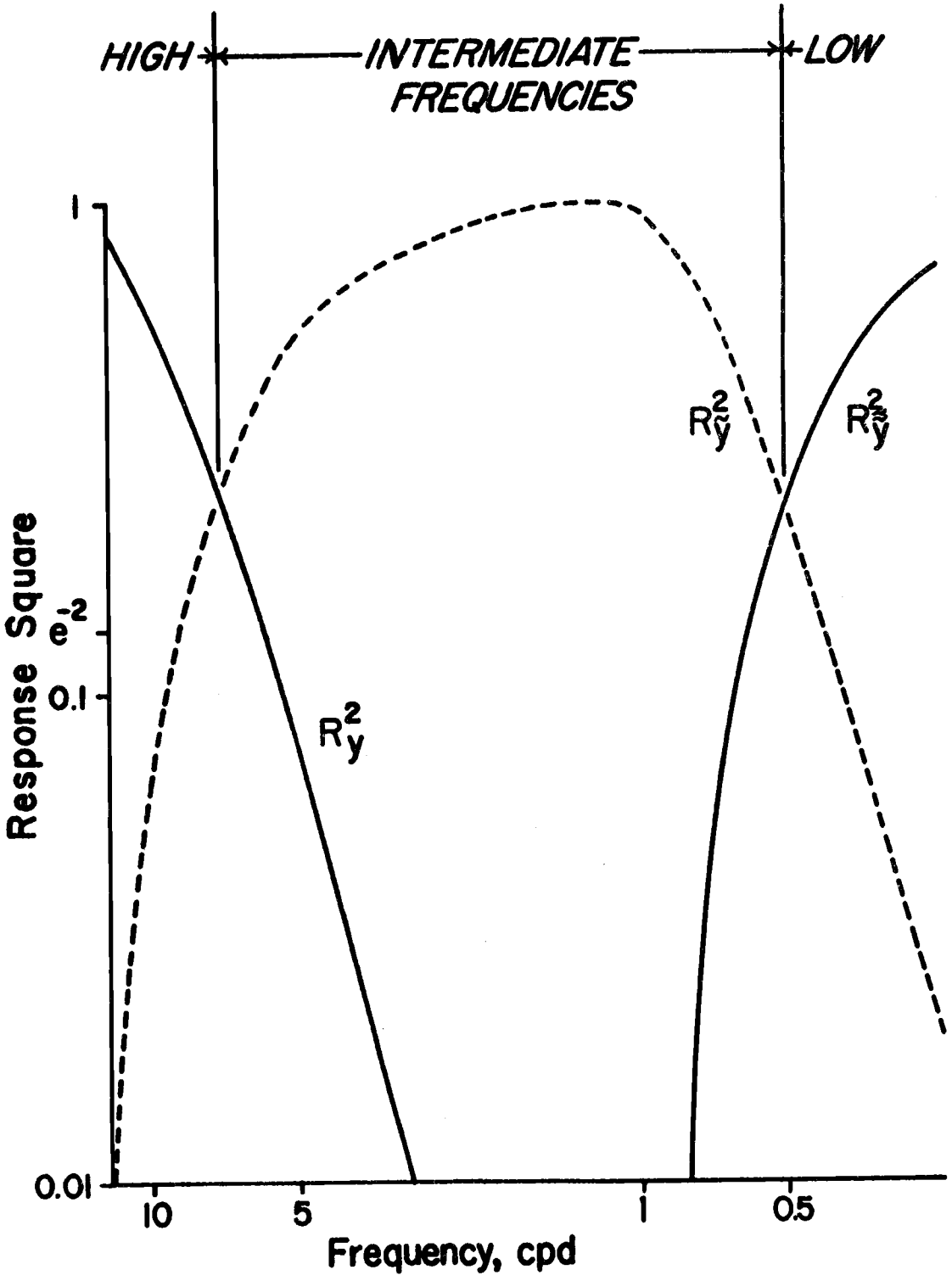

Figure 6. Frequency response of the numerical filters used in this study.

studied with different statistical techniques and from different viewpoints.

Spectral Analysis of Time Series

Introduction

Spectral analysis of time series is used to divide the variance of a time series or the covariance of two time series into discrete frequency bands. Oceanographers were introduced to spectral analysis of observations obtained at regular time intervals by Munk, Snodgrass, and Tucker (1959). Spectral methods have since been applied to many oceanographic studies including analysis of sea level oscillations, temperature oscillations, and current velocity oscillations. Spectral methods have been clearly reviewed by Yampol'skiy (1965) and are in such general use that they have been presented in a recent introductory oceanography text (Neumann and Pierson, 1965).

Computational Procedure

For observed time series $x(t)$, $y(t)$, ..., $t = 1, 2, \ldots, N$,

the mean was computed:

$$\bar{x} = N^{-1} \sum_{t=1}^{N} x(t) ,$$

then the autocovariance:

$$\hat{C}_{xx}(p) = \hat{C}_{xx}(p\Delta t) = \hat{C}_{xx}(\tau) = \frac{1}{N-p} \sum_{q=1}^{N=p} x(q)x(q+p), \; p = 0, 1, \ldots, m, \tag{5-2}$$

and the cross-covariance:

$$\hat{C}_{xy}(p) = \frac{1}{N-p} \sum_{q=1}^{N-p} x(q)y(q+p), \; p = 0, 1, \ldots, m \tag{5-3}$$

$$\hat{C}_{xy}(-p) = \frac{1}{N-p} \sum_{q=1}^{N-p} x(q+p)y(q), \; p = 0, 1, \ldots, m.$$

Note that the variance is estimated by

$$\hat{\sigma}_x^2 = \frac{N}{N-1} \hat{C}_{xx}(0) \sim \hat{C}_{xx}(0)$$

and that the correlation function is

$$\hat{\rho}_{xy}(\tau) = \hat{C}_{xy}(\tau) \left[\hat{C}_{xx}(0) \hat{C}_{yy}(0)\right]^{-1/2} \tag{5-4}$$

The correlation function satisfies the inequality

$$-1 < \rho_{xy}(\tau) < +1 \tag{5-5}$$

The beta coefficient is given by

$$\hat{\beta}_{xy}(\tau) = \hat{C}_{xy}(\tau) \cdot [\hat{C}_{xx}(0)]^{-1} \tag{5-6}$$

(the beta coefficient is the change of y which corresponds to a change of one unit of x).

From the autocovariance function and the cross-covariance function were estimated the power spectrum,

$$\tilde{G}_{xx}(h) = \tilde{G}_{xx}\left(\frac{h\pi}{m\Delta t}\right) = \tilde{G}_{xx}(f) = \frac{2\Delta t}{\pi} \sum_{p=0}^{m} \epsilon_p \hat{C}_{xx}(p) \cos\frac{hp\pi}{m} \quad ; \tag{5-7}$$

the cospectrum,

$$\tilde{X}_{xy}(h) = \frac{\Delta t}{\pi} \sum_{p=0}^{m} \epsilon_p (\hat{C}_{xy}(p) + \hat{C}_{xy}(-p)) \cos\frac{hp\pi}{m} \quad ; \tag{5-8}$$

and the quadrature spectrum,

$$\tilde{Q}_{xy}(h) = \frac{\Delta t}{\pi} \sum_{p=0}^{m} \epsilon_p (\hat{C}_{xy}(p) + \hat{C}_{xy}(-p)) \sin\frac{hp\pi}{m} \quad ; \tag{5-9}$$

where $h = 0, 1, 2, \ldots\ldots, m$ and

$$\epsilon_p = \begin{cases} 1/2, & p = 0, m \\ 1, & 0 < p < m \end{cases} \quad .$$

The cross-spectrum is defined as

$$\tilde{G}_{xy}(f) = \tilde{X}_{xy}(f) + i\tilde{Q}_{xy}(f) \quad . \tag{5-10}$$

Since the variability of estimates (5-7), (5-8), and (5-9) does not decrease with increased sample size for constant N/m, it is necessary to smooth these estimates by "Hamming":

$$\hat{G}_{xx}(0) = .54\tilde{G}_{xx}(0) + .46\tilde{G}_{xx}(1) \tag{5-11}$$

$$\hat{G}_{xx}(h) = .23\tilde{G}_{xx}(h-1) + .54\tilde{G}_{xx}(h) + .23\tilde{G}_{xx}(h+1), \quad 0 < h < m$$

$$\hat{G}_{xx}(m) = .54\tilde{G}_{xx}(m) + .46\tilde{G}_{xx}(m-1) \quad .$$

From these smoothed estimates were calculated the coherence square

$$\hat{\gamma}^2_{xy}(h) = (\hat{X}_{xy}(h)^2 + \hat{Q}_{xy}(h)^2) \cdot (\hat{G}_{xx}(h) \cdot \hat{G}_{yy}(h))^{-1} \tag{5-12}$$

(note that $0 < \gamma^2_{xy}(f) < 1$),

the phase

$$\hat{\phi}_{xy}(h) = \tan^{-1}(\hat{X}_{xy}(h)/\hat{Q}_{xy}(h)), \tag{5-13}$$

and the transfer function from $x(t)$ to $y(t)$

$$\hat{H}_{xy}(h) = |\hat{G}_{xy}(h)|/\hat{G}_{xx}(h). \tag{5-14}$$

These quantities were computed with a "canned" program, BMD02T, at Western Data Processing Center (Dixon, 1962).

Discussion

The power spectrum measures the density of variance as a function of frequency. (It is usual to refer to the density of variance as "energy" density.) Specifically, Equation (5-7) estimates the proportion of total variance of $x(t)$ due to frequencies in a band, centered around $h/2m$ oscillations per time interval, of roughly $1.3/m$ units of frequency in width (Hamon and Hannan, 1963). The estimate of the power spectrum has a chi-square distribution with ν degrees of freedom, where

$$\nu = \frac{2N}{m} \tag{5-15}$$

(Blackman and Tukey, 1958). Hence the interval

$$\left(\frac{\hat{G}_{xx}(f)}{\chi^2_\nu(0.95)}, \frac{\hat{G}_{xx}(f)}{\chi^2_\nu(0.05)} \right) \tag{5-16}$$

is a 90% confidence interval for $\hat{G}_{xx}(f)$ (Borgman, 1967). A peak in a power spectrum is significant at the 90% level if the background spectrum (noise level) does not lie within the 90% confidence interval. The noise level is estimated from values of energy density on either side of the spectral peak.

The cross-spectrum is best interpreted by coherence square and phase. Coherence square measures the strength of association between two series at a given frequency in the same way as correlation

describes the strength of association between two random variables (Hamon and Hannan, 1963). The phase describes the phase lead or lag of $y(t)$ relative to $x(t)$ at a given frequency (Hamon and Hannan, 1963).

Coherence square (and the association between $x(t)$ and $y(t)$) is significant at the 90% level if

$$\hat{\gamma}^2_{xy} > \frac{4}{\nu} \tag{5-17}$$

(Roden, 1965). Further evidence that the relationship between $x(t)$ and $y(t)$ is significant is provided by phase estimates. When phase estimates are steady, or change slowly, from one frequency band to the next, one has greater confidence in estimates of coherence square and in estimates of the amplitude of the cross-spectrum. Unfortunately, there is no quanitative test which uses this information.

For the system

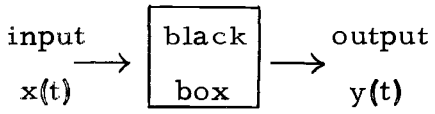

the transfer function provides an estimate of the output $y(t)$ by a linear operation on the input $x(t)$. The transfer function is impedance-like and has an amplitude and a phase. For values of coherence square greater than 0.35, the 90% confidence interval for the transfer function is a circle of radius r centered at $\hat{H}_{xy}(f)$.

$$r^2(f) = \frac{2}{\nu-2}\left(F_{2,\nu-2,0.10}\right)\left[1-\hat{\gamma}^2_{xy}(f)\right]\frac{\hat{G}_{yy}(f)}{\hat{G}_{xx}(f)} \qquad (5\text{-}18)$$

where

$F_{2,\nu-2,0.10}$ = 10% point of an F-distribution with 2 and $\nu-2$ degrees of freedom

(Bendat and Piersol, 1966).

The choice of m, the maximum number of lags, is a compromise between resolution (high m and small bandwidth) and reliability (small m and a large ν). Although in engineering it is usual to maintain between 30 and 100 degrees of freedom (Bendat and Piersol, 1966), in oceanography the use of eight or ten degrees of freedom is not unusual (Sabinin and Schulepov, 1965). In this study ten degrees of freedom were maintained in the low and intermediate frequency domain. Twenty degrees of freedom were used in the high frequency domain.

Misleading results in spectral analysis result from the lack of stationarity of the original time series, quantization of the original signal, aliasing, and limitation due to finite record length. A comment by Borgman (1967) is pertinent:

> .....In view of the many approximations and deviations involved in most time series analysis (e.g. covariance-stationarity, constant mean, instrument accuracy and calibration, and data processing numerical approximations), one should not attempt to be needlessly precise at this point. A tolerant attitude is more in keeping with the realities of the analysis. If the variability of the estimate is extremely important, it would be better to study

> it by repeating the experiment a number of times or by replication of data recording systems at different locations....

A 90% confidence limit was used as a significance test with low frequency and intermediate frequency analysis. A 99% confidence limit was used with high frequency temperature studies.

Amplitude Estimation

If a time series $x(t)$ contains a sinusoidal constituent with a period $2m/h$ time intervals, then the amplitude of this constituent, A, may be estimated from the power spectrum as follows:

$$\hat{A} = \left\{\frac{2\pi}{m\Delta t}\left[\hat{G}_{xx}^{(h-1)} + \hat{G}_{xx}^{(h)} + \hat{G}_{xx}^{(h+1)}\right]\right\}^{1/2} \qquad (5\text{-}19)$$

This estimate of A agrees reasonably well with estimates of A obtained from Fourier and least square analysis (Table 23).

Estimation of Regression Coefficients

The transfer function is difficult to interpret and often a relationship of the form

$$y = \beta x + \alpha$$

is desired. β should contain as much of the information of the transfer function as possible. It may not be possible to obtain a suitable β if the transfer function is strongly frequency dependent.

Consider the special case where the phase between input and output is either zero of 180^{o} for all frequencies.

Then

$$b_{xy}(f) = \hat{X}_{xy}(f) \cdot [\hat{G}_{xx}(f)]^{-1} = \hat{H}_{xy}(f) \qquad (5\text{-}20)$$

Hamon and Hannan (1963) have described how the $b_{xy}(f)$ can be used to estimate β:

> .....Each of the quantities $b_{xy}(f)$ provides an estimate of β and (substantially) this estimate uses the information from the frequency band in an optimal fashion. However each $b_{xy}(f)$ is not equally useful as an estimate of β, and indeed it will be obvious that those $b_{xy}(f)$ from bands where the signal to noise ratio...is high will be the most useful. An estimate of this signal-to-noise ratio is
>
> $$\hat{N}(f) = \hat{G}_{xx}(f) \cdot \left\{\hat{G}_{yy}(f) \cdot [1-\hat{\gamma}^{2}_{xy}(f)]\right\}^{-1}$$
>
> This suggests the formation of a weighted average of the $b_{xy}(f)$,
>
> $$b_{xy} = \frac{\sum_{f} \epsilon(f)\hat{N}(f)b_{xy}(f)}{\sum_{f} \epsilon(f)\hat{N}(f)} \qquad (5\text{-}21)$$
>
> This is the proposed estimator of β. Its variance may be estimated as... (m/N) times the reciprocal of the denominator of b_{xy}... The statistic b_{xy} will be nearly normal when N is large.

Estimation of the Dominant Long Period Constituent

Sinusoidal variations were evident in all low frequency filtered time series and a quanitative estimate of the period and amplitude of these oscillations was desired. Time series were usually not sufficiently long for the power spectrum to be of use, so the autocovariance function, $C_{xx}(\tau)$, was used.

The autocovariance function of the onshore component of current velocity at 20m in July is illustrated in Figure 7. The dominant period, T_d, can be estimated by (i) the first lag at which $C_{xx}(\tau)$ is zero, here $T_d = 4\tau$, (ii) the lag at which $C_{xx}(\tau)$ is a minimum, here $T_d = 2\tau$, and (iii) the lag at which $C_{xx}(\tau)$ is a maximum, here $T_d = \tau$. When possible, the third criteria was used.

The standard deviation, $C_{xx}(0)^{1/2}$, provides a rough estimate of the rms amplitude of the constituent with period T_d. The correlation function at lag τ has been defined (Equation 5-4). For $T_d/4 < \tau < 5T_d/4$, minimum and maximum values of the correlation function correspond to (ii) and (iii). The value of the correlation function corresponding to (i) is zero.

It should be noted that this estimation of the dominant long period constituent is, in fact, a description of the autocorrelation function. To interpret the autocorrelation function in this manner is not entirely correct and results may be misleading. It would be more

accurate to regard the standard deviation as the rms amplitude of the original signal and the correlation at lag T_d a measure of its dispersion or damping. However, amplitudes and periods obtained seemed to adequately describe low frequency data in most cases.

Notation

$\vec{V}_z = u_z i + v_z j$ Current at depth z. Current direction is the direction toward which the current is flowing.

T_z Temperature at depth z.

ζ Sea Level. Measured at the Marine Science Center in Newport with the tide gauge described by Swanson (1965). "0" corresponds to 2.60m on the tide staff, or 1.13m above mean lower low water (USC&GS 1929 datum).

$\vec{W} = x_1 i + x_2 j$ Wind. Wind direction is the direction from which the wind is blowing. For southerly winds, x_2 is positive; for westerly winds, x_1 is positive.

x, y, z Coordinate system. x is positive eastward, y positive northward, and z positive downwards. z is measured in meters.

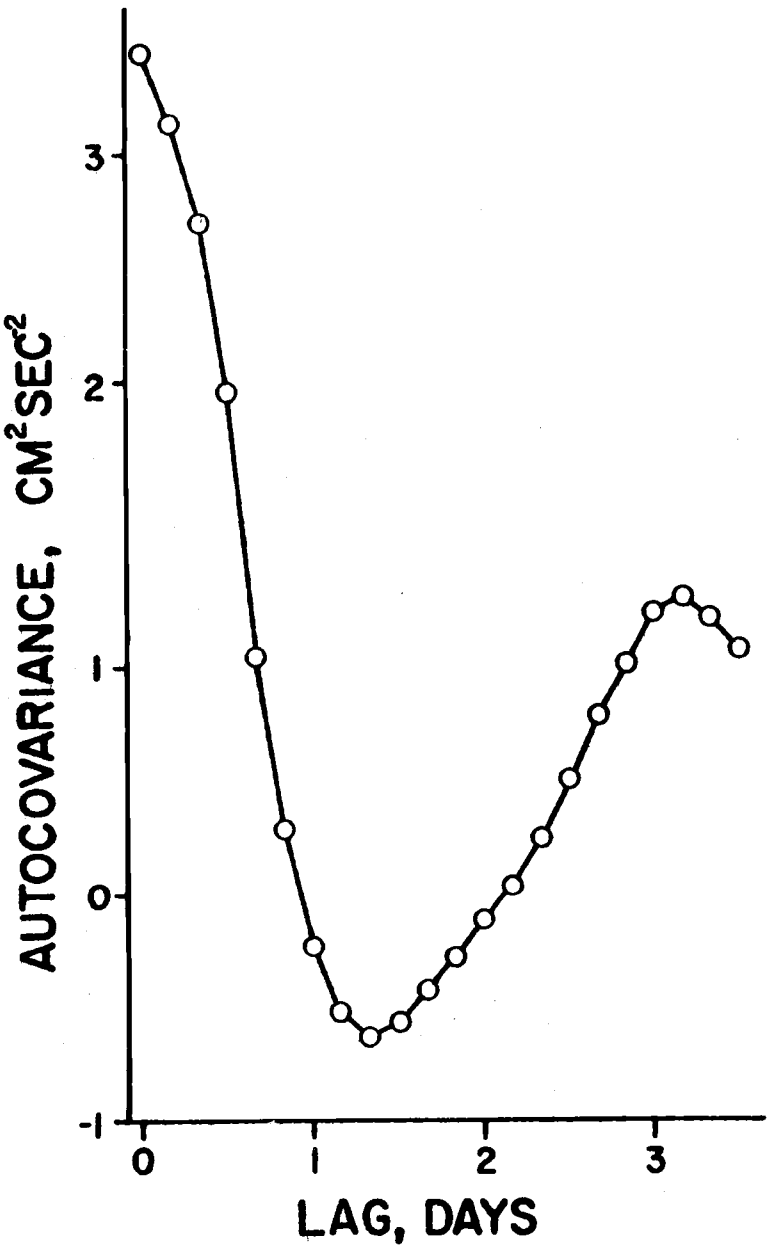

Figure 7. Autocovariance of the onshore component of current velocity at 20m in July 1965.

CHAPTER 6. ELEMENTARY ANALYSIS OF CURRENT VELOCITY

The current velocity observations are summarized using progressive vector diagrams and elementary statistics.

Current Velocities

Velocity statistics are presented in Table 6. Modes were taken from histograms presented by Collins, Creech and Pattullo (1966). In constructing these histograms an interval of 2^{o} was used for speed histograms, an interval of 5 cm sec^{-1} for u and v histograms, and an interval of 10^{o} for direction histograms. It should be noted that means and principal modes seldom coincided and that all but one direction histogram was bimodal. For direction, u and v this is indicative of the fact that flow was usually longshore, either to the north or south. Speed did not have a normal distribution.

Progressive vector diagrams are presented in Figures 8-11.

July

July current flow at 20 meters was southerly and nearly parallel to local bottom topography. The average vector had a direction of 197^{o}. The vector average speed was 16.5 cm sec^{-1} at 20 meters and the mean speed was 21 cm sec^{-1}. The direction histogram for 20m had a single mode at 215^{o} which had a relative

Table 6. Current velocity statistics

Date	Depth (m)	Number of observations	Variable	Mean	Standard Deviation	Maximum	Minimum	Principal Mode	r.f.(%)	Secondary Mode	r.f.(%)
July	20	1472	Speed, cm/sec	21.0	7.5	49.8	5.7	15.7	4.9	17.7	4.2
			u, cm/sec	- 4.7	10.3	26.2	-30.1	-12.5	19.9		
			v, cm/sec	-15.6	11.0	21.4	-49.7	-17.5	20.4		
			Direction, °True					215.	11.4		
	60	1472	Speed, cm/sec	13.3	3.5	29.5	5.7	12.2	13.6		
			u, cm/sec	1.4	6.8	17.7	-18.8	+2.5	27.5		
			v, cm/sec	- 4.1	11.2	22.2	-29.5	-12.5	30.5	7.5	14.9
			Direction, °True					195.	9.3	25.	4.8
September	20	3672	Speed, cm/sec	13.8	4.8	43.8	5.2	9.8	18.4		
			u, cm/sec	0.0	9.1	31.0	-31.5	- 7.5	21.6	7.5	19.3
			v, cm/sec	0.8	11.4	28.2	-33.6	+ 7.5	21.0	-7.5	14.7
			Direction, °True					25.	5.7	225.	4.5
	60	3672	Speed, cm/sec	15.4	5.2	42.9	5.2	12.8	14.5		
			u, cm/sec	- 0.7	8.5	20.5	-31.4	+ 2.5	20.4	- 7.5	17.6
			v, cm/sec	6.1	12.3	35.8	-41.5	+12.5	25.9	-12.5	7.7
			Direction, °True					005.	8.0	175.	2.5
October	20	3600	Speed, cm/sec	19.3	7.4	50.5	5.2	17.1	12.2		
			u, cm/sec	1.2	13.5	49.0	-40.1	+ 7.5	14.9		
			v, cm/sec	3.9	15.0	44.1	-49.0	+12.5	18.5	-12.5	9.6
			Direction, °True					25.	6.5	205.	2.9
February	50	1559	Speed, cm/sec	26.3	14.3	73.1	7.9	12.2	5.0	40.3	1.9
			u, cm/sec	- 3.4	9.3	28.7	-21.7	-12.5	24.1		
			v, cm/sec	- 5.6	27.7	72.6	-55.9	-12.5	13.6	12.5	7.1
			Direction, °True					195.	26.0	15.	9.1
	75	1872	Speed, cm/sec	27.0	13.2	61.1	7.2	13.6	4.6	38.4	2.3
			u, cm/sec	- 4.6	9.8	24.4	-28.1	-12.5	20.2	7.5	12.1
			v, cm/sec	- 9.8	26.3	61.1	-53.2	-37.5	10.5	-12.5	10.2
			Direction, °True					195.	18.3	15.	7.5

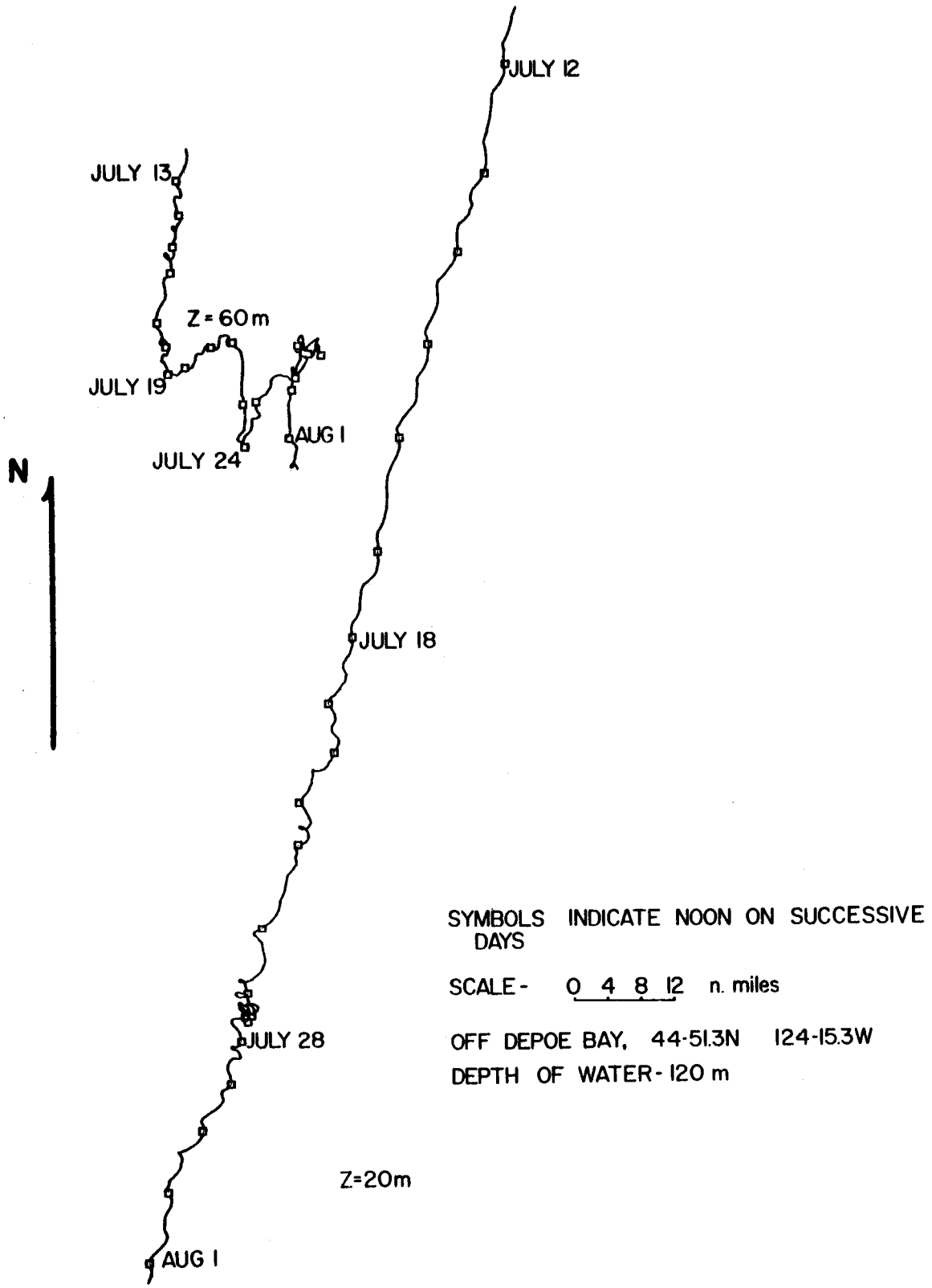

Figure 8. Progressive vector diagrams for currents in July 1965.

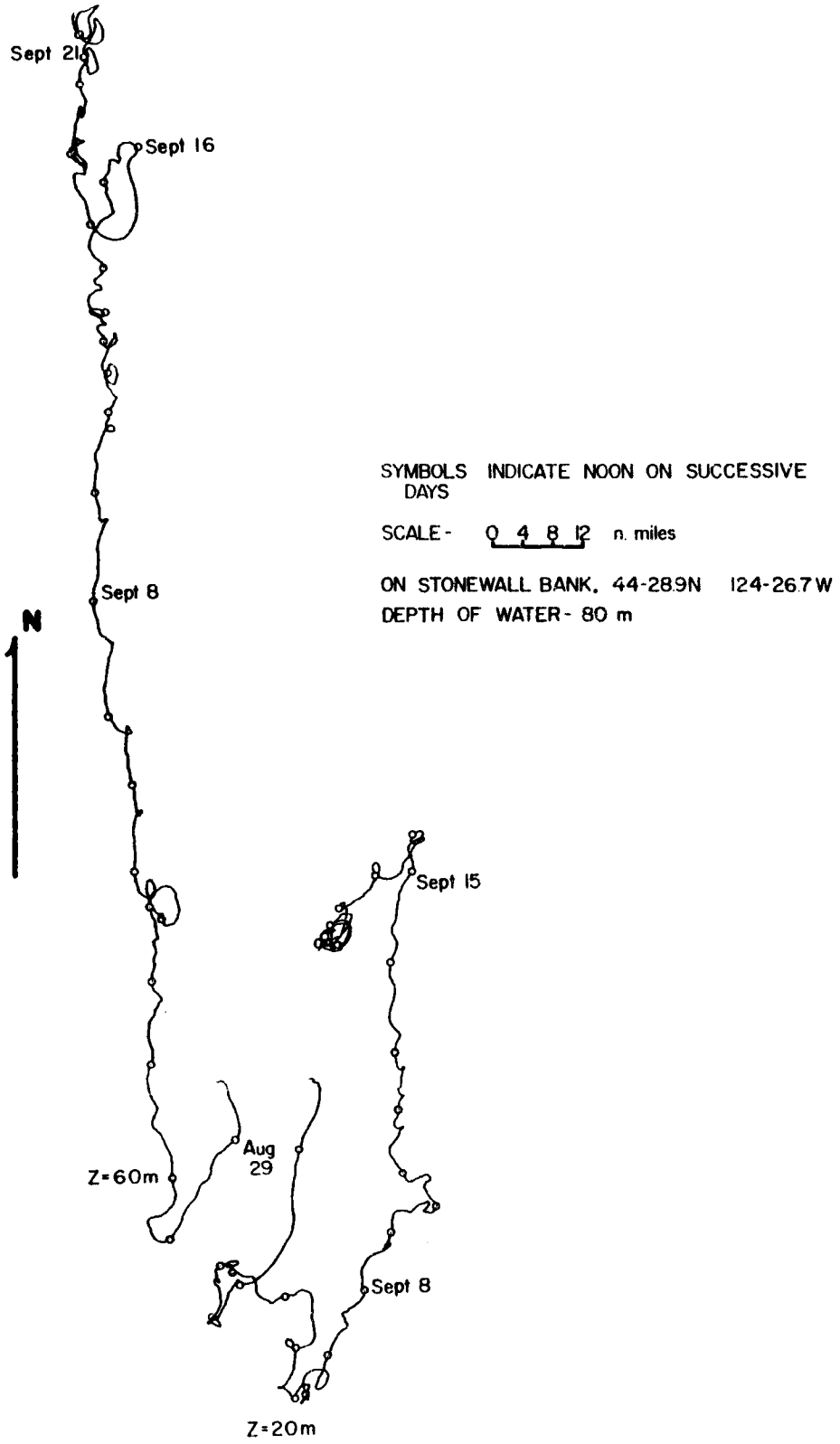

Figure 9. Progressive vector diagrams for currents in September 1965.

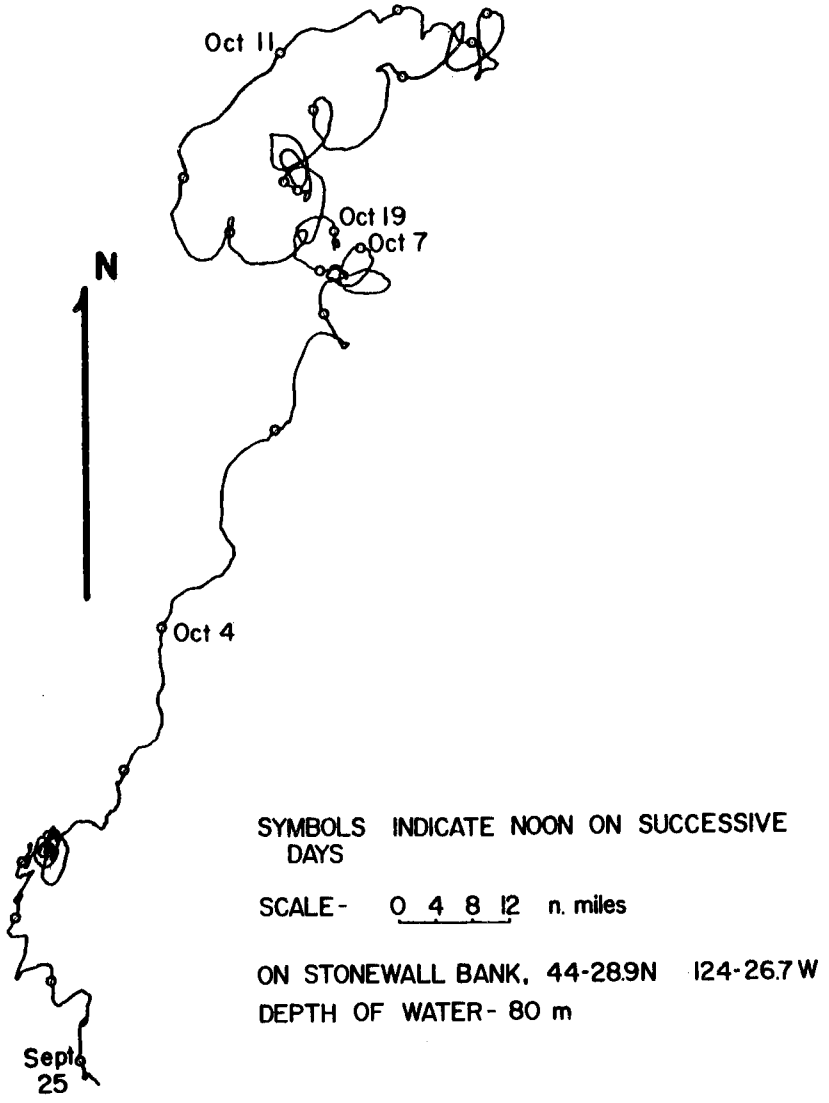

Figure 10. Progressive vector diagram for currents at 20m in October 1965.

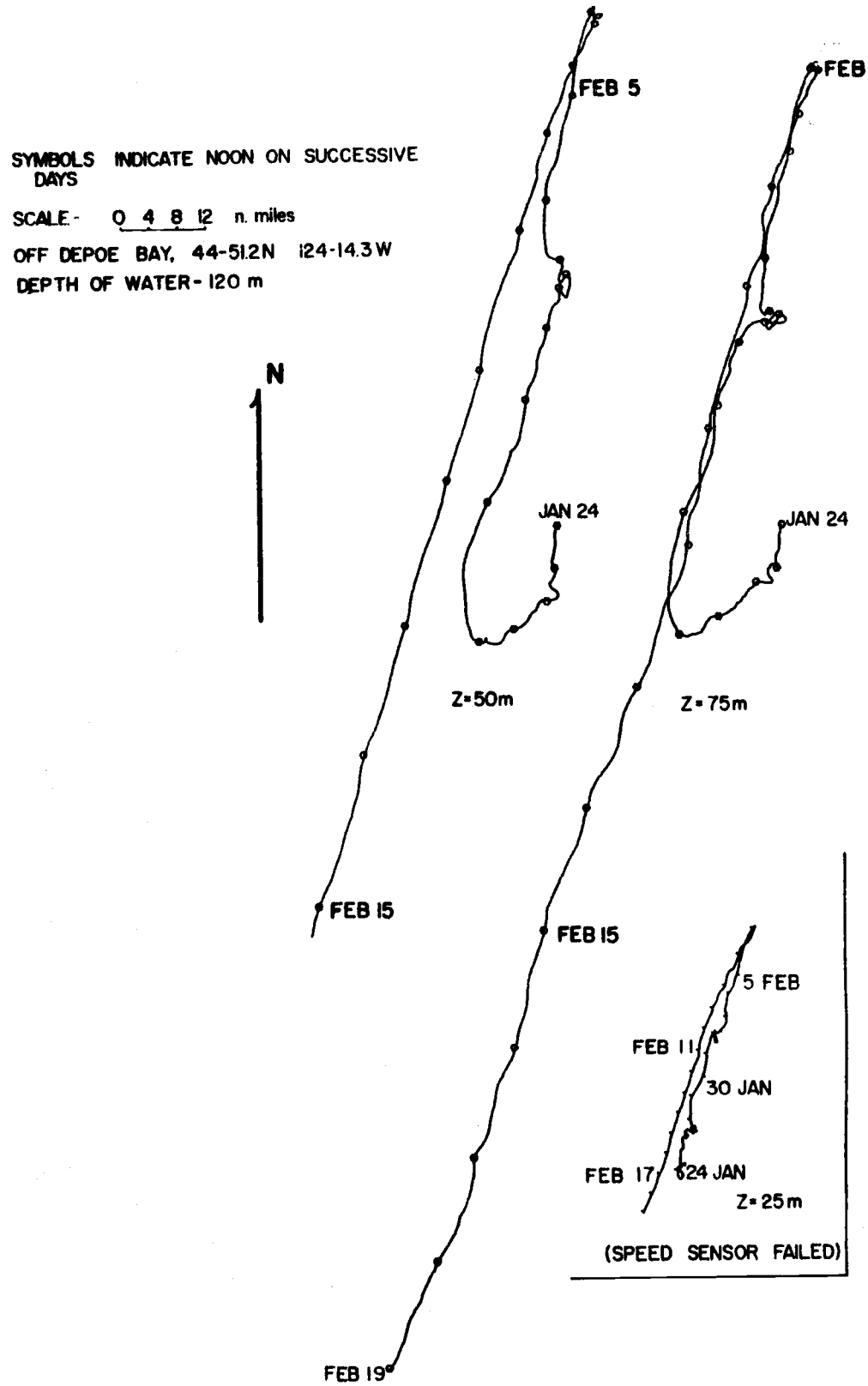

Figure 11. Progressive vector diagrams for currents in February 1966.

frequency of 11.4%.

On July 14 and 15 currents at 40m were observed. The mean current vector had an average direction of 209° and a magnitude of 16.0 cm sec^{-1}. The mean speed was 17.6 cm sec^{-1}.

Current velocity at 60 meters was variable during July. From July 13 to July 19, July 22 to July 24, and July 29 to August 1, flow was southerly with a direction of about 184° and an average vector speed of 2.3 cm sec^{-1}. From 19 July to 22 July and 24 July to 27 July flow was northeasterly (042°) with a vector average speed of 1.9 cm sec^{-1}. Periods of northward flow at 60m corresponded to periods during which the velocity at 20 meters was reduced in magnitude. The direction histogram for 60m was bimodal with a principal mode at 195° (9.3%) and a secondary mode at 025° (4.8%). Flow at 60m was offshore during only one period, 29-30 July. The vector difference between the average flow at 20 meters and the average flow at 60 meters was 13.0 cm sec^{-1}, 202°.

September

Flow was northerly at 20 and 40 meters in September. The vector average flow at 20 meters was 0.8 cm sec^{-1}, 000°, and at 60 meters was 6.1 cm sec^{-1}, 353°. The difference of these vectors, vector average shear, was 5.3 cm sec^{-1}, 352°. The mean speed at 60 meters, 15.4 cm sec^{-1}, was greater than that at 20 meters,

13.8 cm sec^{-1}. The histograms of direction were bimodal.

When the array was installed on 28 August flow was southerly at 20 and 60m with a pattern very similar to July flow. Currents at 60m then rotated to the west (offshore) and became northerly (as did currents at 20m). Again on 16 September southerly flow occurred at 20 and 60m and again 60m current turned to the west and became northerly. This contrasts with the behavior of July 60m currents which always rotated to the east (onshore) to become northerly.

October

Currents were measured at 20m in October. Among the data collected, October data exhibited the largest variance of the u component, 182 $cm^2 sec^{-2}$ (compared to a minimum of 46 $cm^2 sec^{-2}$ for July 60m flow). Vector average flow for October was 4.0 cm sec^{-1}, 018^o, and the mean speed was 19.3 cm sec^{-1}. The principal mode of the direction histogram was 025^o (6.5%).

February

Progressive vector diagrams of February data (Figure 11) are notable for their geometrical similarity (despite failure of the speed sensor at 25 meters), the degree to which flow paralleled bottom contours, and the very large variance of the north-south component of velocity. It is evident that there was little shear

between current meters and that even minor variations in flow, such as the change from 1 February to 2 February, were consistent from depth to depth.

Northerly flow, from 29 January to 31 January and 4 February to 6 February, had a vector average of 8.0 cm sec^{-1}, 013^{o} at 50m and 7.7 cm sec^{-1}, 014^{o} at 75 meters. Southerly flow, from 7 February to 15 February had a vector mean of 8.8 cm sec^{-1}, 197^{o}, at 50 meters and 8.6 cm sec^{-1}, 197^{o} at 75 meters. Hence, vector averages for periods of northerly flow were nearly equal to those for southerly flow.

Direction histograms for February are bimodal. The large values of relative frequency for each mode indicate that onshore or offshore flow does not occur often. In February the mean speeds and the maximum speeds were the largest encountered at depth in our observations.

Considerable offshore flow occurred at 50 and 75m from 25 to 28 January and during this time flow at 25m was northerly with an onshore component. Onshore flow must have occurred in the water column and this suggests that flow was onshore above 25 meters.

Currents at Ten Meters[6]

Additional data on currents at a depth of ten meters were obtained from a current meter suspended from the drilling barge WODECO III. This current meter was operated by Chevron Research Corporation as part of a program to determine drillship motion (Burke, 1966). The meter was sampled randomly in June and July 1965 and somewhat more regularly in September 1965. Current roses are presented for these observations in Figure 12, statistics are given in Table 7, and Figure 13 is a progressive vector diagram which was constructed from 156 September observations.

July

The vector average current had a direction of 157° and a magnitude of 32.9 cm sec^{-1}. Fifty-one percent of the observations indicated southerly flow and no currents with northerly components were observed. The mean speed was 38 cm sec^{-1}.

September

The average current vector had a direction of 225° and a magnitude of 3.0 cm sec^{-1}. Current speeds were weaker than those

---

[6] These data were furnished by Mr. Ben Burke of Chevron Research Corporation.

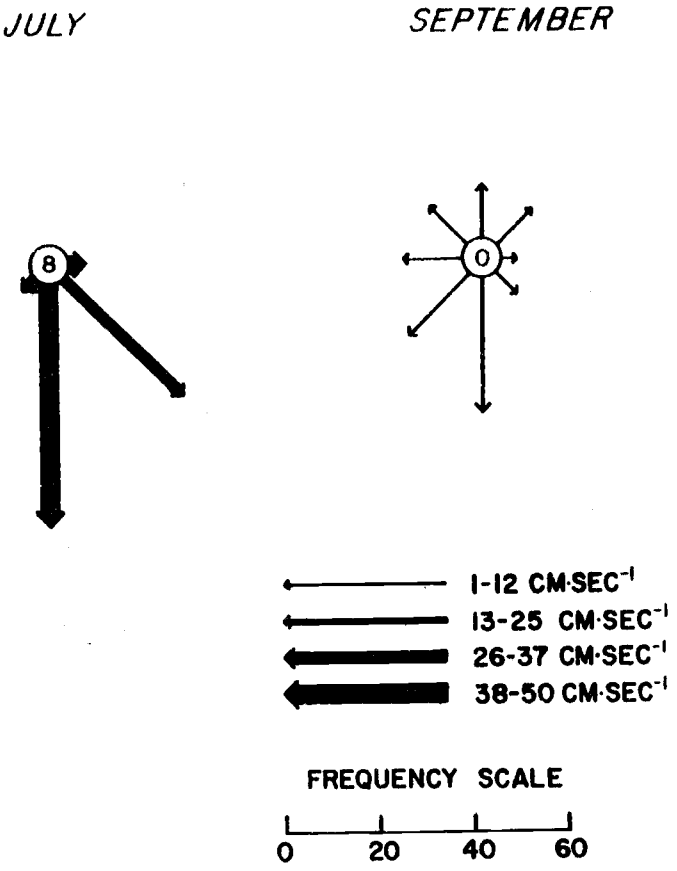

Figure 12. Current roses for the 10m currents in July and September 1965 (data furnished by Chevron Research Corporation).

Table 7. Statistics for 10m currents (data furnished by Chevron Research Corporation)

Month	Variable	Mean $cm\ sec^{-1}$	Variance $cm^2\ sec^{-2}$	No. of Observations
July	speed	37.7	244.	143
	u	7.5	301.	143
	v	-32.0	288.	143
September	speed	8.9	11.	185
	u	-2.0	29.	185
	v	-2.1	53.	185

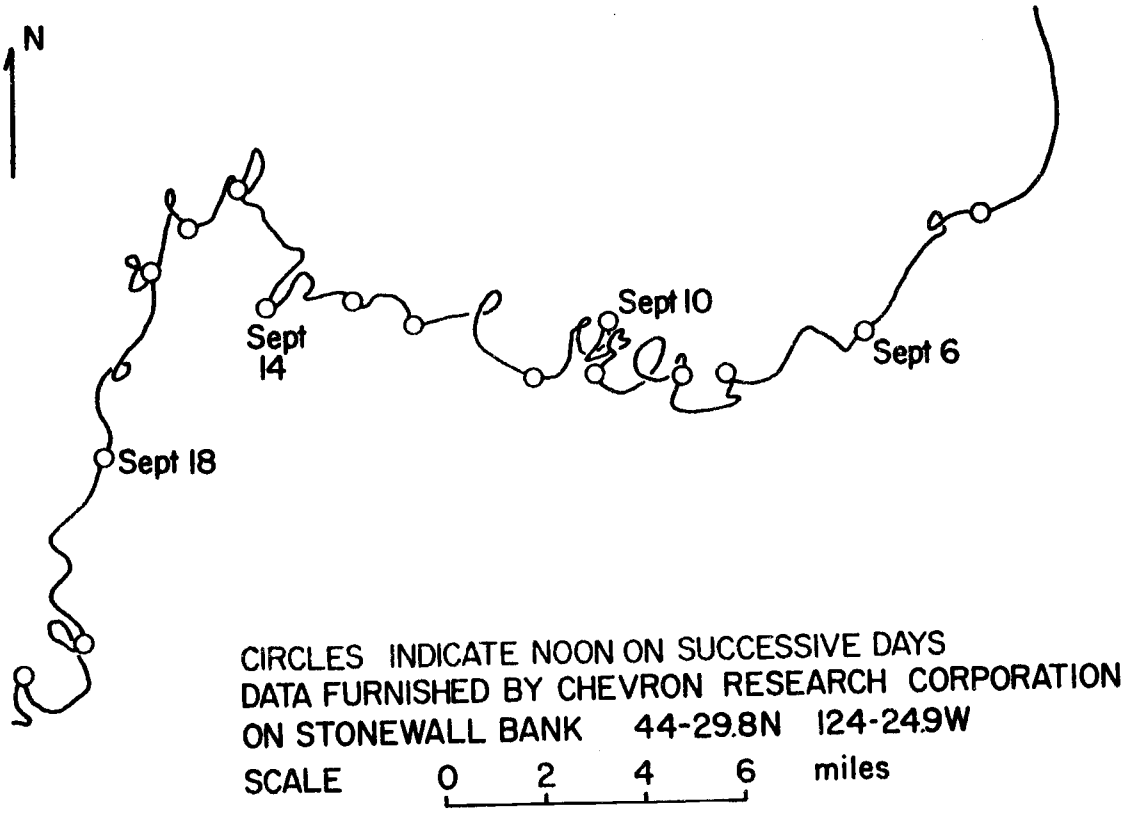

Figure 13. Progressive vector diagram for current velocity at 10m from September 5, 1965, to September 20, 1965.

at 20m and 40m and averaged 8.9 cm sec^{-1}. Southerly currents were observed most frequently (30%) (Figure 12).

Flow at 10m was southerly on 4 September (as it was at 20 and 60m) and then became westerly. From 5 - 15 September, vector mean flow at 10m was 274^{o}, 3.0 cm sec^{-1}, vector mean flow at 20m was 014^{o}, 3.9 cm sec^{-1}, and vector mean flow at 60m was 359^{o}, 5.1 cm sec^{-1}. From 15-20 September, currents were southerly at 10m.

Summary

In July, mean speed decreased with depth. In September mean speed increased with depth.

Strong southerly flow existed at 10, 20 and 40 meters in July. Flow at 60m in July was usually southerly but became northerly on occasion. In September, flow at 60m was to the north; northerly flow at 20m was much weaker than that at 60m and flow at 10m was southerly more often than it was northerly. Flow was onshore at 10 and 60m and offshore at 40m in July; July 20m flow exhibited no on-shore-offshore component. In September flow was offshore at 10m, onshore at 20m, and offshore at 60m. Shear was greater in July than in September, as was the density gradient.

February currents exhibited little shear and flowed both to the

north and the south.

Flow was usually parallel to local topography.

CHAPTER 7. LOW FREQUENCY VARIATIONS

Current velocity, temperature, wind velocity, barometric pressure and sea level time series were numerically filtered to remove inertial and tidal variations. Smoothed (low frequency)[7] sea level observations were adjusted for effects of smoothed barometric pressure using a 1:1 in phase barometric response factor.[8] These time series are illustrated in Figure 14. Several time series were sufficiently long that power spectra with suitable low frequency resolution could be estimated. These spectra are illustrated in Figure 15 (spectra have been compensated for the effect of the numerical filter).

Current Velocity

Smoothed velocity data were resolved into longshore and onshore components. Bathymetry off Depoe Bay is such that bottom

---

[7] Throughout the remainder of the thesis, "smoothed" and "low frequency" will be used interchangeably, i.e. smoothed time series are those which have been generated with equation (5-1).

[8] A mean barometric pressure of 1014 mb was used. Then one cm was subtracted from sea level for each millibar of pressure less than 1014 mb or one cm was added to sea level for each millibar of pressure greater than 1014 mb. This was done so that the effects of barometric pressure would not need to be considered in a later chapter.

Figure 14. Smoothed time series. For velocity time series, the closed dot represents the onshore component and the open dot represents the longshore component.

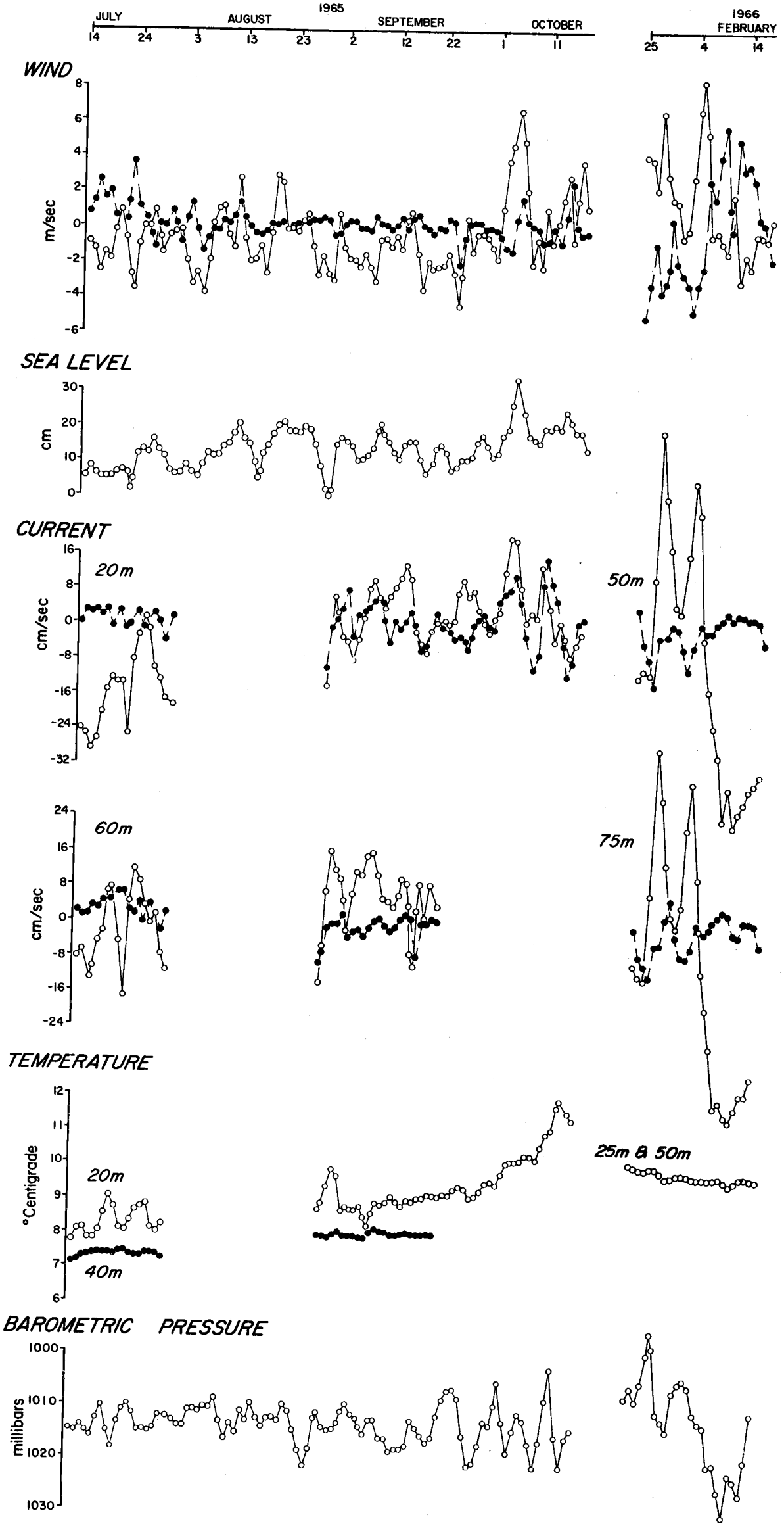
1965
JULY
AUGUST
SEPTEMBER
OCTOBER
1966
FEBRUARY
14 24 3 13 23 2 12 22 1 11 25 4 14
WIND
m/sec
8 6 4 2 0 -2 -4 -6
SEA LEVEL
cm
30 20 10 0
CURRENT
cm/sec
20m
16 8 0 -8 -16 -24 -32
50m
75m
60m
24 16 8 0 -8 -16 -24
TEMPERATURE
°Centigrade
12 11 10 9 8 7 6
20m
40m
25m & 50m
BAROMETRIC PRESSURE
millibars
1000 1010 1020 1030

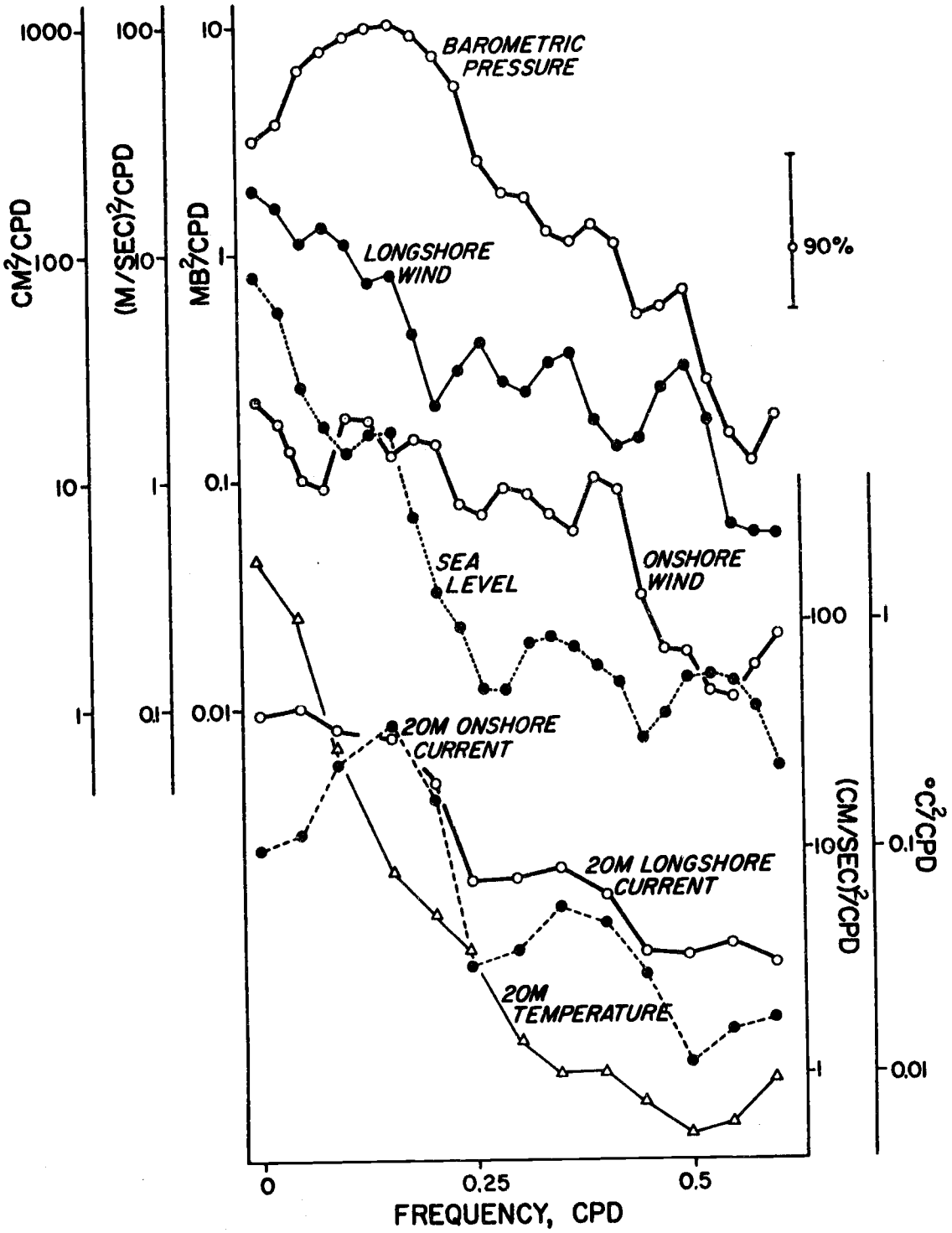

Figure 15. Low frequency power spectra Wind, sea level and barometric pressure were observed from July-October 1965; 20m currents and temperature were observed from September-October 1965.

contours are parallel to 020-200°; bottom contours near the current meter installation site on Stonewall Bank run north-south.

Table 8 gives the variance of low frequency velocities as a percentage of the variance of the unfiltered time series. More than 90% of the variance of longshore current for July 20m and February 50m and 75m was in the low frequency domain.

At 20m the longshore currents had a dominant constituent of 8.0 days in July, 5.5 days in September and 8.3 days in October. Values of the correlation function (Equation 5-4) for these long period constituents were, respectively, -0.09, 0.07, and -0.21; amplitudes were 11.7, 9.7, and 10.0 cm sec^{-1}. The spectrum for September-October 20m longshore flow had no significant peaks, but peaks occurred at 0.05 cpd (20 days), 0.35 cpd (2.9 days) and 0.55 cpd (1.8 days). The amplitudes of these peaks were, respectively, 8.4 cm sec^{-1}, 3.7 cm sec^{-1}, and 1.4 cm sec^{-1}.

20m onshore flow had a dominant constituent of 3.2 days in July, 6.2 days in September, and 7.6 days in October. Values of the correlation function for these long period constituents were, respectively, 0.38, 0.32, and -0.70; amplitudes were 2.6, 5.3 and 9.6 cm sec^{-1}. The spectrum for September-October 20m onshore flow had significant peaks at 0.15 cpd (6.7 days), 0.35 cpd (2.9 days) and 0.60 cpd (1.7 days); the amplitudes of these peaks were, respectively, 6.7, 2.9, and 1.6 cm sec^{-1}.

Table 8. Statistics for smoothed current velocity

Depth m	Month	Low Frequency Variance $cm^2 sec^{-2}$	Percentage of Total Variance %	Dominant Period days	Correlation at Lag T_d -
onshore currents					
20	July	3	5	3.2	0.38
	September	14	17	6.2	0.32
	October	46	25	7.6	-0.70
50	February	17	31	6.3	0.33
60	July	5	6	2.8	0.37
	September	5	8	5.5	-0.35
75	February	18	28	7.2	-0.26
longshore currents					
20	July	68	91	8.0	-0.09
	September	47	36	5.5	0.07
	October	50	22	8.3	-0.21
50	February	735	96	30.0	-
60	July	60	46	5.6	-0.37
	September	39	26	5.1	0.26
75	February	698	96	30.0	-

Longshore flow at 60m had a dominant constituent of 5.6 days in July and 5.1 days in September. The value of the correlation function for these constituents was -0.27 in July and 0.26 in September; amplitudes were 11.0 cm sec^{-1} in July and 8.8 cm sec^{-1} in September. Onshore flow at 60m had a dominant period of 2.8 days in July and 5.5 days in September; associated values of the correlation function were 0.37 and -0.35. Amplitudes were 3.3 cm sec^{-1} in July and September.

February onshore currents had a period of 6.3 days at 50m and 7.2 days at 75m. The values of the correlation function for these constituents were, respectively, 0.33 and -0.26; amplitudes were 5.8 cm sec^{-1} and 6.1 cm sec^{-1}. Longshore currents had a period of 30 days at 50 and 75m; amplitudes were, respectively, 38.3 cm sec^{-1} and 37.3 cm sec^{-1}.

Summary

Longshore velocities had larger values of energy density than onshore currents at most low frequencies. Longshore velocities had dominant periods ranging from 5 days in September to 30 days in February but values of the correlation function were low, usually less than 0.25. Periods near 7 days and near 2.8 days dominated onshore flow; values of the correlation function were usually between 0.2 and 0.4 and amplitudes ranged from 2.6 to 9.6 cm sec^{-1}.

During a single month, periods for 20m flow were longer than those for 60m flow; values of the correlation function were larger at 60m.

Temperature

Statistics for observed temperature are given in Table 9. Column four indicates the percentage of total variance of temperature in the low frequency domain; all of February variance and 76% of October variance were included in the low frequency domain.

Temperature at 20m

Temperatures at 20m were coolest in July; both the average, 8.2C, and the minimum, 7.0C, were the lowest observed. The presence of a temperature inversion in July resulted in the minimum temperature at 20m equalling the minimum temperature at 40m; often temperatures at 40m were warmer than those at 20m. Temperatures were slightly warmer in September and had an average of 8.9C. Although a temperature inversion was not usually present in September, one did develop from 28-29 August and from 5-10 September and during this time it was not unusual for temperatures at 40m to be warmer than those at 20m. This resulted in a cooler minimum temperature at 20m, 7.6C, than at 40m, 7.7C. The temperature increased rapidly in October and a maximum temperature of 12.7C was observed on 15 October.

Table 9. Statistics for temperature data

Month	Mean °C	Standard Deviation °C	Percentage of Variance in the Low Freq. Domain %	Max. °C	Min. °C	Dominant Period days	Correlation at Lag T_d -
at 20m/25m							
July	8.23	0.73	24	10.5	7.0	6.0	-0.37
September	8.94	0.63	28	11.4	7.6	7.3	-0.16
October	10.23	0.98	76	12.7	8.3	-	-
February	9.80	0.14	100	10.4	9.4	-	-
at 40m/50m							
July	7.33	0.16	28	8.5	7.0	9.0	-0.06
September	8.00	0.13	24	9.5	7.7	6.6	0.40
February	9.80	0.16	100	10.3	9.4	-	-

During February the ocean was nearly isothermal between 25 and 50m; in Figure 14 the size of a single point was sufficient to represent the temperatures at both depths. The mean temperature at 25m and 50m was 9.8C; this was cooler than the October mean (10.2C) but greater than either the September mean or the July mean.

October temperatures had the largest variance and February temperatures had the least variance.

Temperatures at 20m had a long period constituent of 6.0 days in July and 7.3 days in September. Values of the correlation function for these long period constituents were, respectively, -0.37 and -0.16; amplitudes were 0.47C and 0.5C. Due to the rapid increase of temperature in October, the spectrum for September-October 20m temperature decreased rapidly from 0 to 0.5 cpd. A peak (which was not significant) occurred at 0.40 cpd; its amplitude was 0.2C.

Temperature at 40m

Temperatures at 40m were coolest in July, 7.3C, slightly warmer in September 8.0C, and much warmer in February, 9.8C. The variances of these time series were nearly the same, about $0.02C^2$. Maximum temperatures at 40m occurred at about the same time as minimum temperatures at 20m.

40m temperatures had a dominant constituent of 9.0 days in July and 6.6 days in September. Values of the correlation function

for these long period constituents were, respectively, -0.06 and 0.40; amplitudes were 0.12C and 0.08C.

Wind

Jones (1918) indicated that summer winds are predominately northwesterly or north-northwesterly and that winter winds are usually southeasterly or southwesterly. Our data follow this pattern (Table 10).

In July the vector average direction of wind was 335^{o}. The mean speed for July wind was 3.7 m sec^{-1}. In August the vector average direction was more northerly, 339^{o}, and the mean speed increased to 3.9 m sec^{-1}. September winds were still more northerly, 356^{o}, and the mean speed was 4.0 m sec^{-1}. In October the vector average direction of wind shifted to southerly, 186^{o}, and the mean speed increased to 5.0 m sec^{-1}. February winds, by far the strongest, had a mean speed of 8.6 m sec^{-1} and a maximum wind speed of 33 m sec^{-1}. The vector average direction of February winds was 186^{o}.

February winds had the largest variance. In February the variance of the onshore component of wind, 38 m^{2} sec^{-2}, was larger than the variance of the longshore wind 31 $m^{2}sec^{-2}$. In July the variance of onshore wind, 5.0 $m^{2}sec^{-2}$, was also larger than the variance of longshore wind, 4.7 $m^{2}sec^{-2}$; however in July this was

Table 10. Statistics for smoothed winds

Month	Mean $m\ sec^{-1}$	Variance $m^2\ sec^{-2}$	Maximum $m\ sec^{-1}$	Minimum $m\ sec^{-1}$	Dominant Period days	Correlation at Lag T_d -
onshore component						
July	1.6	5.0	7.2	-2.4	5.3	0.24
August	0.4	1.5	3.7	-2.7	-	-
September	0.3	0.4	1.8	-1.0	6.9	-0.31
October	0.2	3.0	5.8	-2.5	4.3	-0.29
February	0.3	38.0	11.9	-10.1	29.5	-
longshore component						
July	-1.7	4.7	1.7	-7.1	6.2	0.53
August	-1.5	13.7	5.9	-8.2	-	-
September	-2.9	4.8	1.8	-7.4	2.5	0.06
October	2.2	23.8	15.0	-4.3	9.9	-0.63
February	3.0	31.4	17.6	-5.6	7.2	0.18

largely due to speed changes of the north-northwesterly wind.[9] In other months longshore wind had about ten times more variance than onshore wind.

The spectrum of July-October longshore wind had peaks at 0.08, 0.16, 0.26, 0.40, and 0.50 cpd; the amplitudes of these peaks were, respectively, 3.4, 2.6, 1.8, 1.7, and 1.6 m sec^{-1}. The spectrum of onshore wind had peaks at 0.13, 0.18, 0.29, and 0.40 cpd. The amplitudes of these peaks were 1.3, 1.2, 0.9 and 0.9 m sec^{-1}. The energy density of onshore wind was nearly constant from 0 to 0.4 cpd while the energy density of longshore wind decreased rapidly in this range. At most frequencies, the longshore wind had five to ten times the energy density of the onshore wind.

Longshore wind had a dominant period of 6.2 days in July, 2.5 days in September, 9.9 days in October, and 7.2 days in February. Values of the correlation function for these constituents were, respectively, 0.53, 0.06, -0.63, and 0.18; amplitudes were 3.1, 3.1, 4.9, and 6.2 m sec^{-1}. Onshore wind had a dominant period of 5.3 days in July, 6.9 days in September, 4.3 days in October, and 29.5 days in February. Values of the correlation function for these constituents were 0.24 in July, -0.31 in September,

---

[9] The variance of the north-northwesterly wind was 9.3 m^2 sec^{-2} and the variance of the east-northeasterly wind was 0.4 $m^2 sec^{-2}$.

and -0.29 in October. Amplitudes were, respectively, 3.1, 0.9, and 2.5 m sec^{-1}.

Barometric Pressure

As with wind, February barometric pressure had the largest variance, 72 mb^2, and in February the maximum barometric pressure, 1031 mb, and the minimum barometric pressure, 996 mb, were the extrema noted for all observations (Table 11). The mean barometric pressure was nearly the same for August, September, October, and February, about 1015 mb. The mean barometric pressure for July was slightly lower, 1008 mb.

The spectrum of July-October barometric pressure had a peak at 0.16 cpd (6.4 days) which was significant at the 90% level. This peak had an amplitude of 3.1 mb. Other peaks, which were not significant, occurred at 0.40 cpd and 0.50 cpd; amplitudes were, respectively, 1.1 mb and 0.7 mb.

Barometric pressure had a dominant long period constituent of 5.8 days in July, 5.0 days in September, 5.3 days in October, and 27.3 days in February. Values of the correlation function for these constituents were 0.34 in July, 0.32 in September, and -0.63 in October; amplitudes were 2.8 mb in July, 3.2 mb in September, and 7.0 mb in October.

Table 11. Statistics for smoothed barometric pressure

Month	Mean mb	Variance mb^2	Maximum mb	Minimum mb	Dominant Period days	Correlation at Lag T_d -
July	1008	4	1019	1010	5.8	0.34
August	1015	6	1021	1009	-	-
September	1015	5	1019	1010	5.0	0.32
October	1014	24	1022	1002	5.3	-0.63
February	1013	72	1031	996	27.3	-

Sea Level

The tide gauge did not operate in February. The monthly mean of sea level was lowest in July, 8.5 cm, although the minimum value of sea level, 0 cm, was recorded on 29 August (Table 12). The monthly mean of sea level increased in August to 14.2 cm, decreased to 13.3 cm in September, and was highest, 13.9 cm, in October. The variance of sea level was greatest in October, 26 cm^2, and least in July, 11 cm^2.

Peaks occurred in the spectrum of sea level at 0.16 cpd (6.3 days), 0.34 cpd (2.9 days) and 0.50 cpd (2 days); amplitudes were, respectively, 3.5 cm, 1.4 cm, and 1.1 cm. The 0.5 cpd peak was not significant.

Sea level had a dominant constituent of 9.7 days in July, 6.0 days in September, and 9.3 days in October. Values of the correlation function for these constituents were, respectively, -0.28, -0.29, and -0.35; amplitudes were 4.9 cm, 5.6 cm, and 7.2 cm.

Qualitative Description of Relationship between Time Series

Data presented in Figure 14 were used to obtain a qualitative estimate of changes in sea level, current velocity, and temperature associated with storms. Results are listed in Table 13. In general, northerly winds were associated with a lowering of sea level,

Table 12. Statistics for smoothed sea level

Month	Mean cm	Variance cm^2	Maximum cm	Minimum cm	Dominant Period days	Correlation at Lag T_d -
July	8.5	11.84	17	4	9.7	-0.28
August	14.2	21.81	21	2	-	-
September	13.3	15.34	21	0	6.0	-0.29
October	19.3	25.80	35	11	6.3	-0.35

Table 13. Changes in sea level, current velocity and temperature associated with storms

Date	Wind	Sea Level	Current Velocity	Temperature	Barometric Pressure
1965					
16 July	strong NNW'ly breeze 11 m sec^{-1}	falling slowly (60m)	20m: max S'ly flow, 29 cm sec^{-1} 60m: max S'ly flow, 13 cm sec^{-1}	20m: min 7.7° C 40m: increasing	steady
23 July	moderate NNW'ly gale 17 m sec^{-1}	min 2 cm	20m: max S'ly flow, 24 cm sec^{-1} 60m: max S'ly flow, 18 cm sec^{-1}	20m: min 7.8°C 40m: max 7.5°C	falling
5 Aug	strong NNE'ly breeze 12 m sec^{-1}	min 5 cm	-	-	falling
12 Aug	strong SSW'ly breeze 11 m sec^{-1}	max 21 cm	-	-	rising
29 Aug	moderate N'ly gale 15 m sec^{-1}	min -0 cm	20m: max S'ly flow, 20 cm sec^{-1} 60m: max S'ly flow, 14 cm sec^{-1}	20m: min 8.3°C 40m: steady	falling
16 Sept	moderate NNW'ly gale 15 m sec^{-1}	min +2 cm	20m: max S'ly flow, 6 cm sec^{-1} 60m: max S'ly flow, 10 cm sec^{-1}	20m: min 8.8°C 40m: max 8.1°C	falling
23 Sept	moderate NE'ly gale 15 m sec^{-1}	rising	20m: going from SSW'ly to NNW'ly	20m: increasing	falling
4 Oct	SxE storm 31 m sec^{-1}	max 35 cm	20m: NNE'ly, 23 cm sec^{-1}	20m: increasing	rising
1966					
28 Jan	S'ly hurricane 33 m sec^{-1}	-	50m: max N'ly flow, 47 cm sec^{-1} 75m: max N'ly flow, 42 cm sec^{-1}	-	falling
5 Feb	whole SSE'ly gale 25 m sec^{-1}	-	50m: max N'ly flow, 35 cm sec^{-1} 75m: max N'ly flow, 35 cm sec^{-1}	-	low, 1004 mb
11 Feb	strong NW'ly gale 23 m sec^{-1}	-	50m: max S'ly flow, 45 cm sec^{-1} 75m: max S'ly flow, 45 cm sec^{-1}	-	rising

southerly currents, and cooler temperatures. Southerly winds were associated with a rise in sea level, northerly currents, and an increase in temperature. In the summer and fall, northerly storms were associated with a falling barometer and southerly storms were accompanied by a rising barometer; in the winter the reverse was true.

On 29 August, 1965, current response on Stonewall Bank to a north-northwesterly gale was nearly identical to current response off Depoe Bay to a north-northwesterly breeze on 16 July.

Summary

In July currents were southerly, wind was north-northwesterly, and sea level, barometric pressure, and temperature were low. In September, temperatures were warmer than in July. Currents and winds were northerly in September; sea level and barometric pressure were "average." In October the winds shifted to southerly, and 20m currents, although northerly, were quite variable. Temperatures at 20m rose rapidly in October and sea level was much higher than in September. Barometric pressure was average in October.

In February, currents, winds, and barometric pressure had a larger variance than in other months. Maximum current and wind speeds were observed, as were maximum and minimum values of barometric pressure. Temperatures were warmer in February than

in July and September but cooler than in October. In February the ocean was isothermal between 25 and 50 meters and the variance of temperature time series was negligible.

In summer and fall months of 1965, most smoothed time series had a dominant period close to one week. The amplitudes of these variations were, approximately, 3.1 mb for barometric pressure, 3.5 cm for sea level, 2.6 m sec^{-1} for longshore wind, 1.2 m sec^{-1} for onshore wind, 0.4C for 20m temperature, 0.1C for 40m temperature, and 5 cm sec^{-1} for longshore and onshore currents.

CHAPTER 8. RELATIONSHIPS BETWEEN THE VARIABLES FOR LOW FREQUENCY VARIATIONS

The qualitative relationship between sea level, wind, and longshore flow suggests the following: (i) sea level is elevated or depressed by wind action; (ii) longshore flow adjusts to balance sea level change. The latter relationship is referred to as geostrophic balance and satisfies

$$v = \frac{g}{f}\frac{\partial \zeta}{\partial x} \sim \frac{g}{fL}\zeta \qquad (8\text{-}1)$$

This equation is obtained from the equations of motion by neglecting acceleration, friction, and density differences. The relationship between sea level and longshore flow and the relationship between wind and sea level are discussed in this chapter.

Sea Level and Longshore Current

Cross-covariance functions were computed for sea level and longshore flow. Results are given in Table 14. τ_R is the lag at which the cross-covariance function had the maximum value and it indicates the number of hours that sea level lagged longshore flow. Sea level usually lagged longshore flow by a few hours. Sea level took longer to balance changes in strong longshore flow; in July sea level took two hours longer to balance changes in strong 20m flow

Table 14. Relationship between sea level and longshore current

		from the cross-covariance functions				from spectra	
Month	depth m	τ_R hours	$\hat{C}_{\zeta v}(\tau_R)$ $cm^2\ sec^{-1}$	$\hat{\rho}_{\zeta v}(\tau_R)$ -	$\hat{\beta}_{\zeta v}(\tau_R)$ sec^{-1}	$b_{\zeta v}$ sec^{-1}	σ_b sec^{-1}
July	20	-6	21.1	0.75	1.8	1.4	0.31
	60	-4	16.5	0.62	1.4	1.2	0.33
September	20	0	19.7	0.73	1.3	1.3	0.14
	60	-8	19.2	0.79	1.2	1.2	0.14
October	20	-10	21.1	0.60	0.8	0.5	0.17
September-October	20	-6	22.9	0.60	0.8	1.0	0.09

than weak 60m flow and in September sea level took eight hours longer to balance strong 60m flow than weak 20m flow. The beta coefficient for sea level and longshore flow, $\hat{\beta}_{\zeta v}(\tau_R)$, was greater in July than in September or October. This means that a unit change in sea level was associated with a larger change in longshore velocity in July than in September or October. The fact that the beta coefficients were positive indicates that longshore flow and sea level were in phase, i.e. flow to the south was associated with low sea level.

The transfer function from sea level to 20m longshore current for September-October is illustrated in Figure 16; coherence square and 90% confidence limits are also shown in Figure 16. Phase was steady and coherence square estimates were significant from 0.14 to 0.60 cpd. The amplitude of the transfer function was largest at frequencies of 0.20, 0.35, and 0.60 cpd; this suggests that the shelf was resonant at these frequencies. However the amplitude of the true transfer function could have been constant (independent of frequency) with a value of 0.9-1.7 sec^{-1} and still fit within the 90% confidence interval of each estimate.

Phase estimates indicated that sea level lagged longshore current at most frequencies. The true value of phase could have had a value of 000° to -018° and still fit within the 90% confidence interval of each phase estimate.

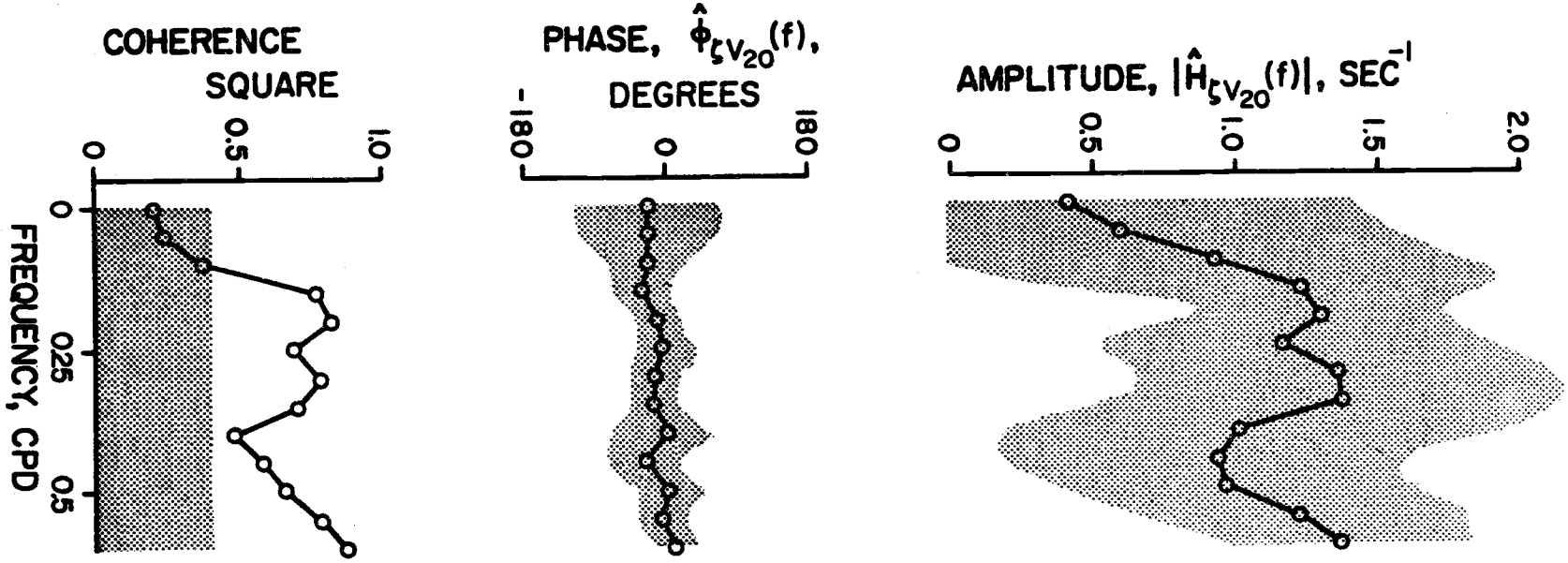

Figure 16. Transfer function from sea level to longshore current for September-October 1965. Stipled area indicates 90% confidence limits.

Estimates of the transfer functions for sea level to longshore flow are tabulated in Table 15 for individual months. Most coherence square estimates were significant and phase estimates were near zero and consistent from one frequency to adjacent frequencies. The amplitude of the transfer function was, in general, largest in July and smaller in October.

Regression coefficients, $b_{\zeta v}$, were calculated by the method of Chapter 4 and are presented in Table 14. The assumption

$$\phi_{\zeta v}(f) = 0, \quad 0 < f < 0.5$$

appears to have been justified (Table 15). Regression coefficients did not differ significantly for July and September and had a value of about $1.3\ \text{sec}^{-1}$. The regression coefficient for October was lower, $0.5\ \text{sec}^{-1}$.

If equation (8-1) is valid, then

$$b_{\zeta v} = \frac{g}{fL} \tag{8-2}$$

i.e. the regression coefficient is a measure of current width, L. A regression coefficient of $1.3\ \text{sec}^{-1}$ requires a current width of 75 km; a regression coefficient of $0.5\ \text{sec}^{-1}$ requires a current width of 180 km.

The width of the Oregon continental shelf is variable. The 100 fathom curve is 28km from the coast off Depoe Bay and 67 km from

Table 15. Transfer functions from sea level to longshore current

depth(m)	month	f cpd	$\lvert\hat{H}_{\zeta v}\rvert$ sec^{-1}	$\hat{\phi}_{\zeta v}$ degrees	$\hat{\gamma}^2_{\zeta v}$ --
20	July	0	1.98	349	0.65
		0.15	1.97	345	0.62
		0.30	1.58	356	0.44
		0.45	1.43	022	0.53
		0.60	0.93	047	0.32
20	Sept.	0	1.58	007	0.47
		0.12	1.31	004	0.50
		0.24	1.21	346	0.71
		0.36	1.32	349	0.82
		0.48	1.43	349	0.84
		0.60	1.40	007	0.86
20	Oct.	0	0.73	335	0.25
		0.12	0.92	331	0.41
		0.24	1.10	335	0.58
		0.36	0.78	321	0.36
		0.48	0.30	331	0.11
		0.60	0.44	050	0.29
60	July	0	1.23	346	0.43
		0.15	1.55	342	0.44
		0.30	2.34	000	0.49
		0.45	1.52	007	0.36
		0.60	0.90	072	0.41
60	Sept.	0	1.32	335	0.77
		0.12	1.34	331	0.86
		0.24	1.37	331	0.79
		0.36	1.49	331	0.56
		0.48	1.75	327	0.56
		0.60	1.77	342	0.55

the coast off Heceta Head. The geostrophic current width deduced from our observations, 75km, is quite close to the latter value. Defant (1952) computed relative sea level heights geostrophically off Northern California and found an inflection in sea level near the edge of the continental shelf. Lee (1967) noted a coastal regime and an offshore regime but he selected a station 200km from the coast as the dividing line and did not study water properties on the continental shelf. An inshore current regime of 75 km explains why Stevenson (1966) measured few northerly currents 80 km offshore while our observations indicate that northerly flow is common.

Several aspects of the sea level-longshore current relationship deserve further comment. If longshore flow is primarily the result of sea level changes, then sea level should lead longshore flow, not vice versa (as observed) However for sea level and longshore flow the value of the cross-covariance function at lag τ_R did not differ significantly from the value of the cross-covariance function at a lag of zero hours. Further, if sea level values were used which were not adjusted for barometric pressure, then longshore flow lagged unadjusted sea level. For example, in September-October longshore current at 20m lagged unadjusted sea level by four hours. Finally, low frequency near-shore or bay processes could affect sea level. Hence the relationship between sea level and longshore flow is approximate and sea level and longshore flow are in-phase as opposed

to being one or two days out of phase.

It seems appropriate to regard Equation (8-1) as a satisfactory approximation. Accelerations are neglected, but for smoothed data acceleration was usually much less than longshore velocity. Friction is also neglected; Rattray (1958) has shown that differential equations which do not consider friction give a satisfactory representation of tides at Umatilla Reef Lightship ($48^{o}10'N, 124^{o}50'W$). The effect of onshore flow on sea level is also ignored, but onshore flow is much less than longshore flow in all months except October. The most serious deficiency of Equation (8-1) is that density differences are neglected. In 1962, the largest change in onshore-offshore density differences occurred in October when sigma-t surfaces 25.5 and 26.0 changed slope (Collins, 1962).

Reasons for the regression coefficient for October being low have been given: (i) a large change in density stratification occurred and is not included in the simple model (Equation (8-10)); (ii) onshore flow is of the same magnitude as longshore flow.

Wind and Sea Level

To compute transfer functions which relate a vector, wind velocity, to a scalar, sea level

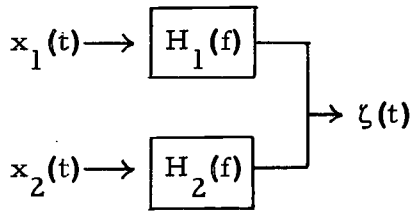

it is necessary to take into account the effects of one component of the wind, say $x_2(t)$, on sea level when computing the transfer function from the other component of wind, $x_1(t)$ to sea level. The following procedure does this (Bendat and Piersol, 1966): (i) First residual spectra are computed

$$\hat{G}_{x_1\zeta.x_2}(f) = \hat{G}_{x_1\zeta}(f)\left[1 - \frac{\hat{G}_{x_1x_2}(f)\hat{G}_{x_2\zeta}(f)}{\hat{G}_{x_2x_2}(f)\hat{G}_{x_1\zeta}(f)}\right] \tag{8-3}$$

$$\hat{G}_{x_1x_1.x_2}(f) = \hat{G}_{x_1x_1}(f)[1 - \hat{\gamma}^2_{x_1x_2}(f)]$$

$$\hat{G}_{\zeta\zeta.x_2}(f) = \hat{G}_{\zeta\zeta}(f)[1 - \hat{\gamma}^2_{x_2\zeta}(f)] \quad .$$

(ii) Then the transfer function from $x_1(t)$ to $\zeta(t)$ is computed as the ratio of the two terms

$$\hat{H}_{x_1\zeta.x_2}(f) = \frac{\hat{G}_{x_1\zeta.x_2}(f)}{\hat{G}_{x_1x_1.x_2}(f)} \tag{8-4}$$

and (iii) the partial coherence square between $x_1(t)$ and $\zeta(t)$ is given by

$$\hat{\gamma}^2_{x_1\zeta.x_2} = \frac{|\hat{G}_{x_1\zeta.x_2}(f)|^2}{\hat{G}_{x_1x_1.x_2}(f)\hat{G}_{\zeta\zeta.x_2}(f)} \quad . \tag{8-5}$$

(iv) Finally, the multiple coherence square between both inputs, $x_1(t)$ and $x_2(t)$, and the output, $\zeta(t)$, is

$$\hat{\gamma}^2_{\zeta.\vec{W}}(f) = 1 - [\hat{G}_{\zeta\zeta}(f)\cdot \hat{G}^{\zeta\zeta}(f)]^{-1} \tag{8-6}$$

where $\hat{G}^{\zeta\zeta}(f)$ can be computed as the last diagonal element of

$$\begin{bmatrix} \hat{G}_{x_1x_1}(f) & \hat{G}_{x_1x_2}(f) & \hat{G}_{x_1\zeta}(f) \\ \hat{G}_{x_2x_1}(f) & \hat{G}_{x_2x_2}(f) & \hat{G}_{x_2\zeta}(f) \\ \hat{G}_{\zeta x_1}(f) & \hat{G}_{\zeta x_2}(f) & \hat{G}_{\zeta\zeta}(f) \end{bmatrix}^{-1} \quad .$$

The relationship between $x_1(t)$ and sea level is significant at the 90% level if partial coherence square satisfies Equation (5-17); multiple coherence square estimates are significant if

$$\hat{\gamma}^2_{\zeta.\vec{W}}(f) > \frac{4}{\nu-2} \tag{8-7}$$

(Bendat and Piersol, 1966).

The transfer function, partial coherence square, and multiple coherence square for wind and sea level in July-October are illustrated in Figure 17. The transfer function for longshore wind to sea level had steady phase and significant partial coherence square for frequencies from zero to 0.18 cpd ($5\frac{1}{2}$ days); the amplitude of the transfer function was close to one cm m^{-1} sec in this frequency range and peaks occurred at 0.026 cpd (41 days) and 0.132 cpd (7.6 days). Phase, for frequencies from zero to 0.18 cpd, required sea level to lag longshore wind slightly. At frequencies greater than 0.18 cpd, the amplitude of the transfer function was less, about 0.4 cm m^{-1} sec; at these frequencies the phase of the transfer function was not steady and values of partial coherence square were, in general, not significant.

Few estimates of partial coherence square for onshore wind and sea level were significant; phase and amplitude of the transfer function from onshore wind to sea level changed rapidly from one frequency to the next. Near zero frequency, onshore wind and sea level were out of phase; this means that at these frequencies westerly winds depressed sea level. At a frequency of 0.32 cpd (3.1 days), onshore winds and sea level were in phase so onshore winds elevated sea level. It is doubtful that the relationship between onshore wind and sea level was significant. This is due, in part, to the fact that few onshore winds occurred during the July-October period (Table 10).

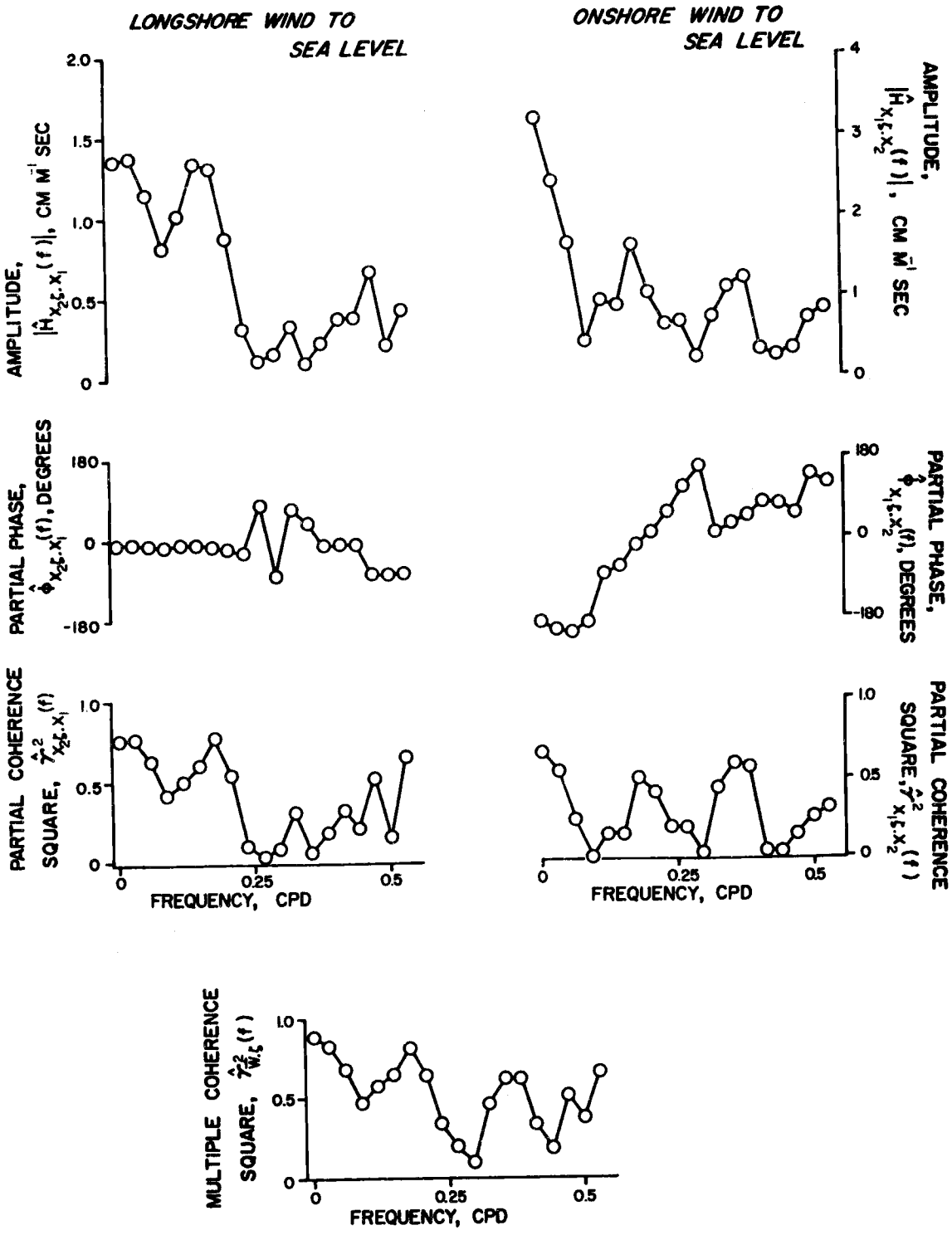

Figure 17. Transfer function from wind to sea level for July-October 1965.

Cross-covariance functions were computed for longshore wind and sea level. Results are given in Table 16. τ_R is the lag at which the cross-covariance function had the maximum value and it indicates the number of hours sea level lagged longshore wind. τ_R varied from three hours in September to 12 hours in October and the value for the merged time series which extended from July to October was eight hours. The value of the cross-correlation function was highest in October, 0.79, and least in July, 0.50. The beta coefficient, $\hat{\beta}_{x_2\zeta}(\tau_R)$, indicates the change in sea level resulting from an increase of longshore wind of one m sec^{-1}. Beta coefficients ranged from 0.8 to 1.0 cm m^{-1} sec. The fact that beta coefficients were positive indicates that longshore wind and sea level were in phase, i.e. northerly winds depressed sea level.

For the wind-sea level case, the regression model is

$$\zeta = \beta_{x_1\zeta \cdot x_2} x_1 + \beta_{x_2\zeta \cdot x_1} x_2 + \alpha \qquad (8\text{-}8)$$

where $\beta_{x_1\zeta \cdot x_2}$ and $\beta_{x_2\zeta \cdot x_1}$ are partial regression coefficients. To estimate the partial regression coefficient, $\beta_{x_2\zeta \cdot x_1}$, Equation (5-21) may be used if

$$b_{x_2\zeta \cdot x_1}(f) = \hat{X}_{x_2\zeta \cdot x_1}(f) \cdot [\hat{G}_{x_2x_2 \cdot x_1}(f)]^{-1} \qquad (8\text{-}9)$$

and

$$\hat{N}(f) = \hat{G}_{x_2 x_2 \cdot x_1}(f)[\hat{G}_{\zeta\zeta \cdot x_1}(f) \cdot (1-\hat{\gamma}^2_{x_2 \zeta \cdot x_1}(f))]^{-1} . \qquad (8\text{-}10)$$

But the assumptions for computing this coefficient are

$$\left.\begin{aligned} &\hat{\phi}_{x_2 \zeta \cdot x_1}(f) = 0 \\ &b_{x_2 \zeta \cdot x_1}(f) = \text{constant} \end{aligned}\right\} \quad 0 < f < 0.5 \qquad (8\text{-}11)$$

and these were not satisfied for the longshore wind-sea level relationship. For example, in July-October the partial regression coefficient relating sea level to longshore wind was 0.4 cm m^{-1} sec for frequencies from zero to 0.5 cpd and 1.1 cm m^{-1} sec for frequencies from zero to 0.18 cpd. The latter value was better because for frequencies from zero to 0.18 cpd (i) partial phase, $\hat{\phi}_{x_2 \zeta \cdot x_1}(f)$, was close to zero and the regression coefficients, $b_{x_2 \zeta \cdot x_2}(f)$, were approximately constant, (ii) all partial coherence square estimates were significant, and (iii) more than 90% of the energy density of the partial cospectrum, $\hat{X}_{x_2 \zeta \cdot x_1}(f)$, was included. To obtain partial regression coefficients for individual months, only significant spectral estimates were used, i.e. estimates for which partial coherence square was significant. Partial regression coefficients are presented in Table 16. Partial regression coefficients were similar to values of the beta function and differences between partial regression coefficients for individual months were not significant. However a change

in longshore wind of one m sec^{-1} was associated with larger sea level changes in September than in July or October.

Wind and Longshore Current

There were no sea level data obtained for February, but it is possible to compare wind with longshore velocity. As onshore winds were strong and variable in February, their effect on current should also be considered. In order to interpret the results, longshore wind and longshore velocity were compared in other months.

February currents seem to flow in a direction determined by the preceding storm. Southerly and easterly winds were associated with northerly flow and westerly and northerly winds were associated with southerly flow. But the ocean responded more readily to westerly winds. For example, a west-northwesterly breeze on 1-2 February was sufficient to disrupt northerly flow at 25, 50, and 75 meters but a similar southerly breeze on 10 February had no effect on southerly flow. Again, southeasterly breezes blew on 25 and 26 January but a reversal of southerly flow at 50 and 75 meters did not occur; yet westerly breezes on 6 February were associated with an immediate reversal of northerly flow at 50 and 75 meters.

Cross-covariance functions were computed for longshore wind and longshore flow for all months. Results are given in Table 17; τ_R is the lag at which the cross-covariance function had the

Table 16. Relationship between longshore wind and sea level

		from the cross-covariance functions			from spectra	
month	τ_R hours	$\hat{C}_{x_2\zeta}(\tau_R)$ m cm sec^{-1}	$\hat{\rho}_{x_2\zeta}(\tau_R)$ -	$\hat{\beta}_{x_2\zeta}(\tau_R)$ cm m^{-1} sec	$b_{x_2\zeta.x_1}$ cm m^{-1} sec	σ_b cm m^{-1} sec
July-Oct	8	15.3	0.67	1.0	1.1	0.13
July	10	3.7	0.50	0.8	0.8	0.15
September	3	4.8	0.56	1.0	0.9	0.19
October	12	19.4	0.79	0.8	0.8	0.14

Table 17. Relationship between longshore wind and longshore current

Month	depth m	from the covariance functions τ_R hours	$\hat{C}_{x_2v}(\tau_R)$ cm m sec^{-2}	$\hat{\rho}_{x_2v}(\tau_R)$ -	$\hat{\beta}_{x_2v}(\tau_R)$ cm m^{-1}	from spectra $b_{x_2v.x_1}$ cm m^{-1}	σ_b cm m^{-1}
July	20	8	12.1	0.70	2.5	1.7	0.48
	60	10	12.2	0.75	2.5	1.8	0.51
September	20	0	9.8	0.65	2.0	1.6	0.33
	60	0	7.1	0.53	1.5	2.1	0.33
October	20	10	18.4	0.53	0.8	0.7	0.46
February	50	15	120.2	0.79	3.9	2.4	1.6
	75	17	118.0	0.80	3.8	2.5	1.5
Sept.-Oct.	20	3	15.2	0.47	0.7	0.7	0.13

maximum value. τ_R indicates the number of hours longshore flow lagged longshore wind. τ_R varied from zero hours for 20 and 60m longshore flow in September to 17 hours for 75m longshore flow in February. In July, longshore flow at 60m took two hours longer to respond to longshore wind than 20m flow. Similarily, in February 75m flow took two hours longer to respond to longshore wind than 50m flow. In September, 20 and 60m longshore flow responded at the same lag, zero hours, to longshore wind.

Values of the cross-correlation function were highest, from 0.7 to 0.8, for July and February and somewhat lower for September and October. Beta coefficients indicate the change of longshore current velocity per unit change of longshore wind velocity. Values of the beta coefficient were smallest for October 20m flow, 0.8 cm m^{-1}, and largest for February 50m flow, 3.9 cm m^{-1}. The fact that beta coefficients were positive indicates that longshore wind and longshore current were in phase, i.e. northerly winds were associated with southerly currents.

For February, cross-covariance functions were computed for onshore wind and longshore flow; results are given in Table 18. Longshore flow lagged onshore wind by three days at both 50 and 75m. Values of the correlation function at this lag were greater than 0.9. Beta functions were negative (this indicates that westerly winds were associated with southerly currents) and a one m sec^{-1} change of

Table 18. Relationship between February onshore wind and longshore current

depth m	τ_R hours	$\hat{C}_{x_1 v}(\tau_R)$ cm m sec^{-2}	$\hat{\rho}_{x_1 v}(\tau_R)$ -	$\hat{\beta}_{x_1 v}(\tau_R)$ cm m^{-1}	$b_{x_1 v . x_2}$ cm m^{-1}	σ_b cm m^{-1}
50	72	-154.9	0.93	-4.1	-2.5	1.4
75	76	-152.2	0.94	-4.0	-2.3	1.4

onshore wind was associated with a four cm sec^{-1} change of longshore current velocity.

Transfer functions for February wind to longshore current are given in Table 19. As with the relationship between wind and sea level, conditions for computing partial regression coefficients (Equation (8-10)) were not satisfied: the transfer function was frequency dependent and phase estimates were not close to zero or 180^{o}. To compute partial regression coefficients for February, only estimates for zero and 0.05 cpd were used. This was justified on the basis that these estimates included more than 95% of the amplitude of the cross spectrum; however phases were still not close to 0^{o} or 180^{o}, especially for the longshore wind-longshore current relationship. For other months, only significant estimates were used in computing partial regression coefficients; in these cases, phases were usually quite close to zero.

Partial regression coefficients for longshore wind and longshore current are given in Table 17. July, September, and February regression coefficients did not differ significantly and had a value of about 2.0 cm m^{-1}. The October regression coefficient was significantly lower than this value, 0.7 cm m^{-1}.

Partial regression coefficients for onshore wind and longshore current are given in Table 18. They were equal in magnitude to the partial regression coefficient for February longshore wind and

Table 19. Transfer functions for February wind to longshore current

	frequency f cpd	amplitude $\lvert\hat{H}_{xv.y}\rvert$ cm m^{-1}	phase $\hat{\phi}_{xv.y}$	coherence square $\gamma^2_{xv.y}$	$\hat{\gamma}^2_{\vec{w}.v}$
from x_1 to v_{50}	0	2.52	-154	.32	.81
	0.12	2.80	-166	.33	.72
	0.24	1.07	054	.09	.58
	0.36	0.18	-018	.03	.73
from x_2 to v_{50}	0	3.96	-037	.43	
	0.12	3.36	-053	.38	
	0.24	1.86	-023	.32	
	0.36	1.52	-056	.30	
from x_1 to v_{75}	0	2.39	-150	.33	.82
	0.12	2.58	-165	.30	.72
	0.24	1.14	055	.10	.58
	0.36	3.13	041	.06	.60
from x_2 to v_{75}	0	4.11	-037	.47	
	0.12	3.35	-050	.39	
	0.24	1.83	-022	.31	
	0.36	1.12	-054	.41	

longshore current and had a value of 2.4 m sec^{-1}. The regression equation which related wind to longshore flow in February is

$$v \sim -2.4x_1 + 2.4x_2 - 16 \ .$$

Clearly, northwesterly winds and southeasterly winds are most effective in producing longshore flow. Based on a careful appraisal of February data, I do not wish to say that the constant term, -16 cm sec^{-1}, indicates a mean drift to the south. Rather, northwesterly winds were more efficient in producing southerly flow than southeasterly winds were in producing northerly flow.

Other Relationships

Other relationships between low frequency variations were noted in Chapter 7. Statistics are given in Table 20 for relationships which had significant values of coherence square.

July

In July temperatures at 20m were coolest when north-northwesterly winds were strong. Temperature at 20m lagged north-northwesterly wind by 27 hours. The beta coefficient and the amplitude of the transfer function indicated that an increase of wind speed of one m sec^{-1} was associated with a temperature decrease of $0.08^{\circ}C$.

Longshore velocity components at 20 and 60m were well

Table 20. Other significant relationships between variables for low frequency oscillations

			from the cross-covariance function				from the transfer function		
			τ_R	$\hat{C}_{xy}(\tau_R)$	$\hat{\rho}_{xy}(\tau_R)$	$\hat{\beta}_{xy}(\tau_R)$	f	$\lvert\hat{H}_{xy}(f)\rvert$	$\hat{\phi}_{xy}(f)$	$\hat{\gamma}^2_{xy}(f)$
Month	x	y	hours	x·y	-	y/x	cpd	y/x	o	
July	ζ	u_{60}	-3	-4.2	0.52	0.8	0.45	1.0	176	0.56
							0.60	0.6	158	0.43
	x_{NNW}	T_{20}	27	0.7	0.65	0.08	0.30	0.08	83	0.54
	v_{20}	v_{60}	-4	52.0	0.84	0.83	0.0	0.7	356	0.81
							0.15	0.8	353	0.74
							0.30	1.3	349	0.70
							0.45	1.2	353	0.65
September	ζ	u_{20}	2	11.2	0.76	0.73	0.0	0.80	356	0.62
							0.12	0.79	0	0.69
							0.24	0.76	18	0.71
	ζ	u_{60}	1	5.9	0.64	0.38	0.0	0.25	36	0.36
							0.12	0.40	29	0.40
							0.24	0.47	18	0.47
							0.36	0.47	342	0.47
	v_{20}	v_{60}	-10	17.8	0.76	1.25	0.0	1.30	345	0.77
							0.12	1.23	331	0.66
							0.24	1.38	309	0.67
							0.36	1.36	317	0.54
							0.48	1.36	320	0.53
	v_{20}	v_{60}	-2	24.2	0.57	0.51	0.0	0.25	313	0.14
							0.12	0.46	330	0.35
							0.24	0.86	342	0.64
							0.36	1.08	342	0.64
							0.48	1.18	348	0.62
	v_{60}	T_{40}	-20	-0.24	0.62	-0.006	0.0	0.007	130	0.40
							0.12	0.009	130	0.62
							0.24	0.008	130	0.57
October	x_2	u_{20}	7	15.2	0.46	0.64	0.36	0.87	052	0.48
							0.48	0.54	058	0.51

correlated in July; 60m flow led 20m flow by four hours and the average of the amplitude of the transfer function from 20m longshore flow to 60m longshore flow was near unity. Values of coherence square were high, greater than 0.65.

Sea level lagged 60m onshore flow by two hours and was out of phase, i.e. easterly flow was associated with low values of sea level. The amplitude of the transfer function from sea level to 60m onshore flow was about 0.8 sec^{-1}.

September

In September sea level was highest when onshore flow occurred at 20 and 60m. 20m onshore flow lagged sea level by 2 hours and 60m onshore flow lagged sea level by one hour. The beta coefficient and the amplitude of the transfer function indicated that an increase of sea level of one cm was associated with an increase of onshore flow of 0.8 sec^{-1} at 20m and 0.5 sec^{-1} at 60m. This is a different relationship than existed in July.

Northerly flow at 60m was strongest when flow at 20m was to the north or onshore. Longshore flow at 20m lagged 60m longshore flow by two hours and 20m onshore flow lagged 60m longshore flow by ten hours. The amplitude of the transfer function indicated that response of 60m longshore flow to an increase of one cm sec^{-1} of 20m longshore flow increased from 0.25 at low frequencies to 1.28

at 0.5 cpd. The amplitude of the transfer function from 20m onshore flow to 60m longshore flow was almost constant from 0 to 0.5 cpd and had a value of 1.3, i.e. an increase of onshore flow at 20m of one cm sec^{-1} corresponded to an increase of longshore flow at 60m of 1.3 cm sec^{-1}.

Temperature at 40m was coolest when 60m longshore flow was to the north; 40m temperature led 60m longshore flow by 20 hours. A one cm sec^{-1} decrease of 60m longshore flow corresponded to a 40m temperature increase of 0.008 C. A similar relationship between 40m temperature and 60m longshore flow existed in July but was not significant.

October

In October, southerly winds were associated with onshore currents. Onshore flow at 20m lagged longshore wind by seven hours; an increase of longshore wind of one m sec^{-1} was associated with an increase of easterly current of 1/2 cm sec^{-1}.

The sharp rise of temperature in October was associated with onshore currents. Largest temperature increases occurred on 3-6 October and 10-13 October when flow was onshore. Offshore flow on 8 and 9 October, associated with northeasterly winds, did not lower temperatures; but offshore and southerly flow on 15 and 16 October (associated with northwesterly breezes) did lower temperature at

20m. An increase of onshore flow of one cm sec^{-1} was associated with an increase of temperature of 0.12C.

Summary

In July when winds were calm:

sea level was higher than usual, 14 cm;

currents at 20m were southerly, 5 cm sec^{-1};

currents at 60m flowed to the north with a speed of 10 cm sec^{-1};

temperatures at 20m were warmer than usual, 8.5C;

temperatures at 40m were cooler than usual, 7.3C.

For each m sec^{-1} increase of northerly wind in July:

sea level was lowered 0.8 cm;

currents at 20 and 60m increased their southerly component 2 cm sec^{-1};

temperature at 20m decreased 0.08 C (at a lag of 27 hours);

temperature at 40m increased 0.01C (at a lag of 36 hours).

In September when winds were calm:

sea level was higher than usual, 18 cm;

currents at 20m were northerly, 4 cm sec^{-1};

currents at 60m were northerly, 10 cm sec^{-1};

temperature at 20m was 9.1C;

temperature at 40m was 8.0C.

For each m sec^{-1} increase of northerly wind in September, changes of longshore current velocity, temperature and sea level had nearly the same values as in July. An important difference between July and September flow regimes is the relationship between onshore flow and sea level. In July onshore flow at 60m corresponds to low values of sea level while in September low values of sea level correspond to offshore flow at 20 and 60m.

In October when winds were calm:

sea level was lower than usual, 21 cm;

currents were north-northeasterly at 20m, 5 cm sec^{-1}.

For each m sec^{-1} increase of southerly wind in October:

sea level rises 0.8 cm (the same relationship as in July and September);

northerly currents increased 1 cm sec^{-1};

easterly currents increased 0.5 cm sec^{-1};

temperature rose 0.12C.

CHAPTER 9. DESCRIPTION OF INTERMEDIATE FREQUENCY OSCILLATIONS

Table 21 indicates the variance of the intermediate frequency data and its percent of total variance. Of velocity data at 20 meters, October data have the largest variance, July the second largest variance, and September the least variance. At 60m, September flow had the largest variance. February velocity data were least variable.

At 20 and 40m temperatures had the largest variance in July.

Sea Level

Sea level intermediate frequency spectra consisted of two bands of energy--one at one cpd (the diurnal tide) and the other at two cpd (the semidiurnal tide). Each energy band consists of many spectral lines which are called partial tides (Munk, Zetler, and Groves, 1965). Of the partial tides, the lunisolar diurnal tide (designated K_1), the principal lunar diurnal tide (O_1), the principal solar tide (S_2), and the lunar semidiurnal tide (M_2) usually account for 70% of the variation of sea level (Defant, 1958).

To obtain values for the amplitude, A, and the phase, ϕ, of each partial tide we fitted a sinusoid of the form

Table 21. Variance of intermediate frequency time series of current velocity and temperature

Variable	Depth m	Month	IF Variance $cm^2 sec^{-2}$	% of total Variance
Northerly flow	20	July	47	39
		September	49	38
		October	138	62
	50	February	37	5
	60	July	48	39
		September	68	45
	75	February	36	5
Easterly flow	20	July	83	79
		September	43	52
		October	101	56
	50	February	20	23
	60	July	23	50
		September	37	50
	75	February	24	25
			$^oC^2$	
Temperature	20	July	0.306	42
		September	0.167	27
		October	0.124	13
	40	July	0.0094	37
		September	0.0069	40

$$z_0 + \sum_{i=1}^{5} A_i \cos(\sigma_i t + \phi_i) \qquad (9\text{-}1)$$

where z_0 = mean sea level,

σ_i = speed of constituent i, and

the extra partial tide was N_2.

Data used was the Newport sea level record for 5 July - 17 October and the computation was done by the method of least squares (Zetler, Schuldt, Whipple, and Hicks, 1965). Results are compared (Table 22) with values obtained for Newport in May, 1964, by Swanson (1965) and by the Coast and Geodetic Survey in 1933. Agreement is good.

Table 22. Tidal constants

	Partial Tide							
	M_2		S_2		K_1		O_1	
Location	A cm	ϕ degrees	A cm	ϕ degrees	A cm	ϕ degrees	A cm	ϕ degrees
Newport:								
USC&GS (1933)	85	347	22	15	42	116	26	98
May, 1964	86	348	21	0	44	104	22	100
This Study	85	347	22	16	44	116	28	98
Stonewall Bank	80	342	22	358	43	114	27	102
Depoe Bay	79	342	26	3	41	109	27	87

From the spectrum of sea level the amplitude of the energy at one cpd was estimated to be 43 cm and the amplitude of the energy at two cpd was estimated to be 86 cm. These equal, respectively, the

amplitude of the K_1 tide and the amplitude of the M_2 tide (Table 22).

Drillship motion data obtained by Chevron Research Corporation on Stonewall Bank and off Depoe Bay were analyzed in the same manner (equation 9-1) and results are also given in Table 22. Agreement with the Newport tide was good. Hence near Newport the tide on the shelf 8-12 miles offshore is adequately represented by sea level observations at Newport.

Current Velocity

Spectra for current velocity are presented in Figure 18. In addition to diurnal and semidiurnal energy peaks, energy was usually significant at a frequency of 1.4 cpd--the inertial frequency for 44^{o}N.

Analysis was first attempted by adding an inertial term to equation (9-1) and fitting this to velocity data by the method of least squares. Results were often not consistent; this was due to the fact that the phase of the inertial oscillation was not constant. Amplitudes for velocity components were obtained from power spectra; phase was obtained from cross spectra with sea level. Table 23 compares time series analysis results with those obtained from Fourier analysis[10] and least squares analysis. Amplitudes and phases

---

[10] Results for Fourier analysis provided by Mr. C. B. Taylor, Mr. Bob Dennis, and Mr. Elmo Smith of the Currents Section, Oceanography Division, Environmental Science Services Administration.

Figure 18. Intermediate frequency spectra of current velocity. The closed dot represents the east-west component of velocity and the open dot represents the north-south component of velocity.

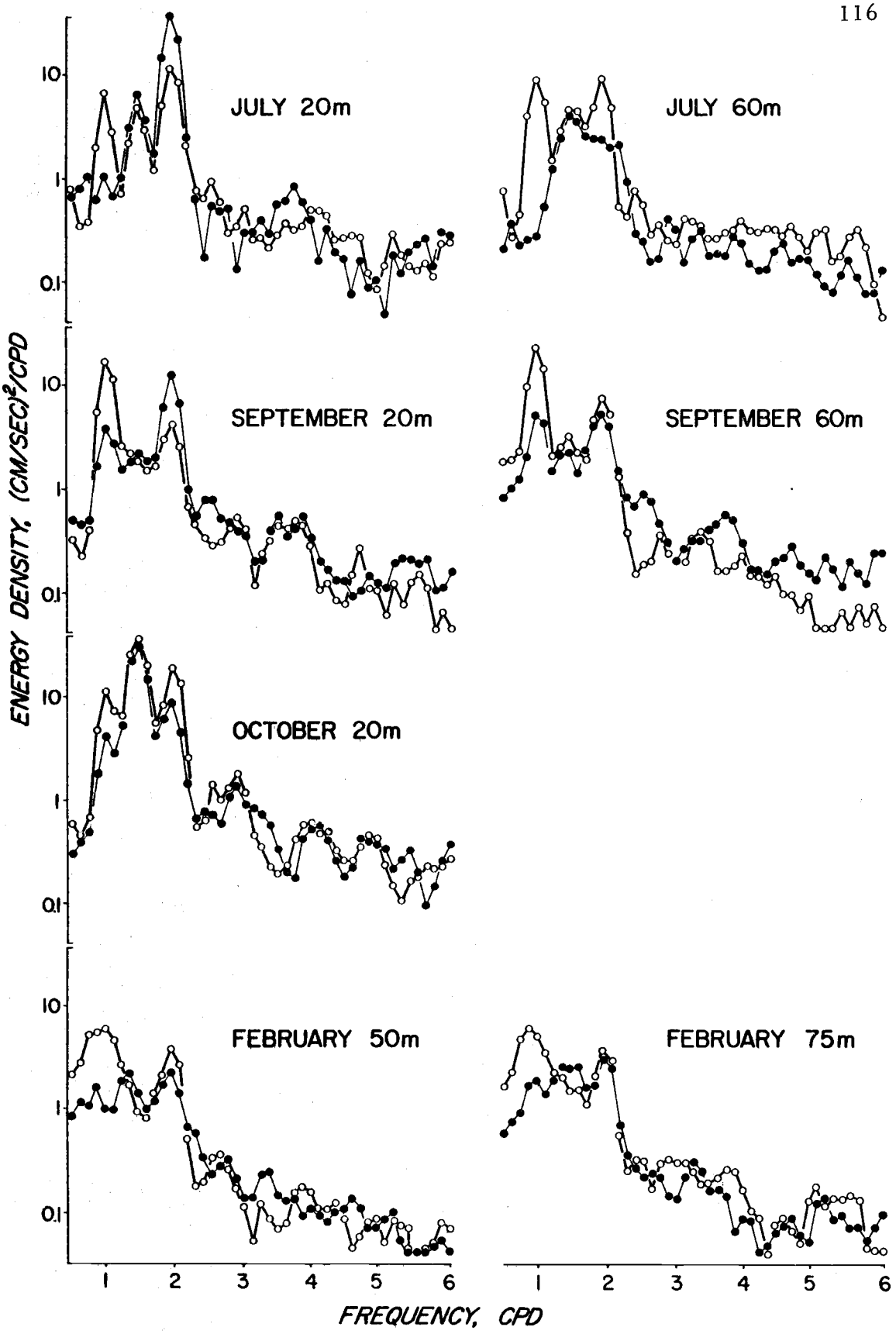
JULY 20m
JULY 60m
SEPTEMBER 20m
SEPTEMBER 60m
OCTOBER 20m
FEBRUARY 50m
FEBRUARY 75m
10
1
0.1
1
2
3
4
5
6
ENERGY DENSITY, (CM/SEC)²/CPD
FREQUENCY, CPD

Table 23. Tidal constants for September 20m velocity

Component	Analysis Method	Partial Tide K_1 cm sec^{-1}	K_1 degrees	O_1 cm sec^{-1}	O_1 degrees	M_2 cm sec^{-1}	M_2 degrees	S_2 cm sec^{-1}	S_2 degrees
v_{20}	Fourier Analysis	8.6	066	2.8	046	2.4	275	1.2	289
	Least Squares	6.0	072	2.0	088	3.1	248	1.0	309
	Time Series Analysis	7.2	050			3.6	280		
u_{20}	Fourier Analysis	3.6	129	1.6	059	6.7	265	1.3	231
	Least Squares	3.6	137	2.0	088	6.2	261	1.3	233
	Time Series Analysis	3.7	110			6.2	267		

obtained from time series analysis compare favorably with Fourier and least square results.

Current ellipses were constructed with standard methods (USC&GS, 1950). These ellipses are illustrated in Figure 19; ellipse dimensions are given in Table 24.

Diurnal Currents

Rotation of the 20m velocity vector was counterclockwise in July and clockwise in September and October. Maximum velocity at 20m was largest in September, $7\frac{1}{2}$ cm sec^{-1}, and smallest in July, 4 cm sec^{-1}. The major axis of the 20m ellipse formed an angle of 026^{o} with the meridian in July; this angle was 018^{o} in September and October. At 20m, maximum easterly flow occured 1 hour before high tide in July, and at high tide in September and October.

Rotation of the 60m velocity vector was counterclockwise in July and clockwise in September. The maximum velocity at 60m was 5 cm sec^{-1} in July and 9 cm sec^{-1} in September. The major axis of the 60m ellipse formed an angle of about 350^{o} with the meridian in July and September. At 60m, maximum easterly flow occurred 11 hours before high tide in July and 6 hours after high tide in September.

February ellipses were nearly straight lines. Maximum velocities were the same at 50m and 75m, about 5 cm sec^{-1};

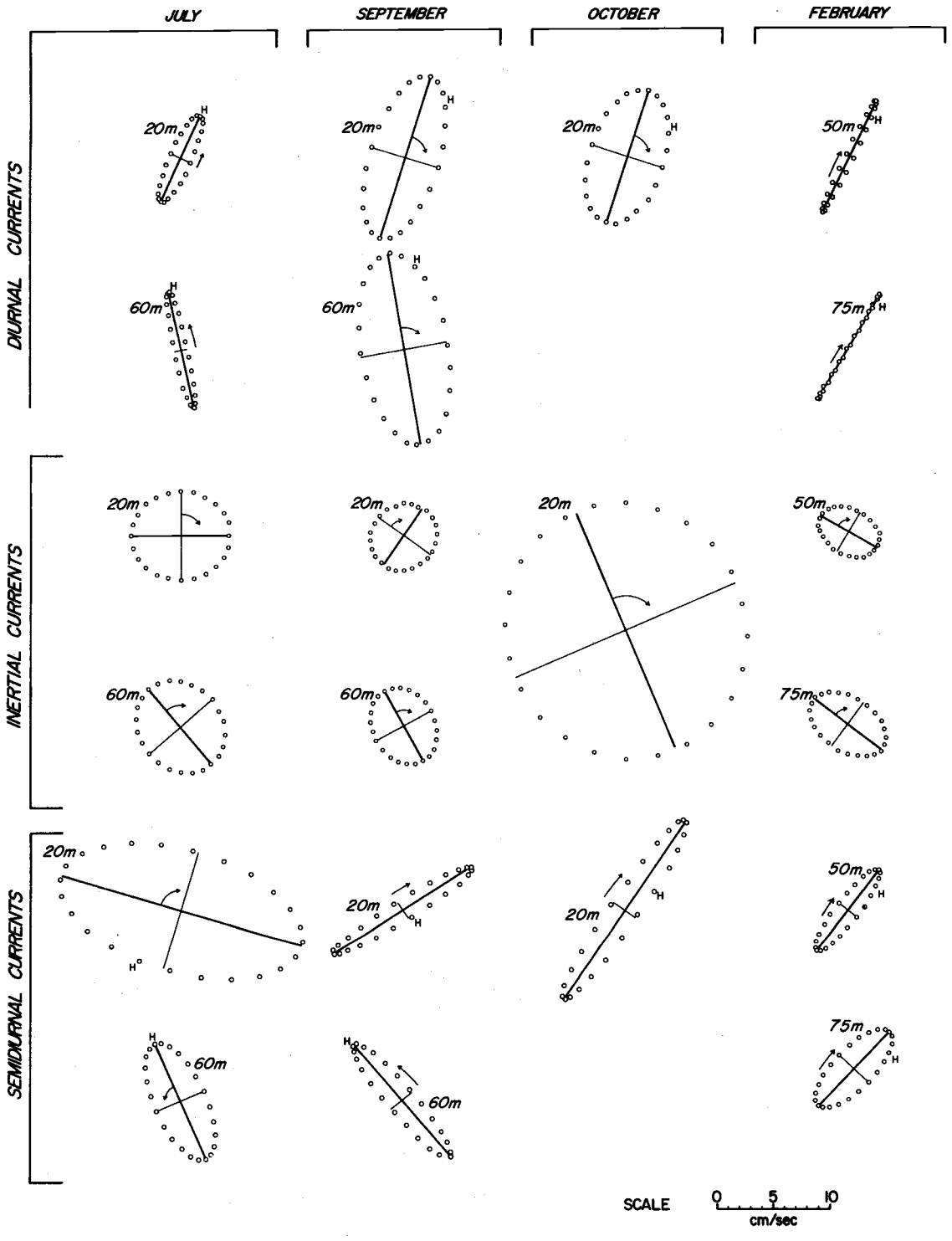

Figure 19. Current velocity ellipses. "H" corresponds to high tide and north is toward the top of the page.

Table 24. Constants for current velocity ellipses

Period	Depth m	Month	Semimajor Axis cm sec^{-1}	Semiminor Axis cm sec^{-1}	Orientation of Major Axis with Meridian	Rotation
Diurnal	20	July	4.1	1.0	026	counterclockwise
		September	7.5	3.1	018	clockwise
		October	6.1	3.2	018	clockwise
	50	February	5.4	0.4	025	counterclockwise
	60	July	5.4	0.6	347	counterclockwise
		September	8.6	3.8	350	clockwise
	75	February	5.5	0.1	031	counterclockwise
Inertial	20	July	4.8	3.5		clockwise
		September	3.3	2.5		clockwise
		October	11.4	10.6		clockwise
	50	February	3.0	2.0		clockwise
	60	July	4.4	3.7		clockwise
		September	3.5	2.8		clockwise
	75	February	3.7	2.3		clockwise
Semidiurnal	20	July	11.0	5.4	286	clockwise
		September	7.4	0.8	058	clockwise
		October	9.6	1.3	034	clockwise
	50	February	4.5	1.0	038	clockwise
	60	July	5.6	2.3	336	counterclockwise
		September	6.6	1.1	320	counterclockwise
	75	February	4.5	1.8	044	clockwise

orientation with respect to the meridian was also the same at each depth, 030°. Maximum easterly flow occurred two hours after high tide.

Inertial Currents

Phase for the u component of inertial current was arbitrarily taken as zero. Phase of the v component of current relative to the u component of current was obtained from the cross-spectrum of u and v.

Inertial currents were significant in July and October. Inertial currents were always clockwise and nearly circular, as required by theory (Sverdrup, et al., 1942). Maximum velocities were 11.4 cm sec^{-1} for October and 4.8 cm sec^{-1} for July.

Semidiurnal Currents

Semidiurnal currents were significant at the 90% level at both depths and during all four months. Rotation at 20m was clockwise; maximum velocity was largest in July, 11 cm sec^{-1}, and smallest in September, 7.3 cm sec^{-1}. The major axis of the 20m ellipse formed an angle of 286° with the meridian in July; this angle was 238° in September and 214° in October. At 20m, maximum easterly flow occurred 3 1/2 hours before high tide in July, 3 hours before high tide in September, and 2 1/2 hours before high tide in October.

Rotation of the 60m velocity vector was counterclockwise in July and September. The major axis of the 60m ellipse formed an angle of 336° with the meridian in July; this angle was 320° in September. Maximum 60m velocities were about 6 cm sec^{-1} in July and September. At 60m maximum easterly flow occurred 4 1/2 hours before high tide in July and 5 1/2 hours before high tide in September.

February semidiurnal currents rotated clockwise at 50m and 75m. The major axis of the 50m ellipse and the major axis of the 75m ellipse formed an angle of about 040° with the meridian. The maximum velocity was the same at each depth, $4\frac{1}{2}$ cm sec^{-1}. In February at 50m and 75m maximum easterly flow occurred two hours after high tide.

Other Significant Oscillations

Other significant oscillations of current velocity occurred near 3 cpd, 4 cpd, and 5 cpd (Table 25). Harmonics of the tide and of the inertial oscillation have frequencies similar to these. Amplitudes decreased with increasing frequency and ranged from 2.7 cm sec^{-1} for a 3 cpd oscillation of v at 20m in October to 0.7 cm sec^{-1} for a 5 cpd oscillation of u at 75m in February.

Table 25. Other significant intermediate frequency oscillations of current velocity

Month	Depth m	f cpd	Variable	Amplitude cm sec^{-1}	$\hat{\gamma}^2_{uv}$	$\hat{\phi}_{uv}$ degrees
July	20	2.6	u	1.6	0.61	247
		3.7	u	1.7	0.68	219
September	20	2.9	v	1.6	0.19	273
		3.7	u, v	1.6, 1.4	0.74	256
		4.7	v	1.0	0.42	198
	60	3.7	u	1.4		
October	20	2.9	u, v	2.3, 2.7	0.85	281
		4.0	u, v	1.6, 1.6	0.03	345
		4.8	v	1.4	0.25	280
February	50	2.6	v	1.0	0.46	190
		3.8	v	0.8	0.20	027
	75	3.2	u	1.3	0.17	260
		5.2	u, v	0.7, 0.8	0.001	049

Temperature

Spectra of intermediate frequency oscillations of temperature are presented in Figure 20. Statistics for spectral peaks which were significant at the 90% level are given in Table 26.

Diurnal and Inertial Energy

Most noticeable was the lack of 1 cpd oscillations of 20m temperature spectra. If temperature oscillations were entirely the result of a barotropic tide, the values of energy density would be directly proportional to the product of the temperature gradient and the amplitude of the surface tide. The amplitude of the diurnal tide averaged 45 cm and the average temperature gradient in July was $-0.25^{\circ}C\ m^{-1}$ at 20m so September barotropic temperature oscillations should have an amplitude of $0.11^{\circ}C$ The energy density at 1 cpd in July was sufficient to account for an amplitude of $0.14^{\circ}C$. Hence energy density was only slightly larger than the energy density which would result from barotropic response.

Diurnal temperature oscillations were significant at 40m in July and September. These were well correlated with current velocity but the correlation (coherence square) with sea level was not significant. Inertial oscillations were significant in October at 20m and had an amplitude of $1^{\circ}C$.

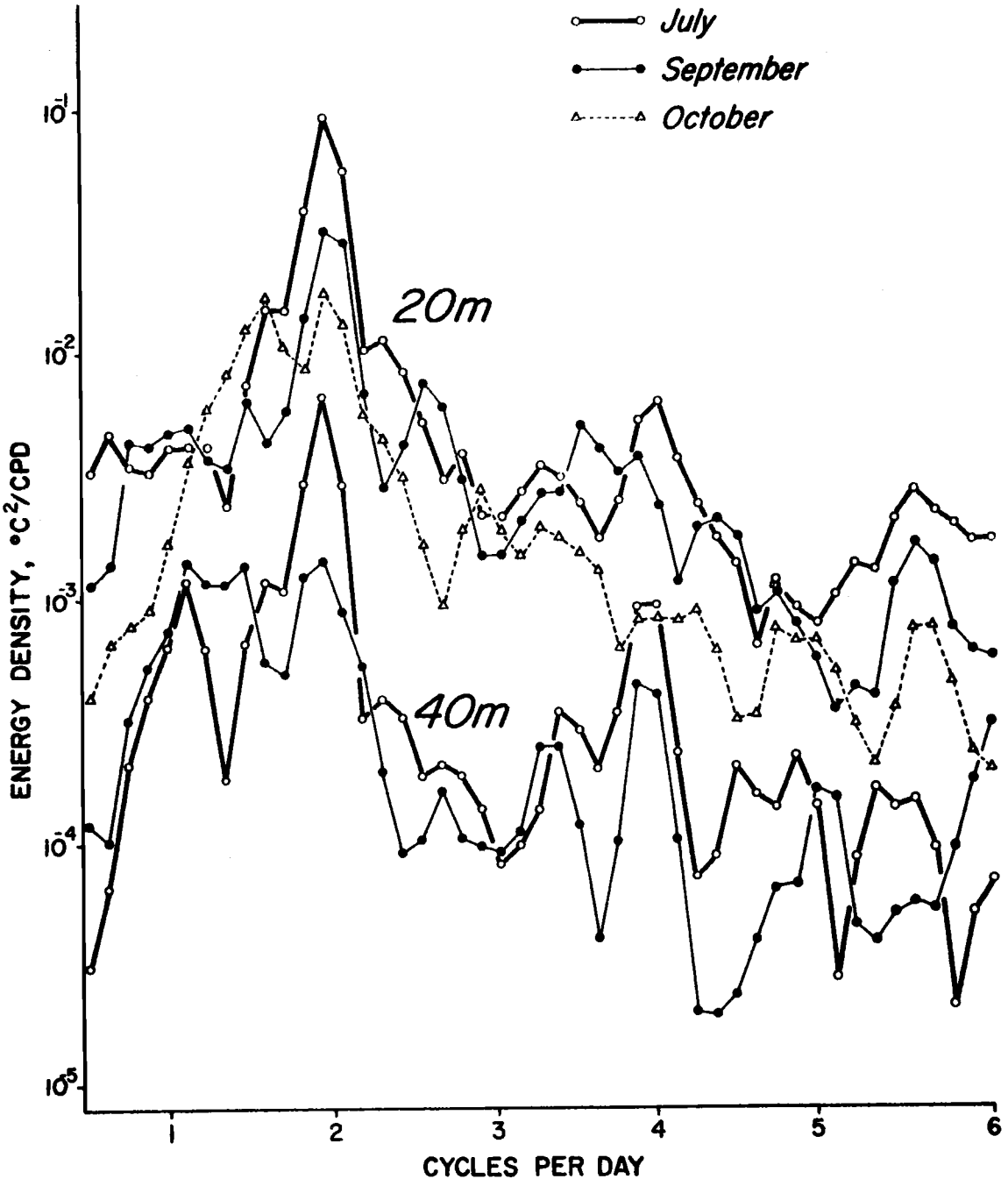

Figure 20. Intermediate frequency spectra of temperature.

Table 26. Significant intermediate frequency temperature oscillations and their relationship to current velocity

				Transfer functions: from T_z to u_z			from T_z to v_z			from T_{20} to T_{40}			from ζ to T_z		
Month	Variable	f cpd	Amp. °C	$\hat{\gamma}^2(f)$ -	$\lvert\hat{H}(f)\rvert$ C cm sec^{-1}	$\hat{\phi}(f)$ °	$\hat{\gamma}^2(f)$ -	$\lvert\hat{H}(f)\rvert$ C cm sec^{-1}	$\hat{\phi}(f)$ °	$\hat{\gamma}^2(f)$ -	$\lvert\hat{H}(f)\rvert$ -	$\hat{\phi}(f)$ °	$\hat{\gamma}^2(f)$ -	$\hat{H}(f)$ C cm^{-1}	$\hat{\phi}(f)$ °
July	T_{20}	1.9	3.19	0.91	18.1	357	0.93	8.3	123				0.75	0.56	255
		3.2	0.21	0.31	5.6	309	0.83	8.5	76				0.08	1.11	233
		4.0	0.18	0.42	4.9	351	0.69	9.3	188				0.11	1.65	316
	T_{40}	1.0	0.25	0.81	31.7	340	0.81	60.2	29	0.63	0.27	156	0.30	0.046	338
		1.9	0.45	0.57	105.9	174	0.62	63.8	57	0.36	0.08	193	0.57	0.067	69
		3.8	0.22	0.46	24.3	141	0.70	23.3	343	0.13	0.10	233	0.07	0.24	171
		4.6	0.15	0.46	26.1	206	0.87	40.6	331	0.41	0.19	122	0.04	0.15	172
		5.5	0.13	0.62	23.6	353	0.31	19.3	273	0.52	0.14	223	0.001	0.02	77
September	T_{20}	1.9	2.00	0.08	5.5	25	0.07	2.4	213				0.02	0.019	302
		2.5	0.98	0.34	5.8	349	0.52	4.9	185				0.26	0.378	55
		3.8	0.84	0.68	9.3	79	0.91	10.7	117				0.19	0.379	84
		5.5	0.48	0.11	3.3	21	0.59	2.1	12				0.01	0.15	138
	T_{40}	1.0	0.30	0.36	36.7	278	0.57	37.2	207	0.24	0.16	335	0.04	0.008	148
		1.9	0.31	0.27	74.6	6	0.56	19.5	61	0.43	0.07	335	0.26	0.008	285
		3.2	0.14	0.15	13.8	335	0.92	11.1	125	0.24	0.12	107	0.14	0.069	161
		3.8	0.17	0.58	34.5	343	0.70	26.5	94	0.83	0.23	340	0.01	0.01	179
		4.9	0.13	0.04	6.0	116	0.65	12.8	348	0.26	0.20	266	0.01	0.02	164
October	T_{20}	1.6	1.49	0.08	7.8	292	0.32	18.5	209				0.14	0.45	152
		1.9	1.47	0.33	12.0	206	0.76	27.2	203				0.69	0.23	103
		2.9	0.61	0.22	10.0	276	0.49	16.5	197				0.15	0.64	81
		4.8	0.35	0.52	15.8	339	0.18	9.8	226				0.01	0.21	114
		5.6	0.33	0.41	10.8	12	0.32	9.3	132				0.01	0.22	288

Semidiurnal Oscillations

Two-cpd oscillations were significant for all temperature time series. Largest oscillations were observed in July, 3.2°C; values of coherence square with 20m velocity components were very high, 0.9, as was the value of coherence square with sea level, 0.75. The value of the transfer function from sea level to July 20m temperature was $0.56^{\circ}C\ m^{-1}$, 255°, at 2 cpd, i.e. the maximum value of temperature occurred 8.4 hours after high tide and had a value which was greater than the mean by

0.56 x amplitude of the semidiurnal tide in meters.

The temperature gradient observed at this depth was $-0.25^{\circ}C\ m^{-1}$, about one half the value of the transfer function, $0.56^{\circ}C\ m^{-1}$. This difference, and the fact that the phase between sea level and 20m temperature was not close to zero, requires the ocean to respond baroclinically to the semidiurnal tide at 20m in July.

The amplitude of the semidiurnal 20m temperature oscillation was 2.0°C in September and 1.4°C in October. September 20m temperature oscillations were not well correlated with either 20m velocity or sea level; October 20m oscillations were well correlated with v (a coherence square of 0.76) and with sea level (a coherence square of 0.69). The value of the transfer function in the latter case was $0.23^{\circ}C\ m^{-1}$, 103°.

Semidiurnal temperature oscillations at 40m had an amplitude of $0.45^{o}C$ in July and an amplitude of $0.31^{o}C$ in September. July 40m temperature was well correlated with v and with sea level; the transfer function from sea level had a value of $0.067^{o}C\ m^{-1}$, 069^{o}; the average value of the temperature gradient at 40m in July was $+0.027^{o}C\ m^{-1}$, about one half the amplitude of the transfer function. The fact that July 40m temperature was out of phase with 20m temperatures is explained by the temperature inversion. September 40m temperature was significantly correlated with v and 20m temperature. In September, 40m temperature was in phase with 20m temperature.

Other Significant Oscillations

Significant temperature oscillations occurred at frequencies greater than two cpd. The amplitude of these oscillations usually decreased with increasing frequency and the oscillations were usually well correlated with 20m current velocity and poorly correlated with sea level.

In July and September an oscillation near four cpd was common to all time series. Its amplitude was largest, $0.8^{o}C$, in September at 20m; the amplitude of the four cpd oscillation was nearly the same at both depths in July, about $0.2^{o}C$. The four cpd oscillation was well correlated with both velocity components and, at 40m, with 20m

temperature. In July the four cpd oscillation at 40m was out of phase with 20m temperature, due to the temperature inversion, and in September it was in phase with 20m temperature.

It should be noted that a four cpd oscillation in the temperature data would result from a two cpd internal wave if the temperature gradient were non-linear. But if the four cpd oscillation in the temperature data was entirely the result of a nonlinear temperature gradient, then the four cpd temperature oscillation would not be well correlated with current velocity as it was in this case.

Winds

Diurnal energy was significant for all wind spectra. Statistics for diurnal wind ellipses are given in Table 27. The major axis of the wind ellipse formed an angle of about 350^{o} with the meridian in each month. The maximum velocity of the diurnal wind was about 3 m sec^{-1} in September, October, and February; in July the maximum velocity of the diurnal wind was 1 m sec^{-1}.[11] The strongest north-northwesterly breezes occurred in the late afternoon or early evening in July, September, and October; in February, north-northwesterly breezes were strongest at 1400.

---

[11] Meteorological data for July were obtained from a different source so numerical differences may not be real.

Table 27. Constants for diurnal winds

Month	Semimajor axis $m\ sec^{-1}$	Semiminor axis $m\ sec^{-1}$	Orientation of Semimajor axis with meridian ^{o}	Rotation	Local Time of maximum NNW'ly wind
July	0.6	0.3	345	clockwise	1900
September	2.6	0.3	350	clockwise	2000
October	1.7	0.2	344	clockwise	1700
February	2.2	0.2	350	clockwise	1400

A sinusoid, similar to equation (9-1) but containing only diurnal, inertial, and semidiurnal terms, was fitted to successive two-day intervals for September and October by the method of least squares. Ellipse areas were computed for winds and 20m currents. Results are presented in Figure 21.

Sea level data show the regular progression of the tide; inertial oscillations of sea level were not significant. Large diurnal winds occurred on 17-18 September, 3-4 October, and 13-14 October. These large diurnal and inertial winds were associated with rapid increases of mean wind speed.

Neither diurnal nor semidiurnal 20m temperature oscillations had a regular pattern. Semidiurnal temperature oscillations were usually greater than diurnal temperature oscillations. Large inertial temperature oscillations occurred on 5-6 October, 0.4C, and 15-16 October, 0.5C.

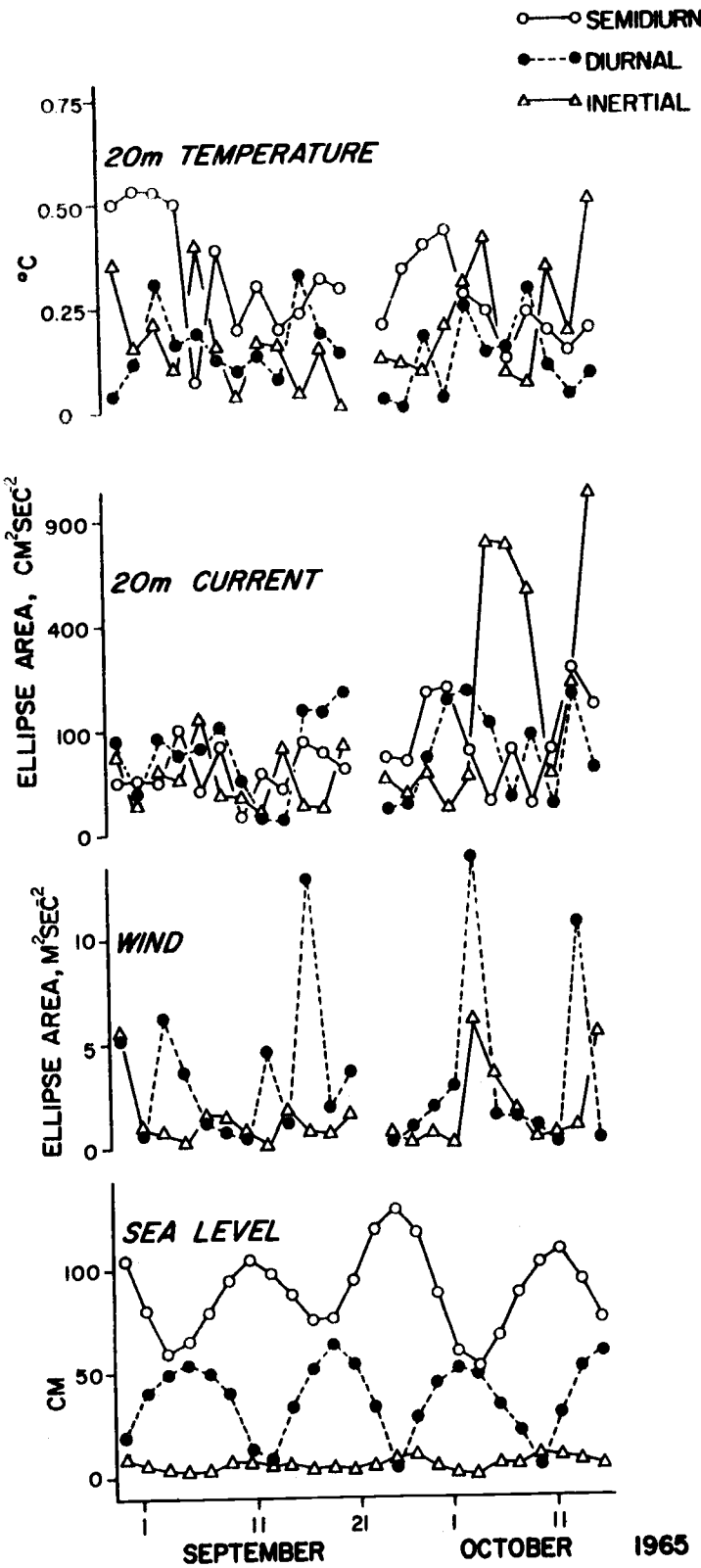

Figure 21. Variations in the amplitude of diurnal, inertial, and semidiurnal oscillations of temperature, current velocity, wind and sea level for successive two-day periods in September and October 1965.

Semidiurnal tidal currents did not exhibit the same pattern as the semidiurnal oscillation of sea level. The area of the semidiurnal current ellipse followed a random pattern and had an average value of 67 $cm^2 sec^{-2}$. Diurnal currents do follow the pattern of the diurnal surface tide but response to diurnal winds was also possible. Unfortunately, large diurnal winds occurred almost simultaneously with the maximum values of the diurnal tide so that the effects of each on current is difficult to ascertain. For example, the area of the diurnal current ellipse reached a maximum, 175 $cm^2 sec^{-2}$, on 3-4 October, as did the area of the diurnal wind ellipse, but the amplitude of the diurnal tide was greatest on 1-2 October.

Inertial currents were associated with large diurnal and inertial winds in October. It took one time unit, two days, for inertial currents to appear after the inertial winds occurred. Inertial currents continued for six days after the storm of 4 October.

Heat Flux

Further insight into the nature of diurnal, inertial, and semidiurnal energy is provided by the cospectrum of onshore flow and temperature at 20m, $\hat{X}_{u_{20}T_{20}}(f)$ (Figure 22). This quantity is usually referred to as heat flux, although for internal oscillations it may not represent a true flux of heat.

In each month, the largest energy density of the cospectrum of

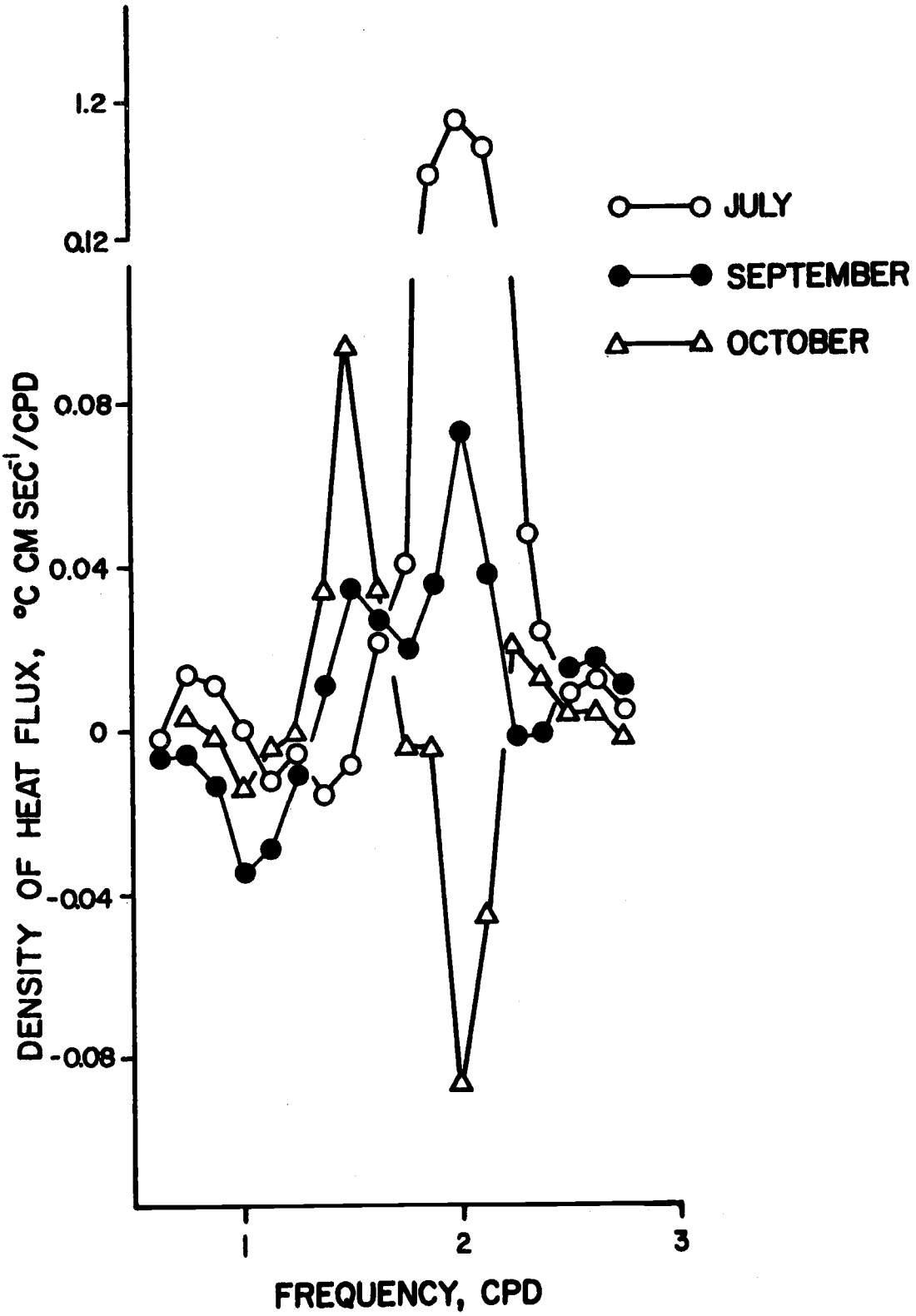

Figure 22. Cospectrum of the onshore component of velocity and temperature at 20m for 0.5 to 3.0 cpd.

20m temperature and onshore velocity occurred at two cpd. In July and September, heat flux was positive so onshore semidiurnal tidal currents were associated with warm temperatures. In October, heat flux was negative at two cpd, so onshore semidiurnal currents were associated with cool temperatures.

Heat flux at the inertial frequency was opposite to that at two cpd in July and October. In October, onshore inertial flow was associated with warm temperatures; in July onshore inertial flow was associated with cool temperatures.

Summary

Sea level spectra showed bands of energy at one cpd and two cpd with corresponding amplitudes of 43 cm and 86 cm. Current velocity spectra had, in addition to significant one and two cpd energy peaks, a peak at the inertial frequency and energy at higher frequencies, some of which was significant. Temperature spectra lack well defined peaks at one and 1.4 cpd and were dominated by energy at two cpd. Significant peaks in temperature spectra also existed at higher frequencies and in particular at 4 cpd.

Considerable baroclinic motion was indicated by the following: (i) When correlation between sea level and temperature was significant, the amplitude of the transfer function from sea level to temperature was larger than the observed temperature gradient; also

the phase between sea level and temperature was close to neither zero nor 180°. (ii) Current velocity ellipses exhibited changes with depth and with month which are not characteristic of barotropic motion. (iii) Temperature and current velocity were better correlated than either current velocity and sea level or temperature and sea level.

Baroclinic response at a frequency of two cpd was much greater than baroclinic response at one cpd. This is in agreement with theoretical results (Cox, 1962).

Inertial currents were associated with storm passage, as were inertial and diurnal winds.

CHAPTER 10. HIGH FREQUENCY TEMPERATURE OSCILLATIONS

Introduction

Oceanographers have viewed high frequency temperature oscillations as internal waves. Groen (1948) showed that the highest frequency at which a particle in a water column can oscillate is given by the maximum value of the Väisälä frequency $N(z)_{max}$, where $N(z)_{max}$ is the largest value of

$$N(z) = (2\pi)^{-1}[\rho^{-1} g(d\rho/dz)]^{\frac{1}{2}}$$

which can occur in the water column. Mooers (1964) and Haurwitz, Stommel and Munk (1959) present evidence that a "break" in the spectrum of temperature occurs near the Väisälä frequency, i.e. that energy density above $N(z)_{max}$ is much less than energy density below $N(z)_{max}$. But others have not noted this (Carsola and Callaway, 1962). Another view, suggested by Haurwitz, Stommel, and Munk (1959) and discussed explicitly by Sabinin and Shulepov (1964) considers the sea as a series of finite layers, each having its own Väisälä frequency. The oscillations of such a sea would resemble a linked pendulum system in which the frequency of the pendulum with the largest mass dominates. Data from the Norwegian Sea support this view (Sabinin and Shulepov, 1964).

Neumann (1949) believes internal oscillations can be cellular waves (standing cellular stability oscillations) which have a frequency given by

$$L_z L_x^{-1} N(z)$$

where L_z and L_x are, respectively, the vertical and horizontal dimensions of the cellular waves. Neumann (1949) found values of L_x/L_z near 3.5 for temperature oscillations in the Baltic.

Method

Spectra were obtained for each month and each depth as follows: first, spectra were calculated for selected two-day periods; then these spectra were normalized, lumped together, and multiplied by the mean value of $\frac{m\Delta t}{\pi} \hat{C}_{xx}(0)$. Finally spectra were compensated for the effect of the original numerical filter and the thermometer lag coefficient.

Two-day spectra obtained for July were classed as "large gradient" spectra or "small gradient" spectra on the basis of the mean temperature difference between 20 and 40 meters. If there was little temperature difference between these depths (less than $0.5^{\circ}C$), the spectrum was classed as a small gradient spectrum; a large temperature difference (greater than $1.0^{\circ}C$) was associated

with a large gradient spectrum. Large gradient and small gradient spectra were each lumped, recoloured and compensated in the same manner as monthly spectra.

The large gradient--small gradient classification is based on the fact that the temperature structure in regions where cold water has been upwelled is more homogeneous than where normal temperature stratification exists. Large gradient spectra should represent waters in which the water is well stratified. Small gradient spectra should represent upwelled water.

Results

Spectra (Figure 23) appeared to have three regions: (a) a region from zero to 0.6 cph where a rapid decrease of energy density occurred with increasing frequency; (b) a region of less rapid decrease of energy density with increasing frequency from 0.6 to 4.5 cph; (c) a region of constant energy density, the "noise" level, from 4.5 to 6.0 cph (40m spectra had an increase in energy density in this frequency band due to compensation for the thermometer lag coefficient).

Twenty meter spectra each had the same "noise" level, about $0.0025C^2$ cph^{-1}. The July 20m spectrum had significantly less energy than September and October 20m spectra in most of the 0.6 to 4.5 cph region. Prominent spectral peaks occurred in the

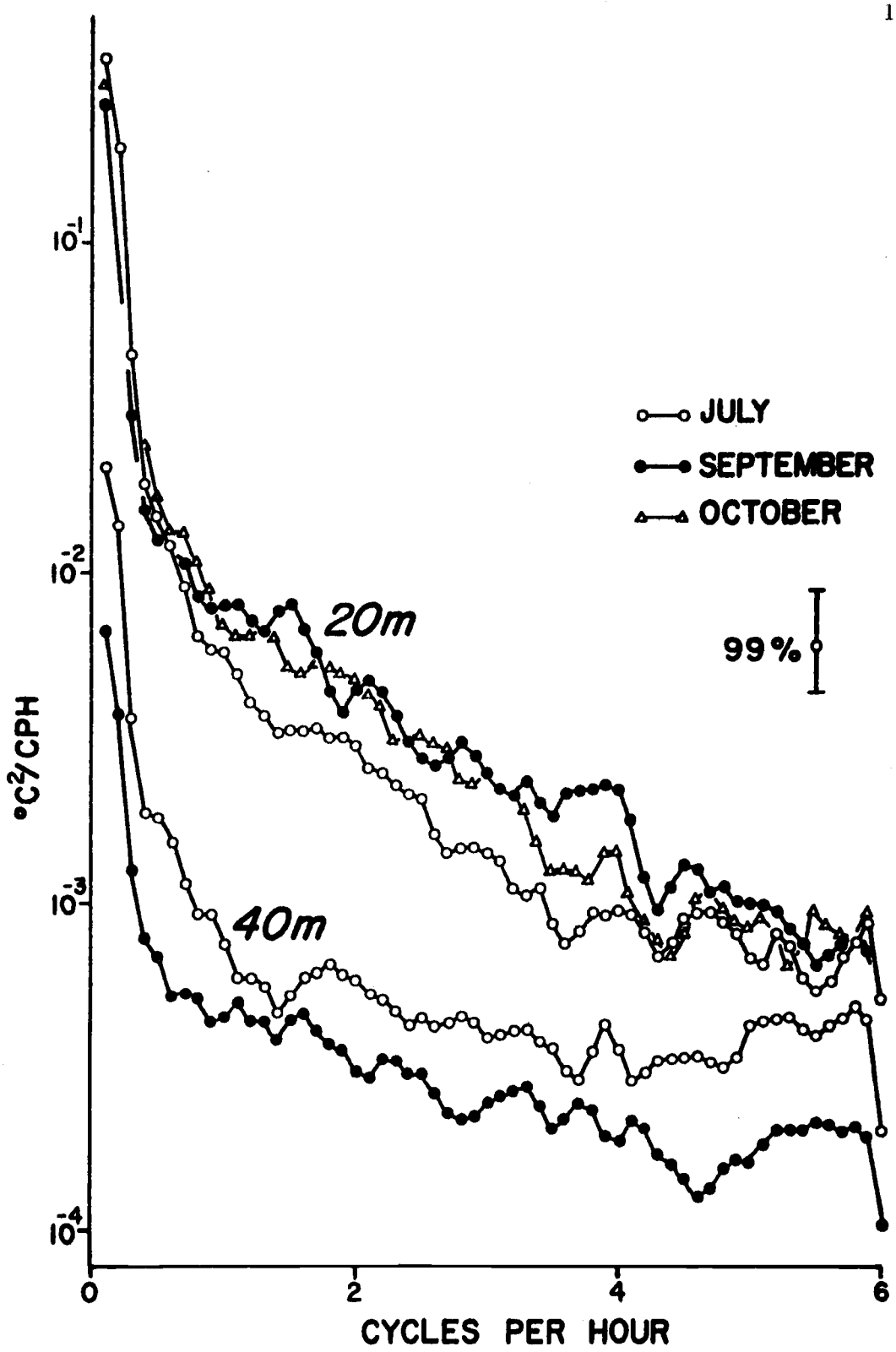

Figure 23. High frequency temperature spectra.

September 20m spectrum at 1.5 cph and 3.9 cph and in the October 20m spectrum at 3.9 cph; these peaks were significant at the 99% level. Spectral peaks occurred at 3.9 and 4.6 cph in the July 20m spectrum but these were not significant at the 99% level.

It is interesting to note that the July 40m spectrum had, at all frequencies, a larger value of energy density than the September 40m spectrum. The July 40m spectrum also had two significant peaks--at 1.8 cph and 4 cph. The September 40m spectrum had no significant spectral peaks. In general, 20m spectra had about ten times the energy density of the 40m spectra.

July small gradient and large gradient spectra are presented in Figure 24. Most noticeable is the peak at 2 cph (99% significant) which occurred on the large gradient spectrum at 40m and on the small gradient spectrum at 20m. At 20m the small gradient spectrum had greater energy density than the large gradient spectrum; at 40m the values of energy density were nearly the same.

Values of coherence square between 20 and 40m were generally not significant, but exceptions occurred. In September, coherence square between lumped 20 and 40m temperatures had a value of 0.13 (significant at the 99% level) at 2.2 cph; phase was 124°. For individual two-day spectra, a maximum value of coherence square, 0.70, was obtained for 17-18 July at a frequency of 3.4 cph; phase was 260° and the mean temperature difference

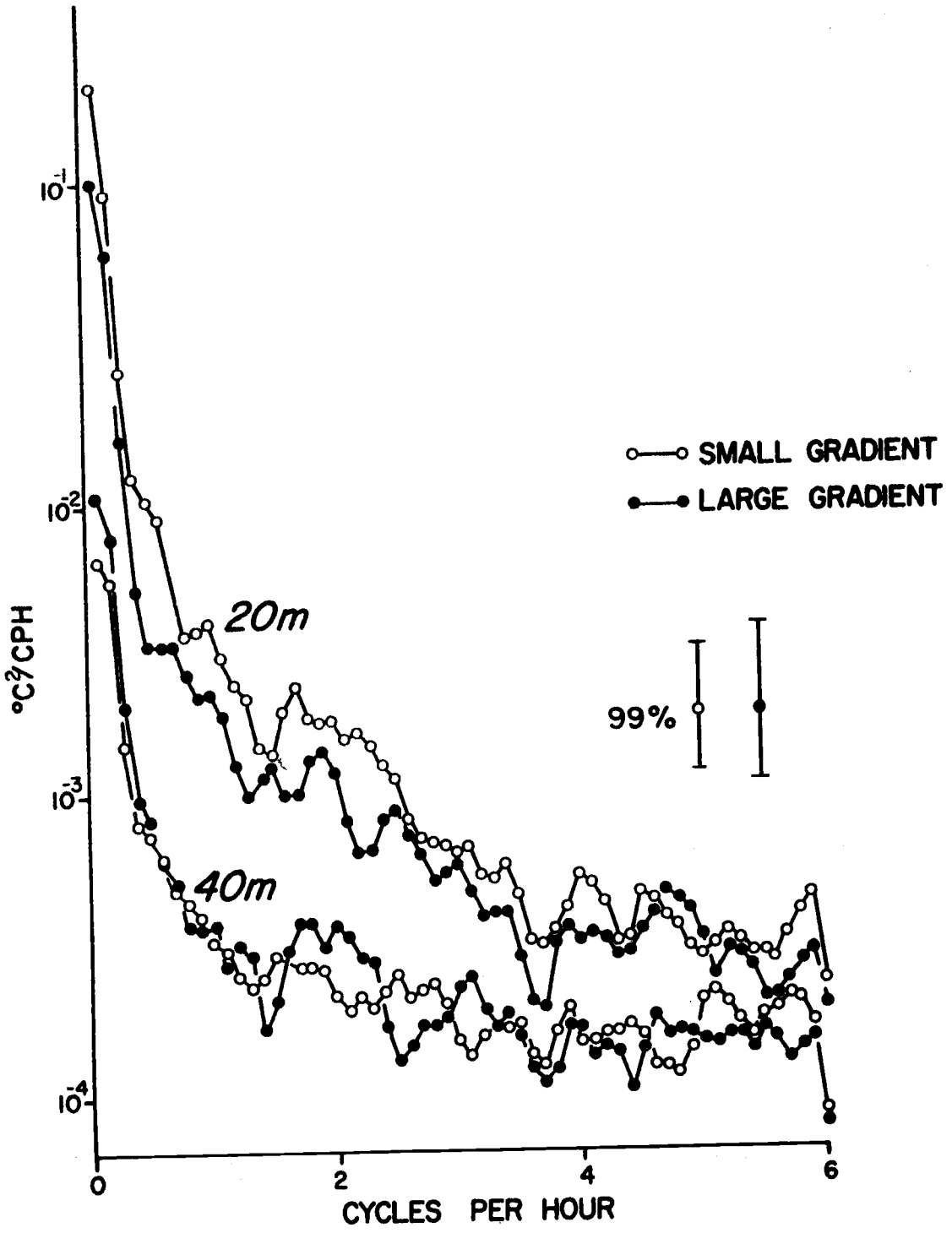

Figure 24. Large gradient and small gradient high frequency temperature spectra for July, 1965.

between 20 and 40m was 0.46°C (a small gradient).

Discussion

Three features are of particular interest: the oscillations at 4 cph, the oscillations at 2 cph, and the low values of energy density for the July 20m spectrum. The latter result is especially surprising in view of the large temperature gradient[12] at 20m in July and the large values of energy density of July 20m temperatures for frequencies of 1-6 cpd (usually greater than September or October). This indicates that high frequency oscillations at 20m were damped, not enhanced, by the large density and thermal gradient.

The opposite situation existed at 40m in July. Due to a temperature inversion, density gradients were a minimum near 40m, much weaker than in September. Yet July 40m energy density values were greater than those for September. Here the weak vertical stability enhanced high frequency temperature oscillations.

Figure 25 illustrates the Väisälä frequency as a function of depth for several hydrographic casts. The maximum value of the Väisälä frequency was near 12 cph in each case. This was beyond the Nyquist frequency for our observations. Minimum values of the

---

[12] The temperature variation associated with an internal oscillation of a given height is directly proportional to the temperature gradient.

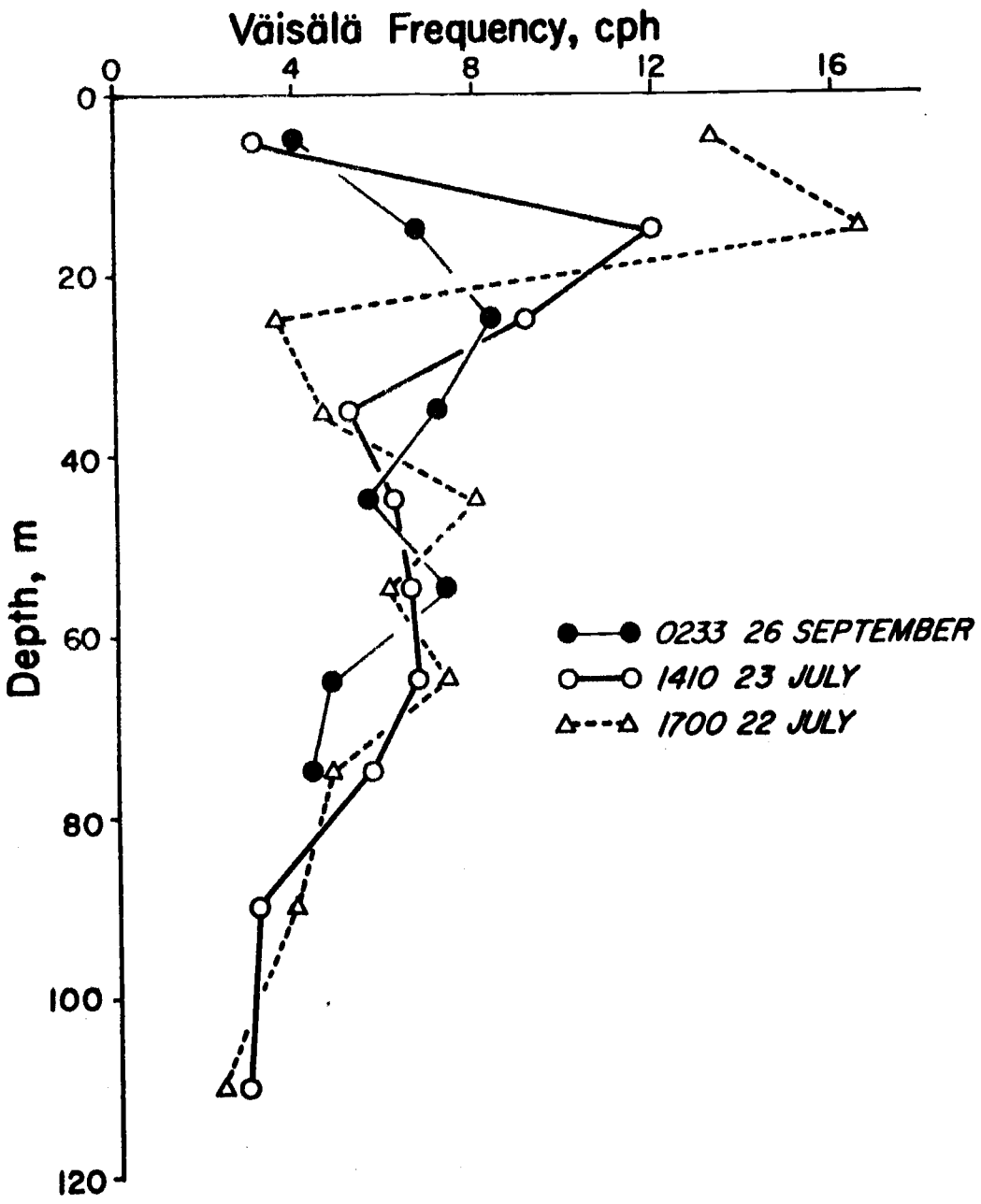

Figure 25. Väisälä frequency versus depth.

Väisälä frequency occurred between 2.4 and 4.0 cph. In September, and at 1410, 23 July (a small gradient case), the Väisälä frequency minimum was at the surface and at depths of 80-110m. For the large gradient profile, 1700, 22 July, the Väisälä frequency minimum was at 50m and at depths greater than 90m; the former was associated with the temperature inversion.

Both the 2 cph oscillations and the 4 cph oscillations can be explained as stability oscillations associated with layer of minimum Väisälä frequency. But if this were the case, two distinct types of stratification are required, one with a Väisälä frequency near 4 cph and the other with a Väisälä frequency near 2 cph. Further, the ocean should proceed gradually from one type of stratification to the next so that oscillations from 2 cph to 4 cph would have occurred. This might have been the case and could explain several features such as the masking of the 2 cph oscillations on the July 20m spectrum. Stability oscillations of upwelled surface water could have been represented by the 4 cph oscillations; stability oscillations of the layer of water in which the temperature inversion occurred could have been represented by the 2 cph oscillations.

Other explanations are possible. For example, the 4 cph oscillations could have been the linked pendulum response. When these oscillations reached a critical amplitude, standing cellular

oscillations could have occurred. Presumably, these had a frequency of 2 cph; hence, L_x/L_z is two.

CHAPTER 11. SUMMARY

Density stratification on the Oregon continental shelf varied from month to month. In July and September the waters were stratified: the density difference between 20 and 60m was 0.75 sigma-t units. In February, conditions were nearly isopycnal between these depths.

With strong density stratification, shear existed between currents at 20 and 60m. In July and September currents at 20m differed from those at 60m; this was true not only for the mean flow, but for low frequency and tidal currents. On the other hand, in February currents at 50m were similar to currents at 75m for all frequencies studied.

Northerly currents are common on the Oregon continental shelf. In February, flow was to the north at 25, 50, and 75m whenever strong southerly breezes blew; this flow seemed to be a direct effect of the wind. In summer and fall, northerly flow was of a different nature. In July, flow was to the north at 60m whenever the north-northwesterly breezes abated. In September, a strong northerly current flowed at 60m despite northerly breezes. Currents at 20m were northerly most of the time in September and October, but were weak. This flow could be a part of the California countercurrent.

In July and September, currents at 10m were usually to the south and were much stronger in July than in September. In July, flow at 20m was also southerly.

In July the following pattern of onshore-offshore flow occurred when north-northwesterly breezes were strong: flow at 10m had an onshore component of 22.5 cm sec^{-1}; at 20m no onshore flow occurred; 40m currents were offshore, 2.5 cm sec^{-1}; flow at 60m was onshore, 0.6 cm sec^{-1}. Temperatures associated with this current pattern were cooler than usual at 20m and warmer than usual at 40m. As north-northwesterly breezes abate, flow is onshore at the surface and at 60m. As a result temperatures increase at 20m and decrease at 40m.

After a summer of northerly breezes, the first strong southerly wind occurred on 4 October. In response to this storm, currents at 20m flowed to the north and onshore; temperatures at 20m warmed and sea level rose. In the wake of this storm, large inertial currents occurred at 20m and these contributed to the flux of heat onshore.

The relationship between variations of sea level and longshore velocity agreed with the geostrophic equation, i.e. southerly currents were associated with low values of sea level and northerly currents with high sea level. Values of coherence square were significant and phase estimates were steady for all low frequencies.

The regression coefficient between sea level and longshore velocity was interpreted as geostrophic current width; the coefficient was constant for July and September and implied a current width of 75 km.

The relationship between wind and sea level was studied. The effect of onshore wind on sea level was not significant. The relationship between longshore wind and sea level was dependent on frequency: longshore winds had a greater effect on sea level at frequencies lower than 0.2 cpd than at higher frequencies. For frequencies lower than 0.2 cpd, an increase of one m sec^{-1} of southerly wind was associated with a one cm rise of sea level.

Spectra of sea level, current velocity, and temperature were studied for frequencies from one to six cycles per day. Sea level spectra showed bands of energy at one and two cpd. Current velocity spectra had, in addition to significant one and two cpd energy, a peak at the inertial frequency, 1.4 cpd. Temperature spectra lacked well defined peaks at one and 1.4 cpd and were dominated by energy at two cycles per day. These differences of spectra were explained as follows. Inertial currents were associated with storm passage. For the stratified ocean, baroclinic response to the diurnal tide was slight, and temperature variations were only slightly greater than would be expected from a barotropic diurnal tide; however, baroclinic response to the semidiurnal tide produced

temperature variations much larger than would be expected from a barotropic semidiurnal tide.

High frequency temperature spectra were dominated by oscillations of 2 cph and 4 cph. Further, at a given depth, values of energy density were inversely proportional to the temperature gradient; this indicates that weak vertical stability enhanced high frequency vertical oscillations.

BIBLIOGRAPHY

Barnes, Clifford A. and Robert G. Paquette. 1954. Circulation near the Washington Coast. Seattle. 31 p. (Washington. University. Dept. of Oceanography. Technical Report no. 17)

Bendat, Julius S. and Allan G. Piersol. 1966. Measurement and analysis of random data. New York, Wiley. 390 p.

Blackman, R. B. and J. W. Tukey. 1959. The measurement of power spectra from the point of view of communi cations engineering. New York, Dover. 190 p.

Borgman, L. E. 1967. Statistical time series. Berkeley, University of California. 120 p.

Brainard, Edward C. 1964. 400 day high accuracy recording thermograph. Pittsburg, Instrument Society of America. 6 p. (Conference Preprint)

Burke, Ben G. 1966. A vessel motion instrumentation system. Journal of Petroleum Technology 18:1041-1046.

Burt, Wayne V. and Bruce Wyatt. 1964. Drift bottle observations of the Davidson Current off Oregon. In: Studies on oceanography, ed. by K. Yoshida. Seattle, University of Washington. p. 166-180.

Carsola, A. J. and E. B. Callaway. 1962. Two short-period internal wave frequency spectra in the sea off Southern California. Limnology and Oceanography 7:115-120.

Collins, Curtis A. 1964. Structure and kinematics of the permanent oceanic front off the Oregon Coast. Master's thesis. Corvallis, Oregon State University. 53 numb. leaves.

Collins, Curtis A., H. Clayton Creech and June G. Pattullo. 1966. A compilation of observations from moored current meters and thermographs. Vol. 1: Oregon continental shelf, July 1965-February 1966. Corvallis, 39 p. (Oregon. State University. Department of Oceanography. Data Report no. 23)

Cox, C. S. 1962. Internal waves. Part II. In: The sea, ed. by M. N. Hill. Vol. 1. New York, Interscience. p. 752-763.

Cromwell, Townsend and Joseph L. Reid, Jr. 1956. A study of oceanic fronts. Tellus 8:94-101.

Curie, R. 1953. Upwelling in the Benguela Current. Nature 171: 497-500.

Defant, A. 1952. Theoretische Überlengungen zum Phanomen des Windstaus und des Auftriebes und Ozeanischen Küsten. Deutsche Hydrographische Zeitschrift 5:69-80.

Defant, A. 1958. Ebb and flow. Ann Arbor, University of Michigan. 121 p.

Dixon, W. J. 1965. BMD biomedical computer programs. Los Angeles, University of California. 620 p.

Dodimead, A. J., F. Favorite and T. Hirano. 1963. Salmon of the North Pacific Ocean. Part 2. A review of oceanography of the Subarctic Pacific region. Vancouver, B. C. 195 p. (International North Pacific Fisheries Commission. Bulletin no. 13)

Fofonoff, N. P. 1965. A technique for analyzing buoy system motion. Geo-Marine Technology 1:222-225.

Fofonoff, N. P. 1966. Oscillation modes of a deep-sea mooring. Geo-Marine Technology 2:327-331.

Gaul, R. D. 1963. Influence of vertical motion on the Savonius rotor current meter. College Station. 73 p. (Texas. Agricultural and Mechanical College. Department of Oceanography and Meteorology. Reference 63-4T, Project 329)

Gaul, R. D., M. J. Snodgrass and D. J Cretzler. 1963. Some dynamical properties of the Savonius rotor current meter. In: Marine sciences instrumentation. Vol. 2. New York, Plenum. p. 119-125.

Groen, P. 1948. Contribution to the theory of internal waves. Mededlingen en Verhandelingen, Ser. B., 2(11):1-23. (Koninklijk Nederlands Meteorologish Institute de Bilt no. 125)

Hamon, B. V. and E. J. Hannan. 1963. Estimating relations between time series. Journal of Geophysical Research 68:6033-6041.

Haurwitz, B., H. Stommel and W. H. Munk. 1959. On thermal unrest in the ocean. In: Rossby memorial Volume, New York, Rockefeller Institute. p. 74-94.

Holloway, J. Leith, Jr. 1958. Smoothing and filtering of time series and space fields. Advances in Geophysics 4:351-388.

Jones, E. Lester. 1918. The neglected waters of the Pacific Coast. Washington. 21 p. (U. S. Coast and Geodetic Survey. Special Publication no. 48)

Lee, Kuo-heng. 1967. Geopotential anomaly and geostrophic flow off Newport, Oregon. Master's thesis. Corvallis, Oregon State University. 40 numb. leaves.

Marmer, H. A. 1926. Coastal currents along the Pacific Coast of the United States. Washington. 91 p. (U. S. Coast and Geodetic Survey. Special Publication no. 121)

Mooers, C. N. K. 1966. A study of ocean variability at a depth of one mile. New London. 92 p. (U. S. Navy. Underwater Sound Laboratory. Report no. 693)

Munk, W. H., F. E. Snodgrass and M. J. Tucker. 1959. Spectra of low-frequency ocean waves. Bulletin of the Scripps Institution of Oceanography of the University of California 7:283-362.

Neumann, Gerhard. 1949. Stabilitätschwingungen und die Innere Thermische Unruhe im Meer und in der Atmosphare. Deutsche Hydrographische Zeitschrift 2:23-45.

Neumann, Gerhard and W. J. Pierson. 1966. Principles of physical oceanography. Englewood Cliffs, Prentice-Hall. 545 p.

Norpac Committee. 1960. Oceanic observations of the Pacific: 1955, the Norpac atlas. Berkeley, University of California. 120 p.

Paquette, R. B. and Bion Hendersen. 1965. The dynamics of simple deep-sea buoy moorings. Santa Barbara. 167 p. (General Motors Defense Research Laboratories. Sea Operations Department. TR65-79)

Pattullo, June G. and Warren Denner. 1965. Processes affecting sea water characteristics along the Oregon Coast. Limnology and Oceanography 10:443-450.

Rattray, Maurice, Jr. 1957. On the offshore distribution of tide and tidal current. Transactions of the American Geophysical Union 38:675-679.

Reid, J. L. and R. A. Schwartzlose. 1962. Direct measurements of the Davidson Current off Central California. Journal of Geophysical Research 67:2491-2497.

Reid, J. L., G. I. Roden and J. G. Wylie. 1958. Studies of the California Current system. In: CALCOFI Progress Report 1 July 1956 to January 1958. Sacramento, California Department of Fish and Game. p. 27-56.

Roden, G. I. 1964. Spectral analysis of Japanese sea level records. In: Studies on oceanography, ed. by K. Yoshida. Seattle, University of Washington. p. 166-180.

Sabinin, K. D. and V. A Shulepov. 1965. Short period internal waves of the Norwegian Sea. Oceanology 5:264-275.

Schwartzlose, R. A. 1964. Nearshore currents of the Western United States and Baja California as measured by drift bottles. In: CALCOFI Progress Report 1 July 1960-June 1962. Sacramento, California Department of Fish and Game. p. 15-22.

Sexton, Robert. 1964. Some tow tank calibrations of the Savonius rotor. 38 p. (Columbia University. Lamont Geological Observatory. Report no. CU-11-64)

Smith, R. L., J. G. Pattullo and R. L. Lane. 1966. An investigation of upwelling along the Oregon Coast. Journal of Geophysical Research 71:1135-1140.

Stevenson, Merritt R. 1966. Subsurface currents off Oregon. Ph.D. thesis. Corvallis, Oregon State University. 140 numb. leaves.

Sunblad, Robert L. 1965. The histogram current meter. Pittsburg, Instrument Society of America. 6 p. (Conference Preprint)

Sverdrup, H. U., M. W. Johnson and Richard H. Fleming. 1942. The oceans: their physics, chemistry and general biology. Englewood Cliffs, Prentice-Hall. 1087 p.

Swanson, R. L. 1965. Tidal prediction and the variation of the observed tide from the predicted tide at Newport, Oregon. Master's thesis. Corvallis, Oregon State University. 99 numb. leaves.

United States Coast and Geodetic Survey. 1950. Manual of current observations. Washington, United States Government Printing Office. 87 p. (Special Publication no. 215)

United States Coast and Geodetic Survey. 1951. Coast Pilot 7, Pacific Coast. Washington, United States Government Printing Office. 578 p.

Webster, Ferris. 1964. Processing moored current meter data. Woods Hole. 35 p. (Woods Hole Oceanographic Institution. Technical Report no. 64-55)

Wooster, W. S. and J. L. Reid. 1963. Eastern boundary currents. In: The sea, ed. by M. N. Hill. Vol. 2. New York, Interscience. p. 253-280.

Yampol'skiy, A. D. 1965. Spectral methods of investigating oceanographic processes. Oceanology 5:1-8.

Zetler, B. D., M. D. Schuldt, R. W. Whipple and S. D. Hicks. 1965. Harmonic analysis of tides from data randomly spaced in time. Journal of Geophysical Research 70:2805-2811.